PB83-252833

Limestone Dissolution in Flue Gas Desulfurization Processes

Texas Univ. at Austin. Dept. of Chemical Engineering

Prepared for

Industrial Environmental Research Lab.
Research Triangle Park, NC

Aug 83

U.S. Department of Commerce
National Technical Information Service
NTIS

EPA-600/7-83-043
August 1983

PB83-252833

LIMESTONE DISSOLUTION IN FLUE GAS DESULFURIZATION PROCESSES

by

Gary T. Rochelle, Pui K. R. Chan, and
Anthony T. Toprac

The University of Texas at Austin
Department of Chemical Engineering
Austin, Texas 78712

EPA Cooperative Agreement R806251

Project Officer

J. David Mobley

Industrial Environmental Research Laboratory
Office of Environmental Engineering and Technology
Research Triangle Park, N.C. 27711

Prepared for:
U.S. Environmental Protection Agency
Office of Research and Development
Washington, D.C. 20460

REPRODUCED BY
NATIONAL TECHNICAL
INFORMATION SERVICE
U.S. DEPARTMENT OF COMMERCE
SPRINGFIELD, VA 22161

TECHNICAL REPORT DATA
(Please read Instructions on the reverse before completing)

1. REPORT NO. EPA-600/7-83-043	2.
3. RECIPIENT'S ACCESSION NO. PB83 252833	
4. TITLE AND SUBTITLE Limestone Dissolution in Flue Gas Desulfurization Processes	5. REPORT DATE August 1983
	6. PERFORMING ORGANIZATION CODE
7. AUTHOR(S) G. T. Rochelle, P. K. R. Chan, and A. T. Toprac	8. PERFORMING ORGANIZATION REPORT NO.
9. PERFORMING ORGANIZATION NAME AND ADDRESS The University of Texas at Austin Department of Chemical Engineering Austin, Texas 78712	10. PROGRAM ELEMENT NO.
	11. CONTRACT/GRANT NO. Cooperative Agreement R806251
12. SPONSORING AGENCY NAME AND ADDRESS EPA, Office of Research and Development Industrial Environmental Research Laboratory Research Triangle Park, NC 27711	13. TYPE OF REPORT AND PERIOD COVERED Final; 3/79 - 4/83
	14. SPONSORING AGENCY CODE EPA/600/13

15. SUPPLEMENTARY NOTES IERL-RTP project officer is J. David Mobley, Mail Drop 61, 919/541-2578.

16. ABSTRACT The report gives results of the measurement of dissolution rates of reagent CaCO3 and commercial limestones (9 types/19 grinds) at constant pH and solution composition by batch titration with HCl. Conditions were selected to simulate flue gas desulfurization. A mass transfer model has been developed which includes theoretical effects of particle size and equilibrium acid/base reactions. The cumulative rate of mass transfer is calculated by integrating over a particle size distribution obtained by Coulter Counter and screening measurements. The mass transfer model predicts measured dissolution rates with a standard deviation of 30%, without any allowance for limestone type. Therefore, particle size distribution was found to be the most significant factor governing limestone reactivity. The mass transfer model accurately predicted the effects of solution composition and temperature, at pH 4-7, 25-55 C, 0-20 mM organic acid, 0-1 atm CO2, and 0-0.1 M Ca(+2). The dissolution rate is a strong function of pH and a weak function of temperature. Buffers, such as adipic acid and low concentrations of sulfite, enhance mass transfer by increasing acidity transport to the limestone surface. Mn(+2), Fe(+2), Mg(+2), and SO3(-2) inhibit limestone dissolution, probably by formation of adsorption surface layers.

17. KEY WORDS AND DOCUMENT ANALYSIS

a. DESCRIPTORS	b. IDENTIFIERS/OPEN ENDED TERMS	c. COSATI Field/Group
Pollution Calcium Carbonates Limestone Dissolving Flue Gases Desulfurization Measurement Mass Transfer Mathematical Models	Pollution Control Stationary Sources	13B 14B 07B 08G 14G 07D 12A 21B 07A

18. DISTRIBUTION STATEMENT Release to Public	19. SECURITY CLASS (This Report) Unclassified	21. NO. OF PAGES 110
	20. SECURITY CLASS (This page) Unclassified	22. PRICE

EPA Form 2220-1 (9-73)

NOTICE

This document has been reviewed in accordance with U.S. Environmental Protection Agency policy and approved for publication. Mention of trade names or commercial products does not constitute endorsement or recommendation for use.

BEGIN FIRST LINE OF TEXT HERE
TYPING GUIDE SHEET
CENTER OF PAGE
TOP OF IMAGE AREA
DROPPED HEAD. BEGIN SECTION HERE

ABSTRACT

Dissolution rates of reagent $CaCO_3$ and commercial limestones (8 types/ 18 grinds) have been measured at constant pH and solution composition by batch titration with HCl. Conditions were selected to simulate flue gas desulfurization.

A mass transfer model has been developed which includes theoretical effects of particle size and equilibrium acid/base reactions. The cumulative rate of mass transfer is calculated by integrating over a particle size distribution obtained by Coulter Counter and screening measurements. The mass transfer model predcits measured dissolution rates with a standard deviation of 30%, without any allowance for limestone type. Therefore, particle size distribution was found to be the most significant factor governing limestone reactivity.

The mass transfer model accurately predicted the effects of solution composition and temperature, at pH 4 to 7, 25 to 55°C, 0 to 20 mM organic acid, 0 to 1 atm CO_2, and 0 to 0.1 M Ca^{++}. The dissolution rate is a strong function of pH and a weak function of temperature. Buffers, such as adipic acid and low concentrations of sulfite, enhance mass transfer by increasing acidity transport to the limestone surface. Mn^{+2}, Fe^{+2}, Mg^{+2}, and $SO_3^{=}$ inhibit limestone dissolution, probably by formation of adsorption surface layers.

BEGIN LAST LINE OF TEXT
BOTTOM OF IMAGE AREA
LAYOUT DIMENSIONS FOR TABLES AND ILLUSTRATIONS
EPA-287 (Orig.) (4-74)

CONTENTS

Section		Page
Abstract		iii
Illustrations		vi
Tables		viii
	PROJECT SUMMARY	1
	Mass Transfer Model	2
	Experimental Methods	3
	Results	4
	Conclusions	9
	Recommendations	9
1	INTRODUCTION	12
2	LITERATURE REVIEW	13
3	THEORY	15
	General Model/Stagnant	16
	Simplified Model/Stagnant	21
	Simplified Model/Turbulent	22
	CSTR Model	24
	Diffusivities	25
4	EXPERIMENTAL APPARATUS AND PROCEDURES	27
5	RESULTS	33
	Effect of Solution Composition	33
	Effect of Type and Grind	45
	CSTR Calculated Results and SO_2 Removal	54
	Results Calculated with a Log Gamma Distribution	59
	Additional Results	60
6	CONCLUSIONS	86
7	RECOMMENDATIONS	89
Literature Cited		90
Appendices		
	A. Particle Size Distributions	93
	B. Compositions of Limestone Samples	99
	C. Nomenclature	100

Preceding page blank

ILLUSTRATIONS

Figure		Page
S-1	Effect of Sulfite, N_2 Sparging, 25° and 55°C. Curves Calculated from Mass Transfer Model using $CaCO_3^\circ/CaSO_3^\circ$ Solid Solution (Figure 11)	5
S-2	CSTR Mass Transfer Model Dissolution Rates for Various Limestone Types and Grinds	9
1	Dissolution Reactor.	28
2	pH-Stat Apparatus.	29
3	Dissolution curves for Reagent Grade $CaCO_3$ at 25°C with N_2 Sparging.	31
4	Dissolution Rate of Reagent $CaCO_3$ with CO_2 Sparging in 0.1 M $CaCl_2$.	34
5	Dissolution Rate of Reagent Grade $CaCO_3$ with N_2 Sparging in 0.1 M $CaCl_2$.	35
6	$CaCO_3$ Dissolution at 25°C in 0.1 M $CaCl_2$, Effect of Acetic Acid.	36
7	Dissolution Rate of $CaCO_3$ in 0.1 M $CaCl_2$ with N_2 Sparging at 25°C, and 3 mM Adipic Acid	37
8	Effect of Organic Acids on Dissolution Rate in 0.1 M $CaCl_2$ with N_2 Sparging, 25°C and pH 5.	38
9	Effect of Sulfite, N_2 Sparging, 25° and 55°C. Curves Calculated from Mass Transfer Model using $CaCO_3^\circ/CaSO_3^\circ$ Solid Solution (Figure 11)	39
10	Effect of Acetate on Dissolution Rate with 3 mM of Total Sulfite, pH 5 and 25°C	40
11	Calculated Solution Composition at $CaCO_3$ Surface, N_2 Sparging and 25°C	44
12	Dissolution Curves for Georgia Marble Fine at pH 5 with N_2 Sparging	50
13	Dissolution Curves for Fredonia Extra Coarse at pH 4 with CO_2 Sparging	51

Figure		Page
14	Dissolution Curves for Fredonia Fine at pH 5 with N_2 Sparging.	52
15	CSTR Mass Transfer Model Dissolution Rates for Fredonia Limestone Grinds	57
16	CSTR Mass Transfer Model Dissolution Rates for Various Limestone Types and Grinds	57
17	Correlation of SO_2 Removal with Limestone Relative Reactivity as Determined by CSTR Mass Transfer Model.	58
18	Generalized Log Gamma Distributions for $\beta = 2$.	61
19	Correlation of α to Dispersivity Ratio d_{90}/d_{50} for Log Gamma Distribution, $\beta = 2$.	62
20	Correlation of d_{100} to α for Log Gamma Distribution, $\beta = 2$	63
21	CSTR Dissolution Curves Based on Log Gamma Distributions, $\beta = 2$, $d_{50} = 10\ \mu m$	65
22	CSTR Dissolution Curves Based on Log Gamma Distributions, $\beta = 2$, $d_{50} = 40\ \mu m$	66
23	Effect of Mn and Mg on Reagent $CaCO_3$ Dissolution, 25°C, 2.5 mM Ca^{++}	68
24	Effect of Fe^{+2} on Reagent $CaCO_3$ Dissolution, CO_2 Sparging, 0.1 M Na_2SO_4, 25 mM Ca^{++}, 25°C	69
25	Effect of Fe^{+2} on Reagent $CaCO_3$ Dissolution, N_2 Sparging, 0.1 M Na_2SO_4, 2.5 mM Ca^{++}, 25°C.	70
26	Effect of Dissolved Sulfite on Reagent $CaCO_3$ Dissolution, 1.0 M Na_2SO_4, N_2 Sparging, pH 6.5, 25°C.	71
27	Effect of DIssolved Sulfite on Reagent $CaCO_3$ Dissolution in 0.3 M $MgSO_4$, pH 5, N_2 Sparging	72
28	Effect of Ionic Strength on Reagent $CaCO_3$ Dissolution, pH 5, 0.1 M $CaCl_2$, N_2 Sparging, 25°C, and on H^+ Diffusion in NaCl (Roberts and Northey, 1972)	74
29	Effect of Dissolved Sulfite on Dissolution of Fredonia 100-140 Mesh, 0.1 M Na_2SO_4, 2.5 mM Ca^{++}, pH 5, 25°C.	76
30	Comparison of Dissolution Rates of Calcite and Dolomite with the Same Particle Size Distribution, N_2 Sparging	83

TABLES

Table		Page
S-1	Summary of Measured and Predicted Values of Time Required to Dissolve 50% (t_{50}) and 80% (t_{80}) of the Initial Available $CaCO_3$.	7
1	Diffusivities at 25°C.	26
2	Values of B Obtained from the Experimental Data.	47
3	Summary of Measured and Predicted t_{50} and t_{80}.	48
4	Relative Dissolution Rates as a Function of Agitation Level. .	53
5	Dissolution in 10 mM NaAc Solution, pH 5.0, N_2 Sparge.	55
6	Comparison of Log Gamma Fit with Coulter Counter Data.	64
7	Dissolution of 100-140 Mesh Fredonia, pH 5.0	75
8	Effects of Boiler Cleaning Acid.	78
9	Effects of Ethylenediamine, Reagent $CaCO_3$, pH 6.0, 0.1 M $CaCl_2$, N_2 Sparging.	79
10	Effect of Gypsum Saturation, Reagent $CaCO_3$, 25°C, pH 5, 0.1 M $CaCl_2$, CO_2 Sparging.	80
11	Effect of Reagent $CaCO_3$ Solids Concentration, pH 5.0, CO_2 Sparging, 0.1 M $CaCl_2$, Titration by 10 N H_2SO_4	82
12	Dissolution of Thornton Dolomite, -325 Mesh, 25°C, N_2 Sparging	85

PROJECT SUMMARY

The rate of limestone ($CaCO_3$) dissolution directly affects the overall performance of flue gas desulfurization (FGD) processes based on scrubbing with limestone slurry. In combination with gas/liquid mass transfer and calcium sulfite ($CaSO_3$) dissolution/crystallization, the rate of $CaCO_3$ dissolution determines the relationship of SO_2 removal and $CaCO_3$ utilization. It also affects the potential for scaling by $CaSO_3$ and calcium sulfate ($CaSO_4$) in the scrubber.

The operating pH of a $CaCO_3$ slurry scrubber is a tradeoff of better SO_2 removal at higher pH and improved limestone utilization at lower pH. The rate of limestone dissolution is also significantly affected by dissolved CO_2, sulfite/bisulfite, and other buffer components in the solution. In addition to quantifying these effects of solution composition, it is also important to predict the effects of variations in the type and grind of limestone.

Previous investigators in geochemistry developed the pH-stat to measure $CaCO_3$ dissolution rates (Berner and Morse, 1974; Plummer et al., 1978). They concluded that rates were controlled by H^+ diffusion below pH 5.0 and by surface reaction kinetics above pH 5.0. Previous work in flue gas desulfurization has concentrated primarily on methods of getting relative reactivity as a function of type and grind.

This project adapted the pH-stat method to measure absolute dissolution rates at FGD conditions as a function of solution composition and limestone type and grind. Particle size distributions of the $CaCO_3$ samples were measured by a Coulter Counter. A mass transfer model was developed which includes effects of particle size, diffusion of H^+ with equilibrium buffer reactions, and the finite-rate reaction of CO_2 in the mass transfer boundary layer. With no allowance for surface reaction kinetics, this model accurately predicts limestone dissolution rates over the entire range of experimental data, from pH 4 to pH 7, from 1 to 100 μm particle size,

with 8 different sources of $CaCO_3$. Particle size distribution is shown to be the primary factor determining reactivity of naturally-occurring limestone.

The results of this project have also been reported in theses and papers on effects of solution composition (Chan, 1981; Chan and Rochelle, 1982) and on effects of type and grind (Toprac, 1981; Toprac and Rochelle, 1982; Chang et al., 1982).

MASS TRANSFER MODEL

Several computer programs were developed using mass transfer theory to predict the dissolution rate of limestone as a function of particle size. The dissolution rate (cm^3/sec) of a single spherical particle of diameter d_p(cm) and volume V_p(cm^3) is given by the mass transfer expression:

$$\frac{dV_p}{dt} = -\pi d_p^2 \, k_L \Delta C/\rho_m \qquad (1)$$

where k_L = mass transfer coefficient (ℓ/cm^2-sec)

ΔC = effective concentration driving force (M)

ρ_m = molar density of limestone (0.0271 gmol/cm^3)

For particles from 1 to 100 μm, the mass transfer coefficient was taken to be the sum of one term representing diffusion in stagnant solution and one term representing the effect of agitation. The rate was correlated in terms of the constants K(cm^2/sec) and B(cm^{-1})

$$\frac{dV_p}{dt} = -K(V_p^{1/3} + BV_p^{2/3}) \qquad (2)$$

The constant K was found to be 1.5 times its theoretical value:

$$K = \frac{1.52(6\pi^2)^{1/3} D\Delta C}{\rho_m \cdot 1000} \qquad (3)$$

where D = effective diffusivity (cm^2/sec)

This empirical adjustment of 1.5 is probably a correction for nonspherical shape of the particles.

$CaCO_3$ mass transfer is enhanced by acid/base reactions. Therefore, the effective $D\Delta C$ was calculated by numerical solution of equilibria and material balances in the boundary layer for the species H^+, OH^-, Ca^{++}, $CO_3^=$,

HCO_3^-, $SO_3^=$, HSO_3^-, $A^=$, HA^-, and H_2A (adipic acid or other buffer). In the simplest case, it was assumed that HCO_3^- does not react with H^+ in the boundary layer.

This theoretical calculation of K assumes that the $CaCO_3$ solid is in equilibrium with the solution at its surface. The reaction of $CaCO_3$ solid with aqueous solution is assumed to be instantaneous.

The constant B should be independent of particle size and was given by:

$$B = \frac{0.167}{D} \left[\frac{\varepsilon\nu}{\rho^2}\right]^{1/4} \left[\frac{\nu}{D}\right]^{-2/3}$$

where ε = agitation power (cm^2/sec^3)

ν = kinematic viscosity of solution (cm^2/sec)

ρ = density of solution (g/cm^3)

The adjustable constant, 0.167, based on data from this project was within 50 percent of that predicted by literature correlations. At typical levels of agitation with mass transfer controlled by H^+ diffusion the value of B was 400 cm^{-1}.

Eq. (2) gives the dissolution rate of a single particle of size V_p. In order to model dissolution rates in a batch reactor at constant solution composition, Eq. (2) was integrated to give the fraction of undissolved $CaCO_3$ as an implicit function of time. The total fraction $CaCO_3$ remaining was obtained by summing over the fraction remaining in each size fraction of the initial particle size distribution obtained by a Coulter Counter. Predictions of limestone utilization in a scrubber system were made by an additional integration over a stirred tank residence time distribution. These calculations were implemented on a computer.

EXPERIMENTAL METHODS

The absolute dissolution rates of 9 limestone types and 19 grinds were successfully measured by the pH-stat method. A batch of 0.5 g limestone sample was dissolved in one liter of agitated solution at constant pH. The reactor was sparged with N_2 or CO_2 to maintain constant dissolved CO_2 and constant dissolution stoichiometry. The pH was controlled at values from 4.0 to 7.0 by titration with hydrochloric acid. The cumulative dissolution of $CaCO_3$ was obtained as a function of time directly from the titration

volume of HCl by the stoichiometry:

$$CaCO_3(s) + 2\ HCl \rightarrow Ca^{++} + CO_2(g) + 2\ Cl^- + H_2O$$

Constant concentrations of other components were obtained by initially adding $CaCl_2$, Na_2SO_4, Na_2SO_3, organic acids, and other soluble salts. This procedure was precisely performed with an automatic digital pH titrimeter. However, satisfactory results were also obtained with manual pH control by titration from a burette.

Particle size distributions from 0.7 to 160 μm were obtained with a Coulter Counter. These data were necessary to use the mass transfer model, but not to determine reactivity of the samples. A method was developed to use a two-parameter log gamma size distribution in the model, so that simple techniques such as screening could be used with the mass transfer model.

RESULTS

The mass transfer model correlated all of the measured effects of solution composition and limestone type and grind on the $CaCO_3$ dissolution rate. The two adjustable constants, K and B, were found to be about 50 percent greater than the theoretical or predicted values. If surface reaction kinetics were significant, K and B would be less than their predicted values. Since mass transfer is controlling, the primary effect of limestone type and grind results from the particle size distribution of the ground stone.

Effects of Solution Composition

Figure S-1 illustrates typical results obtained with reagent $CaCO_3$ in 0.1 M $CaCl_2$ solution. The rate constant, k, was obtained from experimental data and from the model by neglecting the second term of Eq. (2). Because of the small effect of agitation, it is equal to 1.25 times the constant K. The curves in Figure S-1 were calculated by the mass transfer model.

The rate data show the strong effect of pH. With no dissolved sulfite and N_2 sparging at 25°C, the dissolution rate increases from 1.4×10^{-10} cm^2/sec at pH 6.0 to 2×10^{-9} cm^2/sec at pH 4.5. $CaCO_3$ dissolves faster at lower pH because there is a proportionately larger driving force for H^+ diffusion from bulk solution to the limestone surface.

Solution components that buffer between the pH of the bulk solution

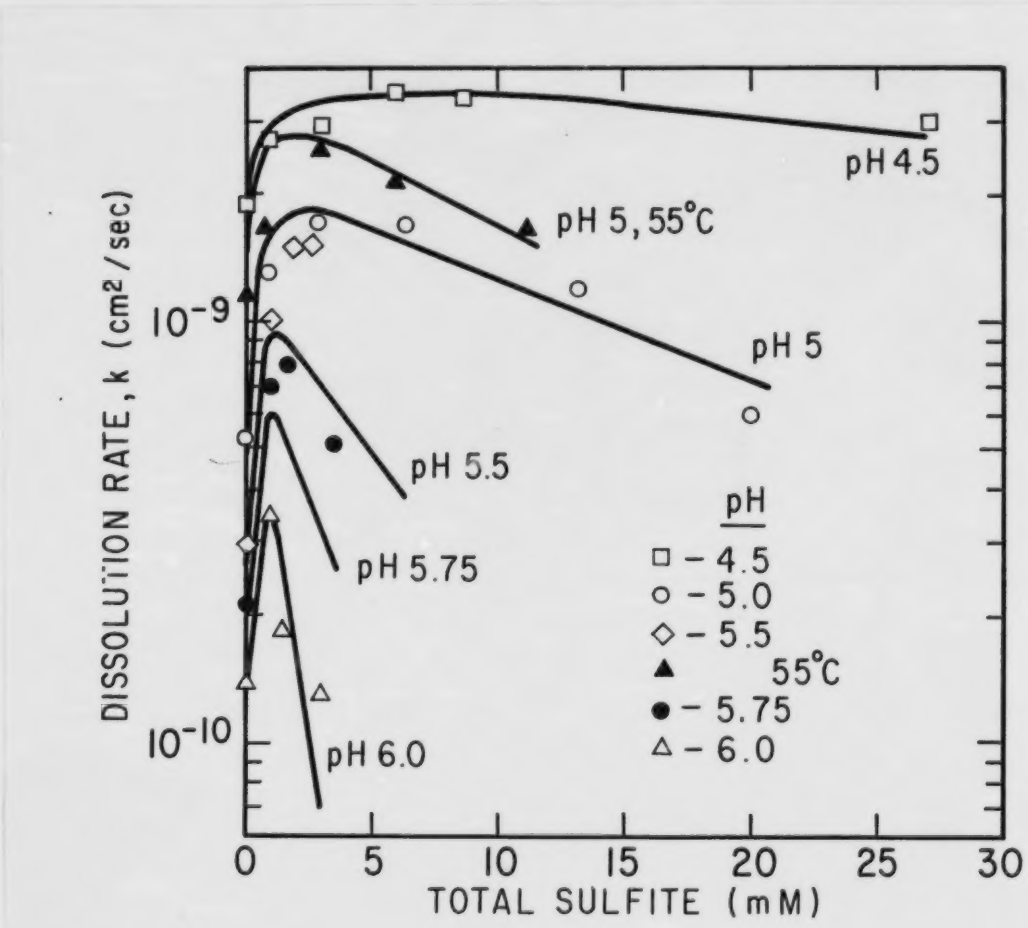

Figure S-1. Effect of Sulfite, N_2 Sparging, 25° and 55°C. Curves Calculated from Transfer Model Using $CaCO_3^\circ/CaSO_3^\circ$ Solid Solution

and the pH of the limestone surface (typically 5.5 to 8.0) enhance the effective H^+ transport. Figure S-1 shows that at pH 5.0, 1 mM of $SO_3^=/HSO_3^-$ buffer enhances the dissolution rate by a factor of 3.0. Similar but less dramatic effects were obtained with acetate, adipate, and other organic acid buffers.

The equilibrium at the $CaCO_3$ solid/solution interface is modified by the adsorption of ionic species on the limestone surface. Figure S-1 shows that higher concentrations of $SO_3^=/HSO_3^-$ inhibit $CaCO_3$ dissolution. This effect was successfully modeled by assuming that the solubility of $CaCO_3$ is depressed by the presence of dissolved $CaSO_3$ at the $CaCO_3$ surface. The inhibiting effect of sulfite depends primarily on the $CaSO_3$ saturation in the solution. At extreme values of $CaSO_3$ saturation, $CaCO_3$ dissolution stopped completely, probably because of irreversible crystallization of $CaSO_3$ on the $CaCO_3$ surface. Similar inhibiting effects were measured with Mn^{++}, Fe^{++}, and polyacrylic acid.

Dissolved CO_2 inhibits $CaCO_3$ dissolution when the bulk solution is nearly saturated to $CaCO_3$. However, at lower pH, dissolved CO_2 can enhance the dissolution rate by acting as a buffer (CO_2/HCO_3^-) to carry acidity. Unlike most other buffers, CO_2 reacts with H_2O at a finite rate to produce H^+ and HCO_3^-. Therefore the contribution of CO_2 is important only with large particles (>50 μm) under conditions where other buffers, such as $SO_3^=/HSO_3^-$, are not present. The effect of the CO_2 reaction was observed as an empirical adjustment in the constant B when using CO_2 sparging.

Effects of Type and Grind

The effect of type and grind was determined by 31 experiments with 9 limestone types and 19 different particle size distributions. Experiments were performed at 25°C in 0.1 M $CaCl_2$ at pH 4 or 5 with sparging by N_2 or CO_2. The results are presented in Table S-1 as the time required to dissolve 50 percent (t_{50}) or 80 percent (t_{80}) of the $CaCO_3$ in the sample.

The data were correlated by Eq. (2) with integration over time and summation over particle size. With N_2 sparging the value of B was found to be 400 cm^{-1}. Because CO_2 enhances or inhibits dissolution more with coarse particles, the value of B with CO_2 sparging was found to be 880 cm^{-1} at pH 5 and 260 cm^{-1} at pH 4. Table S-1 shows that the predicted values of t_{50} agree

Table S-1: Summary of Measured and Predicted Values of Time Required to Dissolve 50% (t_{50}) and 80% (t_{80}) of the Initial Available $CaCO_3$

Limestone Type	Grind	d_{50} (μm)	d_{90}/d_{50}	pH	Sparge	t_{50} (min) meas	t_{50} (min) meas/calc	t_{80} (min) meas	t_{80} (min) meas/calc
Ash Grove %A = 96.7[a]	-325	12.7	2.30	5	CO_2	7.88	0.99	32.6	1.17
Brassfield %A = 84.0	120-200	100	1.35	4	CO_2	39.0[b]	0.98	85.1	1.08
Fredonia %A = 95.0	Coarse	38.1	3.73	4	CO_2	6.95	1.16	57.1	1.33
	Extra Coarse	40.3	4.02	4	CO_2	6.10	0.91	38.7	0.79
	Feedbelt	7.7	6.60	5	N_2	3.91[b]	0.92[d]	60.2	1.32
	Fine	8.0	8.51	5	N_2	6.1	1.37	72.8	0.98
	100-140	130	1.20	4	CO_2	54.2	0.93	107	0.94
				4	N_2	40.0	0.95		
				5	CO_2	208[b]	1.05		
				5	N_2	494[b]	1.03	893	1.18
	120-200	125	1.24	4	CO_2	63.0	1.65[d]	131	1.68
	170-270	66	1.36	4	CO_2	14.6	0.71		
				4	N_2	13.9	0.87		
				5	CO_2	81.5	1.01		
				5	N_2	145	1.00		
	200-325	66.4	1.95	4	CO_2	22.0	0.90[d]	44.1	0.87
Georgia Marble %A = 96.5	Coarse	42.0	2.86	4	CO_2	11.9[b]	1.34	48.9[b]	1.34
				5	CO_2	47.0	1.17		
	Fine	24.0	2.06	5	N_2	27.0[c]	0.95	108	1.21
Longview %A = 95.0	Coarse	17.9	8.60	4	CO_2	2.80[b]	1.31	24.9	0.980
	Fine	15.0	3.63	5	CO_2	7.88[b]	0.87		
Maysville %A = 98.4	-325	8.3	4.31	4	CO_2	0.675[b]	1.01	3.54	0.794
Pfizer %A = 98.7	120-200	19.8	2.82	4	CO_2	3.70[d]	1.48	20.3	1.92
	200-325	21.8	2.34	4	CO_2	4.60[d]	1.63	23.6	2.02
Reagent Grade %A = 100		11.4	1.35	4	CO_2	1.26	1.07		
				4	N_2	1.17	1.07		
				5	CO_2	8.39	1.09		
				5	N_2	10.7	1.08		
Stoneman %A = 86.0	Coarse	40.3	2.90	4	CO_2	6.9[c]	0.90		
	Fine	22.0	2.30	5	CO_2	14.9	1.01	81.4	1.34
				5	N_2	20.3[c]	0.94		

a - %A = percent available for dissolution (wt % $CaCO_3$ + $MgCO_3$)
b - represents an average value from several runs
c - obtained in early apparatus with magnetic stirrer
d - 700 rpm

with measured values within a standard deviation less than 30 percent. This close agreement is maintained for samples with values of t_{50} varying over two orders of magnitude.

For limestone sources of reasonable purity (85 percent $CaCO_3$), the particle size distribution of the ground sample is the primary factor determining reactivity, rather than the limestone type or composition. With lower purity or greater than 90% utilization, the dissolution of dolomite or other impurities may have more pronounced effects on the rate of $CaCO_3$ dissolution.

Experiments with pure dolomite ($MgCO_3 \cdot CaCO_3$) established that it dissolves 3 to 10 times slower than calcite ($CaCO_3$). Therefore, the dissolution rate of dolomtie is controlled by surface reaction kinetics rather than mass transfer. If dolomite is present in a limestone sample, it will dissolve slower than calcite, but it will still dissolve with some release of Mg^{++} into the solution.

Design Implications

In terms of limestone dissolution, a slurry scrubbing system can be defined as a continuous stirred tank reactor (CSTR) with a residence time, τ, equal to the molar ratio of calcium solids inventory and $CaCO_3$ feedrate. Given a particle size distribution, the computerized mass transfer model can calculate a relationship of stoichiometric ratio (SR) and relative reactivity ($1/K\tau SR$), as shown in Figure S-2 for 6 limestone grinds. The constant K can be determined experimentally or by the computer model as a function of solution composition, shown in Figure S-1.

In a typical scrubber hold tank, the limestone has a residence time, τ, of 10 hours. In the absence of equilibrium limitations, Figure S-2 shows that K can easily obtain a value approaching 10^{-9} cm^2/sec at pH 5.5 with dissolved sulfite. With a stoichiometric ratio near 1.0, these values of K and τ give relative reactivity of 3×10^{-4} μm^{-2}, suggesting an actual stoichiometry from Figure S-2 of 1.05 to 1.1 depending on the limestone grind. In practice, stoichiometric ratios of 1.2 to 1.5 give pH values of 5.5 to 6.0. Therefore, hold tanks may operate near equilibrium with respect to $CaCO_3$ or the $CaCO_3 \cdot CaSO_3$ adsorption layer. If the hold tank is operating near equilibrium, its volume will have only a small effect on system

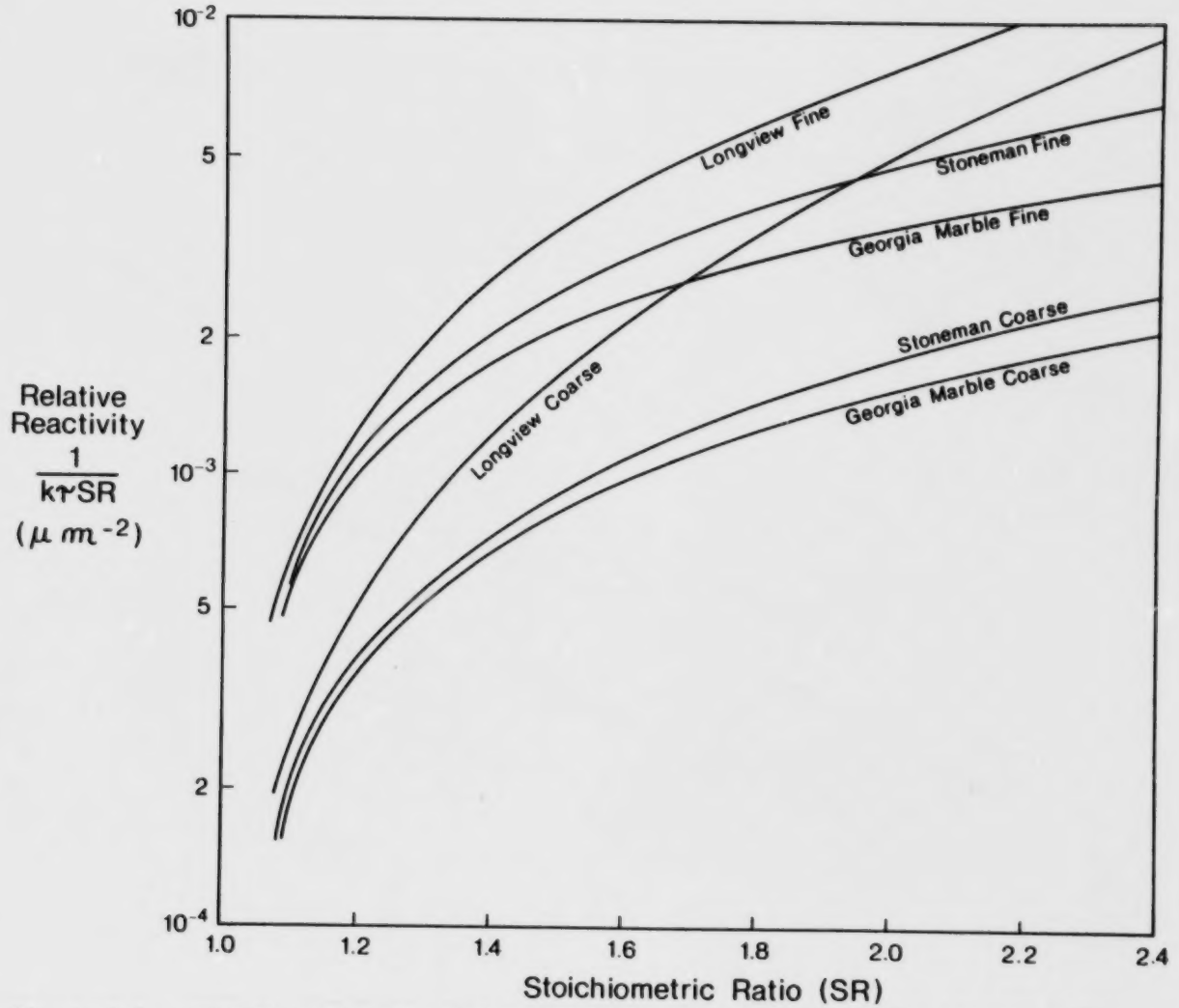

Figure S-2. CSTR Mass Transfer Model Dissolution Rates for Various Limestone Types and Grinds

performance.

In a typical scrubber, the limestone residence time is as much as 100 times less than in the hold tank, for example 0.1 hours. However, the pH is typically much lower, giving a faster rate of $CaCO_3$ dissolution. At pH 4.5 with dissolved sulfite and in the absence of equilibrium limitations, Figure S-1 shows that K can easily be as large as 5×10^{-9} cm^2/sec. The combination of large K and small τ still gives a relative reactivity approaching 4×10^{-3} μm^{-2} and a stoichiometry of 1.5 to 2.0 with fine grind limestones. Therefore, it is conceivable that a significant fraction of the limestone could dissolve in the scrubber rather than the hold tank.

CONCLUSIONS

1. The pH-stat method is effective for determining absolute and relative reactivity of limestone samples.
2. $CaCO_3$ dissolution is controlled by diffusion of H^+, OH^-, and buffer species, not by surface reaction kinetics.
3. Dissolution rates of relatively pure limestones do not depend on limestone type or source, only on particle size distribution.
4. Particle size distributions can be measured by a Coulter Counter. Other methods can be used to give approximate results.
5. Sulfite/bisulfite, adipic acid, and other buffers enhance limestone dissolution.
6. Sulfite, Fe^{++}, Mn^{++}, Mg^{++}, and polyacrylic acid inhibit $CaCO_3$ dissolution, possibly by reducing the effective solubility of $CaCO_3$.
7. The dissolution rate of limestone is relatively fast; therefore, a significant fraction of limestone can dissolve in the scrubber itself, and solution in the hold tank will be near equilibrium with the $CaCO_3$ solids.

RECOMMENDATIONS

1. Dissolution rates should be measured with 1 to 15% solids concentration.
2. Diffusivities of H^+, OH^-, HCO_3^-, $SO_3^=$, and Ca^{++} should be measured in solutions of 0.1 to 2.0 M $CaCl_2$, $MgSO_4$, and Na_2SO_4.
3. Careful measurements of $CaCO_3$ dissolution rates near equilibrium pH are needed to quantify effects of $SO_3^=$, metal ions, and Mg^{++} on the effective solubility of $CaCO_3$.
4. Careful measurements of limestone reactivity at high utilization are needed to establish any second order effects of limestone type and impurities.

LITERATURE CITED

Berner, R. A., and Morse, J. W., Amer. J. Sci., 274, 108 (1974).

Chan, P.K.R., M.S. Thesis, University of Texas, Austin, Texas, 1981.

Chan, P. K., and G. T. Rochelle, ACS Symp. Ser., 188, 75-97 (1982).

Chang, C-S., J. H. Dempsey, R. H. Borgwardt, G. T. Rochelle, and A. J. Toprac, Env. Prog., 1(1), 59-65 (1982).

Plummer, L. N., Wigley, T.M.L., and Parkhurst, D. L., Amer. J. Sci., 278, 179 (1978).

Toprac, A. J., M.S. Thesis, The University of Texas, Austin, Texas (1981).

Toprac, A. J., and G. T. Rochelle, Env. Prog., 1(1), 52-58 (1982).

SECTION 1

INTRODUCTION

Limestone ($CaCO_3$ dissolution is an important phenomenon in stack gas desulfurization processes using limestone slurry to absorb SO_2 and produce $CaSO_3/CaSO_4$ waste solids (Rochelle and King, 1978). The rate of dissolution directly determines the need for excess limestone and interacts strongly with SO_2 removal and scale-free operation in the absorber. There is a need to know the dependence of dissolution rates on both solution composition and the type and grind of limestone. This report develops a mass transfer model and presents experimental results on the dissolution of reagent $CaCO_3$ (calcite) and naturally occurring limestones as a function of solution composition and limestone type and grind.

In the slurry scrubbing process, limestone dissolves at pH 4 to 6 and 55°C in both the absorber and the hold tank/crystallizer. Because of HCl accumulation from the flue gas, typical scrubbing solution contains 0.01 to 0.2 M $CaCl_2$. CO_2 partial pressure can vary from near zero with forced oxidation to one atmosphere with CO_2 evolution from the hold tank and is typically 0.1 atm in the absorber. Sulfite/bisulfite buffer can be present in concentrations up to 0.1 M. $CaSO_3$ and/or $CaSO_4$ crystallization must occur simultaneously with limestone dissolution. Buffer additives such as adipic acid should enhance both SO_2 removal and $CaCO_3$ dissolution at concentrations of 3 to 10 mM (Rochelle, 1977).

Additional details and summaries of this work are given in master's theses and papers on effects of solution composition (Chan, 1981; Chan and Rochelle, 1982) and on effects of type and grind (Toprac, 1981; Toprac and Rochelle, 1982).

SECTION 2

LITERATURE REVIEW

The most significant previous work on calcite dissolution has been done by geochemists in water or a seawater environment as reviewed by Plummer et al. (1979). Berner and Morse (1974) measured dissolution rates of reagent $CaCO_3$ using the pH-stat method. Plummer et al. (1978) studied dissolution of coarse Iceland spar using the free drift and pH-stat methods. These investigators both found a linear dependence of dissolution rate on H^+ concentration and P_{CO_2} and a constant forward rate in the near absence of H^+ and CO_2. Near equilibrium pH Plummer observed a reverse reaction rate proportional to the product of Ca^{++} and HCO_3^-.

Some previous investigators have modelled calcite dissolution as limited by diffusion of H^+ at pH less than 4 to 5 (Berner and Morse, 1974; Barton and Vatanatham, 1976). Plummer (1979) modeled by surface kinetics above pH 5.0. Other investigators have reported a dependence on agitation (Sjoberg, 1976; Erga and Terjesen, 1956; Ottmers et al., 1974).

The reported activation energy of calcite dissolution varies from 1.5 to 14 kcal/gmol (Plummer et al., 1978; Sjoberg, 1976; Barton and Vatanatham, 1976; Ottmers et al., 1974; Sjoberg, 1981). The trend of data gives low activation energy at pH 2 - 4 and high activation energy at pH 8 - 10.

Several investigators have studied inhibition of calcite dissolution near equilibrium pH by surface adsorption of insoluble salts. Berner and Morse (1974) showed inhibition by phosphate at 10^{-6} M. Terjesen et al. (1961) modelled the inhibiting effects of metal ions as an apparent reduction in the equilibrium pH. Koss and Moller (1974) studied the apparent equilibrium pH in the presence of Ni, Fe, Mg, and other metal ions. Sjoberg (1981) measured inhibition by phosphate and by Mg^{++}.

The previous investigators at seawater conditions have performed experiments with many sources of limestone over a wide range of particle size and

agitation. However, no investigator has covered a wide range of limestone particle size and source in a single apparatus. Plummer et al. (1979) reviewed this work and interpreted all the results as rate per unit surface area, implying that limestones differ from each other only in exposed surface area. He introduced no factors to account for the specific geological characteristics of the limestone samples.

Work by previous investigators under conditions typical of flue gas desulfurization has given apparent effects of particle size and limestone type. Drehmel (1972) found for samples of constant mesh size that marl was as much as five times more reactive than marble. He also found a strong effect of particle size in experiments with different screen fractions. Ottmers et al. (1974) found that the dissolution rate was inversely proportional to particle size. Recent work by Meserole et al. (1981) showed that screened limestones from three different sources gave the same dissolution rate at pH 5.8.

SECTION 3

THEORY

The rate of $CaCO_3$ dissolution can be calculated by mass transfer theory assuming that the solution is in equilibrium with calcite at the limestone surface. Both a general model and a simplified model have been developed to quantify effects of solution composition by the theory of mass transfer with chemical reaction. The effects of particle size and fluid mechanics have been quantified by assuming stagnant solution or by an empirical fit of data for turbulent mass transfer. Cumulative dissolution rates are obtained by summing over the particle size distribution of a limestone sample.

The extensive data on effects of solution composition obtained with reagent grade limestone were correlated by the simplified model assuming a stagnant solution. The model-predicted rates were increased by a factor of 1.88 to fit the experimental data. A factor of 1.25 is consistent with the effect of agitation. The balance of the adjustment (a factor of 1.5) may be due to non-spherical shape.

The data with fine and coarse grinds of limestone were correlated by the simplified model with an additional correlation of mass transfer coefficient as a function of particle size.

The effect of solution composition can be obtained by solution of steady-state mass transfer theory assuming instantaneous equilibria of all solution species except CO_2 and using a different diffusivity for each species. The general model accounts for the finite-rate, reversible reaction of CO_2 and H_2O to give H^+ and HCO_3^- by iterative, numerical integration of a second-order, nonlinear differential equation and a set of nonlinear algebraic equations. On the other hand, the simplified model assumes that the relative contribution of CO_2 is independent of particle size. It requires the iterative solution of a set of nonlinear algebraic equations. Because the CO_2 reaction is not important in most cases, the simplified model is usually accurate and is much easier to solve than the general model.

GENERAL MODEL/STAGNANT

The general mass transfer model calculates dissolution rate as function of bulk solution composition, particle diameter, and temperature. It assumes instantaneous equilibrium of the solution species H^+, H_2O, OH^-, $CaCO_3^\circ$, Ca^{++}, $CO_3^=$, HCO_3^-, $SO_3^=$, HSO_3^-, and a general buffer represented by the species H_2A, HA^-, and $A^=$. This assumption gives the following equilibria which apply throughout the mass transfer boundary layer (constants at 25°C):

$$K_{CaCO_3^\circ} = \frac{a_{Ca^{++}} a_{CO_3^=}}{a_{CaCO_3^\circ}} = 6.3 \times 10^{-4} \text{ M (Garrells and Thompson, 1962)} \quad (1)$$

$$K_{HCO_3^-} = \frac{a_{H^+} a_{CO_3^=}}{a_{HCO_3^-}} = 4.69 \times 10^{-11} \text{ M (Harned and Scholes, 1941)} \quad (2)$$

$$K_{HSO_3^-} = \frac{a_{H^+} a_{SO_3^=}}{a_{HSO_3^-}} = 6.24 \times 10^{-8} \text{ M (Tartar and Garretson, 1941)} \quad (3)$$

$$K_{H_2O} = a_{H^+} a_{OH^-} = 1.008 \times 10^{-14} \text{ M}^2 \quad (4)$$

At 55°C, K_{H_2O} was taken to be $7.26 \times 10^{-14} M^2$ and other constants were evaluated according to Lowell et al. (1970). Activities were calculated as the product of concentration and activity coefficient. Activity coefficients were estimated using an extended Debye-Huckel limiting law as implemented by Lowell et al. (1970).

Because it was inconvenient to include directly the ion pair species $CaSO_3^\circ$ and $CaOH^+$, these were lumped with $SO_3^=$ and OH^-, respectively. To account for the $CaSO_3$ ion pair, an effective $K'_{HSO_3^-}$ was defined as:

$$K'_{HSO_3^-} = K_{HSO_3^-} \left(1 + \frac{a_{Ca^{++}}}{K_{CaSO_3^\circ}}\right) \quad (5)$$

$$K_{CaSO_3^\circ} = \frac{a_{Ca^{++}} a_{SO_3}}{a_{CaSO_3^\circ}} = 4.0 \times 10^{-4} \text{ (Lowell et al., 1970)}$$

Similarly, to account for $CaOH^+$ ion pair, an effective K'_{H_2O} was defined as

$$K'_{H_2O} = K_{H_2O} \left(1 + \frac{a_{Ca^{++}}}{K_{CaOH^+}}\right) \tag{6}$$

$$K_{CaOH^+} = \frac{a_{Ca^{++}}\, a_{OH^-}}{a_{CaOH^+}} = 3.5 \times 10^{-2}\ M \quad \text{(Lowell et al., 1970)}$$

The general buffer equilibria were defined by the relations:

$$K_{H_2A} = \frac{a_{H^+}\, [HA^-]}{[H_2A]} \tag{7}$$

$$K_{HA^-} = \frac{a_{H^+}\, [A^=]}{[HA^-]} \tag{8}$$

where K_{H_2A} and K_{HA^-} are effective equilibrium constants which include activity coefficients for the buffer species. In 0.1 M CaCl, the K_{H_2A} and K_{HA^-} values were measured by Cavanaugh (1978) and are 1.05×10^{-4} M and 1.38×10^{-5} M for adipic acid and 7.94×10^{-4} M and 3.98×10^{-5} M for sulfosuccinic acid. For acetic and acrylic acids, K_{HA} was estimated to be 7.94×10^{-4} M and 3.98×10^{-5} M, respectively.

The general model assumes that dissolved CO_2 is in equilibrium with other species in the bulk solution, but that its concentration in the boundary layer is given by the finite-rate, reversible reaction:

$$CO_2 + H_2O \rightleftarrows H^+ + HCO_3^-$$

$$K_{CO_2} = \frac{a_{H^+}\, a_{HCO_3^-}}{a_{CO_2}} = 4.45 \times 10^{-7} M \quad \text{(Harned and Bonner, 1954)} \tag{9}$$

The net rate of this reaction is given by:

$$\frac{d[CO_2]}{dt} = k_{CO_2}\, [CO_2] \left(\frac{a_{H^+}\, a_{HCO_3^-}}{K_{CO_2}\, a_{CO_2}} - 1\right) \tag{10}$$

At infinite dilution, k_{CO_2} is 0.026 s^{-1} at 25°C and 0.27 s^{-1} at 55°C (Pinsent et al., 1956). The rate constant was assumed to be independent of ionic strength.

The differential material balance for total CO_2 species at steady state in spherical coordinates gives:

$$\frac{1}{r^2}\left[D_{CO_2}\frac{\partial}{\partial r}\left(r^2\frac{\partial[CO_2]}{\partial r}\right)+D_{HCO_3^-}\frac{\partial}{\partial r}\left(r^2\frac{\partial[HCO_3^-]}{\partial r}\right)+\right.$$

$$\left.D_{CaCO_3^\circ}\frac{\partial}{\partial r}\left(r^2\frac{\partial[CaCO_3^\circ]}{\partial r}\right)+D_{CO_3^=}\frac{\partial}{\partial r}\left(\frac{\partial[CO_3^=]}{\partial r}\right)\right]=0 \qquad (11)$$

Substituting x = (1-d/2r) where d is the particle diameter and r the distance from the center of the sphere, equation (11) reduces to:

$$D_{CO_2}\frac{\partial^2[CO_2]}{\partial x^2}+D_{HCO_3^-}\frac{\partial^2[HCO_3^-]}{\partial x^2}+D_{CaCO_3^\circ}\frac{\partial^2[CaCO_3^\circ]}{\partial x^2}+$$

$$D_{CO_3^=}\frac{\partial^2[CO_3^=]}{\partial x^2}=0 \qquad (12)$$

Integrating Eq. (12) with respect to x gives:

$$D_{CO_2}[CO_2]+D_{HCO_3^-}[HCO_3^-]+D_{CaCO_3^\circ}[CaCO_3^\circ]+$$

$$D_{CO_3^=}[CO_3^=]=\alpha_1+\beta_1 x \qquad (13)$$

where α_1 (M cm^2 sec^{-1}) and β_1 (M cm^2 sec^{-1}) are constants of integration.

Similarly, other steady-state balances give for Ca^{++} species:

$$D_{Ca^{++}}[Ca^{++}]+D_{CaCO_3^\circ}[CaCO_3^\circ]=\alpha_2+\beta_2 x \qquad (14)$$

For charge balance:

$$D_{H^+}[H^+] + 2D_{Ca^{++}}[Ca^{++}] - D_{HCO_3^-}[HCO_3^-] - 2D_{CO_3^=}[CO_3^=]$$

$$- D_{HA^-}[HA^-] - 2D_{A^=}[A^=] - D_{HSO_3^-}[HSO_3^-] - 2D_{SO_3^=}[SO_3^=]$$

$$- D_{OH^-}[OH^-] = \alpha_3 + \beta_3 x \qquad (15)$$

For H_2A species:

$$D_{H_2A}[H_2A] + D_{HA^-}[HA^-] + D_{A^=}[A^=] = \alpha_4 + \beta_4 x \qquad (16)$$

For sulfite species:

$$D_{HSO_3^-}[HSO_3^-] + D_{SO_3^=}[SO_3^=] = \alpha_5 + \beta_5 x \qquad (17)$$

By reaction stoichiometery, the flux of calcium from the limestone surface must be equal to the flux of total CO_2:

$$\frac{\partial}{\partial x}\left(D_{Ca^{++}}[Ca^{++}] + D_{CaCO_3^\circ}[CaCO_3^\circ]\right) = \frac{\partial}{\partial x}\left(D_{CO_2}[CO_2] + \right.$$

$$\left. D_{HCO_3^-}[HCO_3^-] + D_{CaCO_3^\circ}[CaCO_3^\circ] + D_{CO_3^=}[CO_3^=]\right) \qquad (18)$$

Therefore $\beta_1 = \beta_2 = \beta$. Since the net fluxes of H_2A species, sulfite species, and charged species are zero, β_3, β_4, and β_5 are zero. If β is known, the constants α_1, α_2, α_3, α_4, and α_5 can be obtained from the compositions of the bulk solution (at x = 1.0).

The finite-rate CO_2 reaction (Eq. (10)) gives the following differential material balance for the CO_2 species alone:

$$(1-x)^4 D_{CO_2} \frac{4}{d^2} \frac{\partial^2[CO_2]}{\partial x^2} = k_{CO_2}[CO_2]\left(1 - \frac{a_{H^+} a_{HCO_3^-}}{K_{CO_2} a_{CO_2}}\right) \qquad (19)$$

This equation is integrated numerically with a trial-and-error solution for the boundary conditions. A trial value of β is selected and the constants α_1, α_2, α_3, α_4, and α_5 are calculated from the bulk composition. At each step in the numerical integration, the algebraic equations representing equilibria (1, 2, 3, 4, 7, 8) and other differential material balances (13, 14, 15, 16, 17) are solved by trial and error to give a_{H^+} and a $_{HCO_3^-}$.

To initiate the numerical integration, the solution was assumed to be in equilibrium with calcite at the solid surface (x = 0) giving:

$$[CaCO_3^\circ] = 6.8 \times 10^{-6} \text{ M} \quad \text{(Lowell et al., 1970)}$$

The CO_2 concentration at the surface was calculated from the equilibria and material balances. Since no reaction of CO_2 can occur in the infinitesimal volume element at the solid surface, $d[CO_2]/dx$ was taken to be zero at x = 0.0. Eq. (19) was then integrated by the Simpson-Kutta method (Nielson, 1964) from x = 0 to x = 0.85. A cubic fit of $[CO_2]$ from x = 0.7 to x = 0.85 was used to extrapolate to x = 1.0. This extrapolation is expected to add little error since $[CO_2]$ varies little over this range. If the calculated value of $[CO_2]$ at x = 1.0 was equal to the specified solution composition, then the selected value of β was correct. Otherwise, a new value of β was selected and the integration was repeated.

The finite rate, reversible CO_2 reaction (Eq. (1)) enhances limestone dissolution with high P_{CO_2} at pH 5 by the stoichiometry:

$$CaCO_3 + CO_2 + H_2O \rightarrow Ca^{++} + 2HCO_3^-$$

At pH 4, the CO_2 reaction occurs in reverse and consumes H^+, thereby inhibiting $CaCO_3$ dissolution by requiring two H^+ rather than one:

$$CaCO_3 + 2H^+ \rightarrow Ca^{++} + CO_2 + H_2O$$

The rate of the CO_2 reaction is greater with high P_{CO_2} (CO_2 sparging) and negligible with N_2 sparging. The contribution of the CO_2 reaction to the dissolution rate varies with the volume of the mass transfer boundary layer, which typically varies directly with the surface area of the particle.

SIMPLIFIED MODEL/STAGNANT

The dissolution rate of a single particle of volume V is given by:

$$\frac{dV}{dt} = \frac{-2x10^{-3}\ \beta\pi d^2}{d\ \rho_m} \tag{20}$$

where ρ_m is the molar density of calcite (0.0271 gmol/cm^3). Particle size (d) and volume (V) are related and ρ_m is a constant. If we assume that the contribution of the CO_2 reaction to β is independent of particle size, then β is also a constant. Therefore, Eq. (20) can be integrated to give the fraction $CaCO_3$ remaining (f) as a function of time:

$$f = \frac{V}{V_i} = (1 - \frac{8x10^{-3}\beta\ t}{\rho_m d_i^2})^{3/2} \tag{21}$$

The rate constant k (cm^2/sec) is defined:

$$k = 1.88 \times 8 \times 10^{-3}\ \beta/\rho_m \tag{22}$$

The factor 1.88 is a constant which has been adjusted to account for deviation of experimental results from the unadjusted model. Values of β and k are obtained from the general mass transfer model as a function of solution composition and temperature at a particle diameter of 10 μm. Use of k gives:

$$f = (1 - \frac{kt}{d_i^2})^{1.5} \tag{23}$$

With a polydisperse size distribution, the total fraction remaining, F, can be determined by summing over the differential size distribution ϕ_j where ϕ_j is the fraction of total particle volume with initial diameters from d_j to d_{j+1}:

$$F = \sum_{j=1}^{n} \phi_j \cdot f_j = \sum_{j=1}^{n} \phi_j\ (1 - \frac{kt}{d_j d_{j+1}})^{1.5} \tag{24}$$

$f_j = 0$ when $kt > d_j d_{j+1}$

If a batch experiment gives the fraction remaining, F, as a function of time at constant composition, the rate constant, k, can be calculated from the experimental data and the mass transfer model. Two experimental data points (F_1,t_1) and (F_2,t_2) can be combined with two calculated data points at F_1 and F_2 with $[F_1,(kt)_1]$ and $[F_2,(kt)_2]$ to get the rate constant k_{exp}:

$$k_{exp} = \frac{(kt)_2 - (kt)_1}{t_2 - t_1} \tag{25}$$

This simplified model assumes that the contribution of the CO_2 reaction to the dissolution rate is independent of particle size. Since this assumption is not strictly true, the simplified model will be accurate when the CO_2 reaction contributes little to the overall rate. This condition applies to particles less than 20 μm, to systems with P_{CO_2} less than 0.2 atm, or to systems with high buffer concentrations.

SIMPLIFIED MODEL/TURBULENT

Limestone dissolution rate is given by the steady-state mass transfer expression:

$$\frac{dV_p}{dt} = \frac{-\pi d_p^2 k_L \Delta C}{\rho_m} \tag{26}$$

The mass transfer coefficient, k_L, is given by a Sherwood number $(k_L d_p/D)$ of 2 for very small particles or stagnant solution.

Levins and Glastonbury (1972) reviewed mass transfer coefficients for particles suspended in agitated vessels and found that k_L for larger particles is generally independent of particle diameter and depends weakly on agitation intensity. The combination of the stagnant result with a typical correlation of k_L for agitated conditions by Calderbank and Moo-Young (1961) gives the dissolution rate as:

$$\frac{dV_p}{dt} = -\frac{\pi \Delta C}{\rho_m}\left[2\,D d_p + 0.13\left(\frac{\varepsilon\nu}{\rho_c}\right)^{1/4}\left(\frac{D}{\nu}\right)^{2/3} d_p^{\,2}\right] \tag{27}$$

This is similar to correlations proposed by Levins and Glastonbury (1972) and Harriott (1962).

Eq. 27 may be rewritten as

$$\frac{dV_p}{dt} = -KV_p^{1/3} - KBV_p^{2/3} \tag{28}$$

The constant K(cm^2/sec) is available from the simplified solution composition model and is equal to 0.8 k (Eq. (22)). B (cm^{-1}) gives the enhancement of mass transfer due to agitation:

$$B = \frac{0.0807}{D} \left(\frac{\varepsilon\nu}{\rho^2}\right)^{1/4} \left(\frac{D}{\nu}\right)^{2/3} \tag{29}$$

For large particles the $-KBV_p^{2/3}$ term dominates the dissolution rate. Because the contribution of the CO_2 reaction also varies with $V_p^{2/3}$, the empirical value of B reflects not only the effects of turbulence but also inhibition or enhancement by the CO_2 reaction. For small particles, the $-KV_p^{1/3}$ term, which is independent of P_{CO_2}, dominates dissolution rate. Therefore, the CO_2 reaction will have a negligible effect on the dissolution rate of very small particles but a significant effect on the dissolution rate of large particles.

For a given size fraction j of particles with initial average volume V_j, the dissolution rate expression (Eq. (28)) may be written as:

$$\frac{df_j}{dt} = \frac{-Kf_j^{1/3}}{V_j^{2/3}} - \frac{KBf_j^{2/3}}{V_j^{1/3}} \tag{30}$$

where f_j is V_p/V_j, the fraction of undissolved $CaCO_3$. Eq. (30) may be integrated in closed form to yield f_j as a nonlinear implicit function of t given by

$$t = \frac{3}{KB^2}\left[\ln\left(\frac{1+BV_j^{1/3}f_j^{1/3}}{1+BV_j^{1/3}}\right) + BV_j^{1/3}(1-f_j)\right] \tag{31}$$

The total fraction undissolved $CaCO_3$ in a batch vessel is given by

$$F_b = \sum_{j=1}^{n} \phi_j f_j$$

where ϕ_j is the weight fraction of initial particles of volume V_j.

The simplified model applied to turbulent systems includes an empirical correction for the enhancement of mass transfer by agitation. The effect of the CO_2 reaction can be partially accounted for by adjusting the constant B. The simplification permits efficient summation of the dissolution rate over a particle size distribution.

STIRRED TANK (CSTR) MODEL

Because the scrubber system has a large circulation rate relative to the feed rate of limestone slurry, it can be treated as a continuously stirred tank reactor (CSTR). The probability that a limestone particle will leave the system in dt about t is given by:

$$P(t)dt = \frac{1}{\tau} e^{-t/\tau} dt \qquad (33)$$

The average residence time τ is the total molar Ca inventory in the system divided by the molar limestone feed rate.

The total fraction of undissolved $CaCO_3$ (F_c) can be obtained by integrating over all possible times for each size fraction and by summing over all size fractions.

$$F_c = \sum_{j=1}^{30} \phi_j \quad \frac{1}{\tau} \int_0^{\infty} e^{-t/\tau} f_j dt \qquad (34)$$

The variable f_j is an implicit function of t given by Eq. (31).

Eq. (34) can be simplified by transforming from an integration over t to an integration over f_j:

$$F_c = \sum_{j=1}^{n} \phi_j \frac{1}{\tau} \int_1^{0} f_j \frac{\exp(-t/\tau)}{(df_j/dt)} df_j \qquad (35)$$

In this numerical integration, t is a function of f_j given by Eq. (31). The integral over f_j was evaluated in this work by direct numerical integration with an f_j step size of 0.01. This step size gave good values of F_c for F_c less than 0.7.

For a given limestone, F_c can be determined as a general function of $K\tau$. The stoichiometric ratio, SR, is given by $1/(1-F_c)$. If two different limestones give the same SO_2 removal, the solution composition must be the same, so K must be constant. However, for constant hold tank volume and a constant concentration of calcium solids (moles Ca/liter solution), the residence time, τ, will be inversely proportional to the stoichiometric ratio. Therefore, the quantity $K\tau \cdot SR$ should be constant at a given SO_2 removal. The reciprocal of this quantity, $(K\tau \cdot SR)^{-1}$, is defined here as the relative reactivity. SO_2 removal should increase with increasing relative reactivity.

DIFFUSIVITIES

Values of diffusivities used in the general model are given in Table 1. Diffusivities for ions are taken to be those in absence of a potential gradient, since there is usually a large excess of $CaCl_2$ to disperse any potential gradient. At 25°C and infinite dilution, ionic diffusivities are given by:

$$D = \frac{RT\lambda_o}{n_j (Fa)^2} \tag{36}$$

where Fa is the Faraday number, n_j is the charge on the jth ion, and λ_o is the equivalent ionic conductivity.

Diffusivities at 55°C were estimated by the Stokes-Einstein relationship:

$$D_{55°C} = D_{25°C} \left(\frac{328°K}{298°K}\right) \frac{\eta_{25°C}}{\eta_{55°C}} \tag{37}$$

where η is the absolute viscosity of water. For the basic and monohydrogen species of sulfosuccinic acid, the diffusivities were reduced by 45% and 25%, respectively, to account for Ca^{++} interaction (Weems, 1981).

Table 1: Diffusivities at 25°C

Species	D $\times_2 10^{+5}$ (cm^2/sec)	Reference
CO_2	2.00	Sherwood et al., 1975
HCO_3^-	1.20	Landolt-Bornstein, 1960
$CO_3^=$	0.70	"
Ca^{++}	0.79	"
H^+	9.30	"
$CaCO_3^o$	0.75	estimated
$SO_3^=$	0.70	Landolt-Bornstein, 1960
HSO_3^-	1.33	"
OH^-	5.27	"
$Adipate^=$	0.705	Jeffrey and Vogel, 1935
$Hadipate^-$	0.71	estimated
Adipic acid	0.736	Albery et al., 1967
Acetate	1.09	Landolt-Bornstein, 1960
Acetic acid	1.19	Lewis, 1955
$Sulfosuccinate^{-3}$	0.73	Albery et al., 1967
$H_2sulfosuccinate^=$	0.53	Weems, 1981
$H_2sulfosuccinate^-$	0.41	Weems, 1981

SECTION 4

EXPERIMENTAL APPARATUS AND PROCEDURE

Rates were measured in a pH-stat with batch dissolution of $CaCO_3$ at constant pH and solution composition (Morse, 1974). The pH was automatically controlled within ± 0.02 units by titration with 0.2 M HCl with the stoichiometry:

$$CaCO_3(s) + 2HCl \rightleftarrows CaCl_2 + H_2O + CO_2\ (g)$$

Either CO_2 or N_2 were sparged at 1750 cm^3/min into the solution to maintain a constant P_{CO_2} and HCO_3^- concentration. The relative change in calcium concentration was usually minimized by dissolving 5 mM $CaCO_3$ into solution with 0.1 M dissolved $CaCl_2$. The cumulative dissolution was determined directly from a recording of HCl volume added versus time.

The dissolution reactor is shown in figure 1. It was agitated by a marine propeller (3 blades, square pitch, 2.5 cm radius) to fluidize fully the sample. Most experiments with reagent $CaCO_3$ were performed at 720 rpm. Experiments for type and grind effects were performed at 1500 rpm.

The pH-stat apparatus is shown in Figure 2. For runs at 55°C, the reactor temperature was controlled at $\pm$ 2°C by a water bath. The CO_2 or N_2 gas was presaturated at reactor temperature. The pH (combination, Ag/AgCl) electrode was calibrated at reactor temperature in pH 4 phthalate and pH 7 phosphate buffers.

The reactor held one liter of 0.1 M $CaCl_2$ solution. Buffers were added in nominal concentrations as needed. The pH was adjusted to the desired value by adding HCl or NaOH. The experiment was initiated by addition of 0.5 g limestone. In runs with sulfite the reactor solution was analyzed by iodimetric titration before and after the experiment.

Reagent $CaCO_3$ (precipitated calcite) was obtained from Fisher. Ground samples of natural limestones were provided by the U. S. EPA

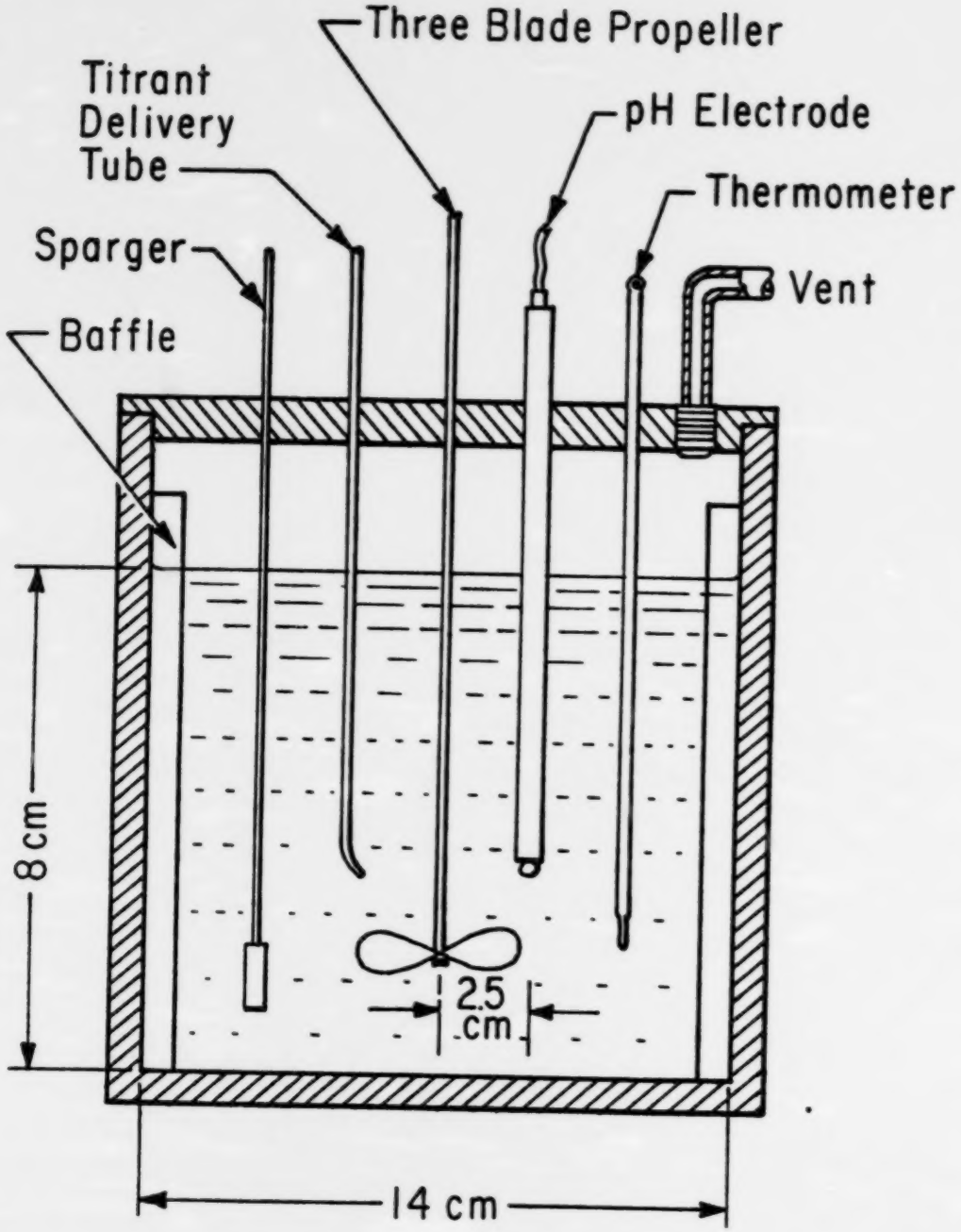

Figure 1. Dissolution Reactor

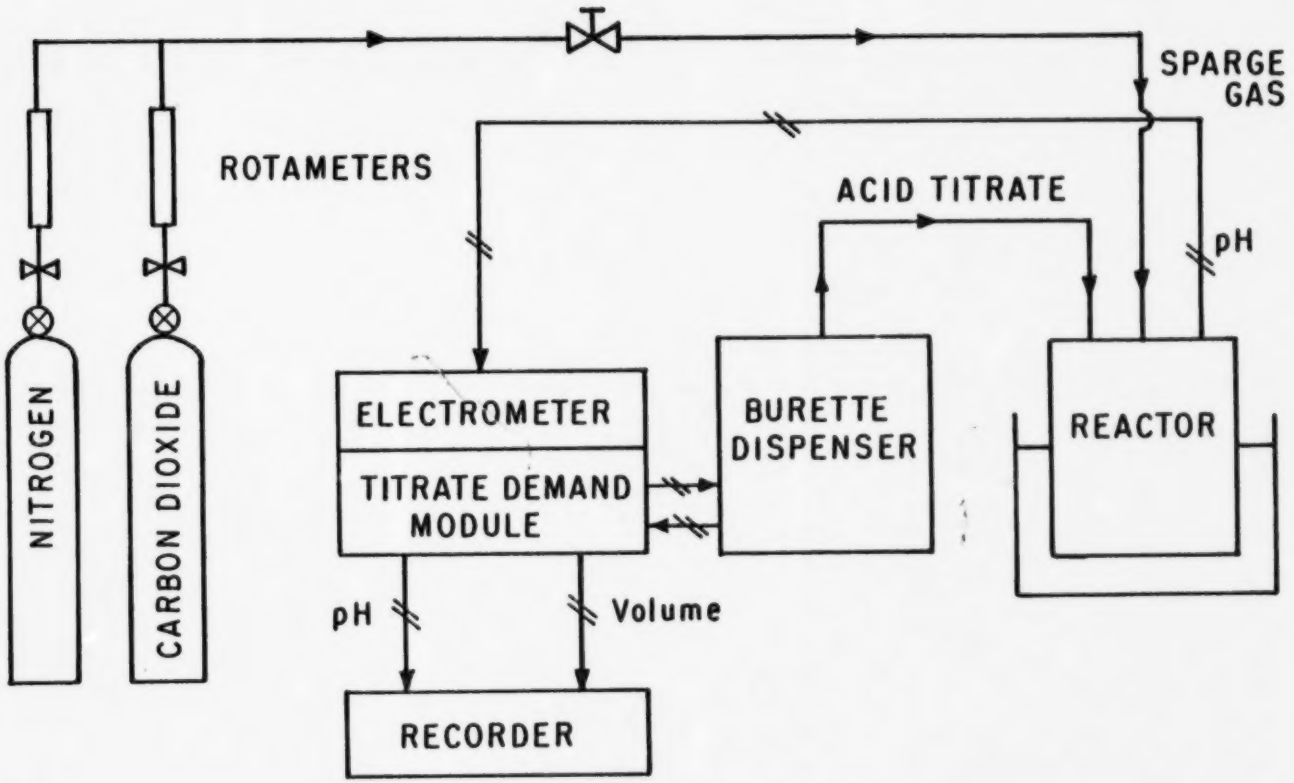

Figure 2. pH-Stat Apparatus

(R. H. Borgwardt), Radian Corp. (F. Meserole), and M. W. Kellogg (R. Cares). The EPA limestones were taken from batches of ground stones used in pilot plant scrubber studies at Research Triangle Park (Chang et al., 1981). The samples provided by Radian were used in their investigations of the effect of solid Mg on limestone reactivity under contract to the Electric Power Research Institute.

Screen size distributions and chemical compositions were provided by the sample suppliers. Composition was given as percent $CaCO_3$, dolomite, solid solution $MgCO_3$, and acid insolubles. The Radian studies have shown dolomite dissolution to be a factor of three to four times slower than calcite dissolution (Meserole, 1982). The percent available for dissolution in a given sample was taken to be the sum of $CaCO_3$ and solid solution $MgCO_3$ content.

A Model TAII Coulter Counter was used to determine size distributions from 0.7 to 160 μm by overlapping distributions obtained with 30, 100 and 400 μm apertures. Wet screening of the sample was necessary for each successively smaller aperture. Dissolution during sizing was minimized by using 0.18 M $CaCl_2$ as electrolyte. Wet screen data provided with the EPA limestones were used to extend size distributions above 160 μm. Particle size distributions for all of the limestones are given in Appendix A.

Typical results of the two experiments with reagent $CaCO_3$ are given in Figure 3. The total fraction remaining, F, calculated from the volume of HCl added is given as a function of dimensionless time, t/t_{50}, where t_{50} is the time required to dissolve 50% of the $CaCO_3$. Calculated curves are also given using the simplified mass transfer model (stagnant) with a single particle size (monodisperse) and with the actual polydisperse size distribution (Appendix A). The polydisperse model fits the shape of the curve very well at all times. The monodisperse model is only satisfactory for t/t_{50} less than 1.

In experiments with Reagent $CaCO_3$, the experimental rate constant, k, was determined by using Eq. (25) with the calculated and measured values of F at kt_{50} and kt_{44}. For the run at pH 5, t_{50} = 11.3 min. From Figure 3:

$$t_{50} - t_{44} = \left(1.0 - \frac{t_{44}}{t_{50}}\right) 11.3 \text{ min} = 96.8 \text{ sec}$$

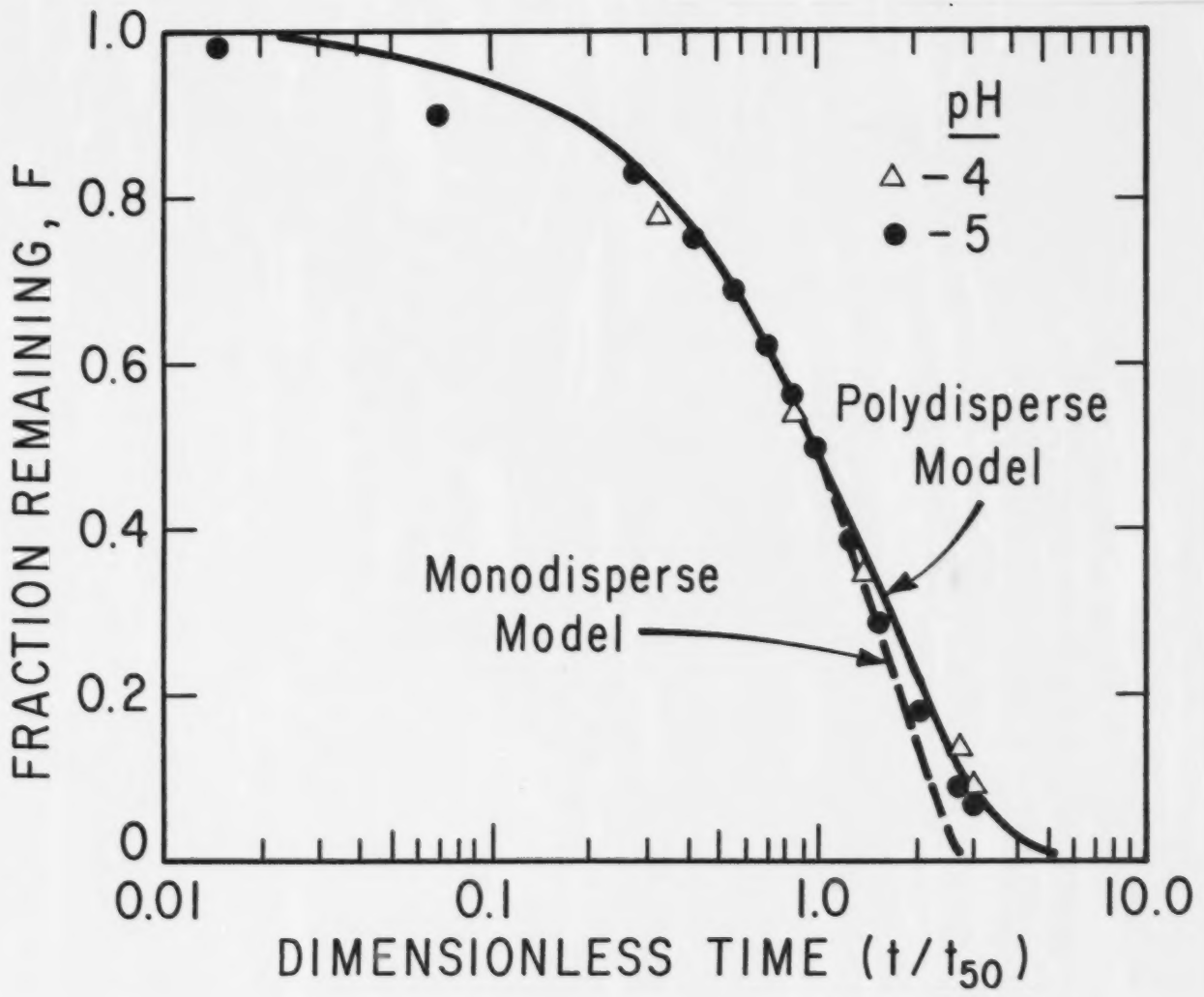

Figure 3. Dissolution Curves for Reagent Grade $CaCO_3$ at 25°C with N_2 Sparging

From the polydisperse model:

$$kt_{50} - kt_{44} = 6.14 \times 10^{-8} cm^2$$

Therefore, $k = 6.34 \times 10^{-10} cm^2/sec$.

In the work on effects of type and grind, the dissolution rate of a given limestone as determined by the pH-stat apparatus was compared to the results of the model by the respective time taken to dissolve fifty and eighty percent of the sample (t_{50} and t_{80}). The shape of the fraction remaining versus time curve generated by the model can be compared to the experimental results independently of the accuracy of the t_{50} prediction by plotting fraction remaining versus normalized time (t/t_{50}).

SECTION 5

RESULTS

There are three sets of results:

1) A large number of experiments were performed with Reagent $CaCO_3$ in 0.1 M $CaCl_2$ over a wide range of solution compositions at 25 and 55°C. These measured rates have been compared with rates calculated by the general stagnant model.
2) Experiments in 0.1 M $CaCl_2$ at pH 4.0 or 5.0 with sparging by N_2 or CO_2 were performed with 9 sources of limestone and 19 total different grinds. These experiments were correlated by the simplified turbulent model to obtain an empirical value of the mass transfer parameter, B.
3) Additional experiments were performed at conditions that were outside the scope of the presently available models. These include experiments on effects of electrolytes other than 0.1 M $CaCl_2$, effects of metal ion inhibitors, and effects of sulfite and temperature with coarse limestones.

EFFECT OF SOLUTION COMPOSITION

The measured rate constants, k, for dissolution of Reagent $CaCO_3$ in 0.1 M $CaCl_2$ are presented in Figures 4 through 10 over the ranges of pH 4.0 to 7.0, 0.0 to 1.0 atm CO_2, 25 to 55°C, 0 to 10 mM buffer additives, and 0 to 28 mM total sulfite.

The curves given in Figures 4 through 10 were calculated by the general mass transfer model with a 10 μm particle diameter and an empirical factor of 1.88. The mass transfer model accurately predicts the effects of all variables except for inhibition by selected organic acids. There is no evidence of any effect of surface kinetics, even at moderate and high values of pH. If surface kinetics were important the measured rate would be less than that predicted by the unadjusted model. However, the measured rate is 1.88 times greater than the unadjusted model. Therefore, it is highly probable that the

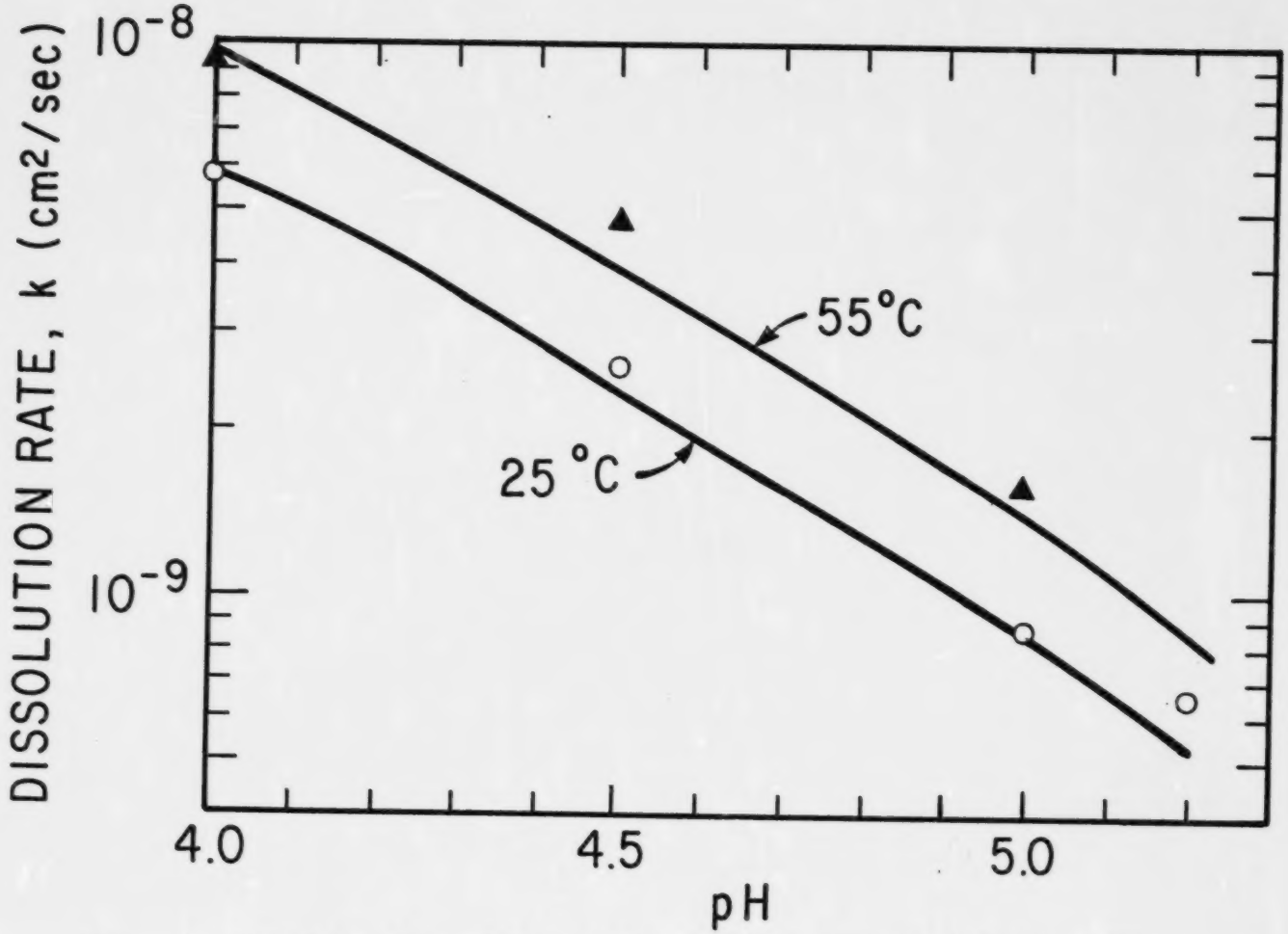

Figure 4. Dissolution Rate of Reagent $CaCO_3$ with CO_2 Sparging in 0.1 M $CaCl_2$

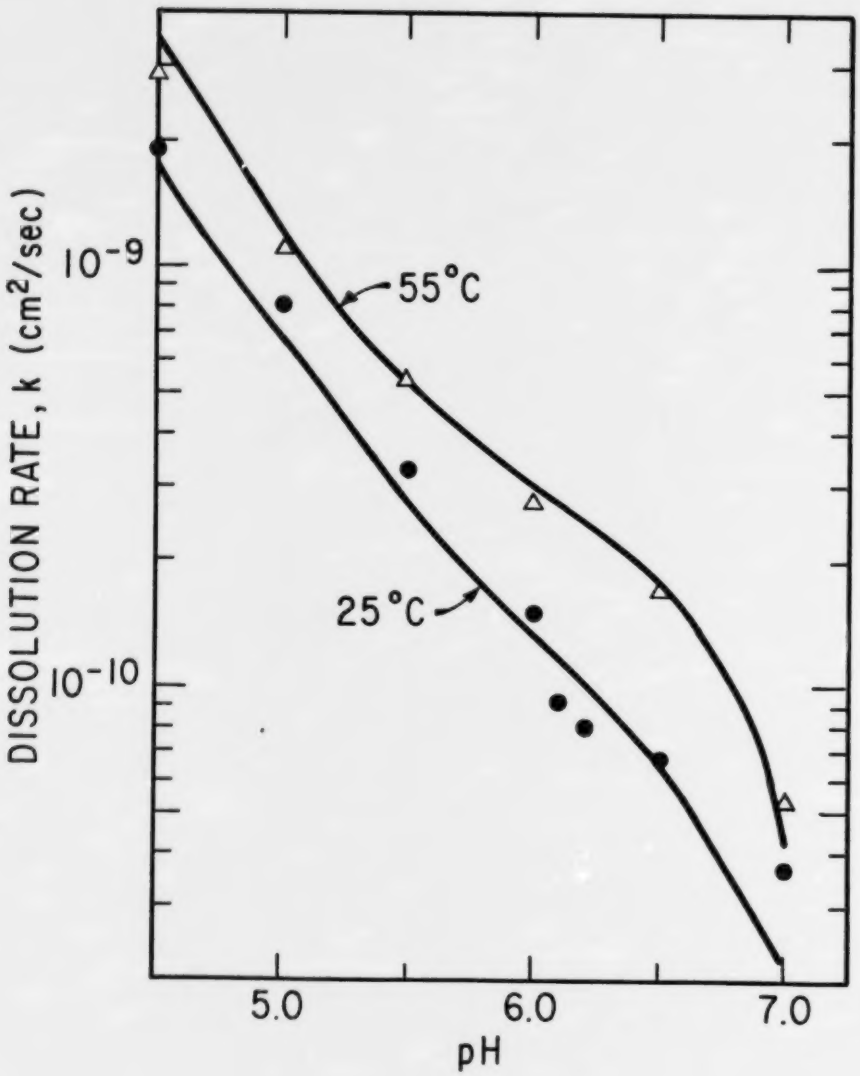

Figure 5. Dissolution Rate of Reagent Grade $CaCO_3$ with N_2 Sparging in 0.1 M $CaCl_2$

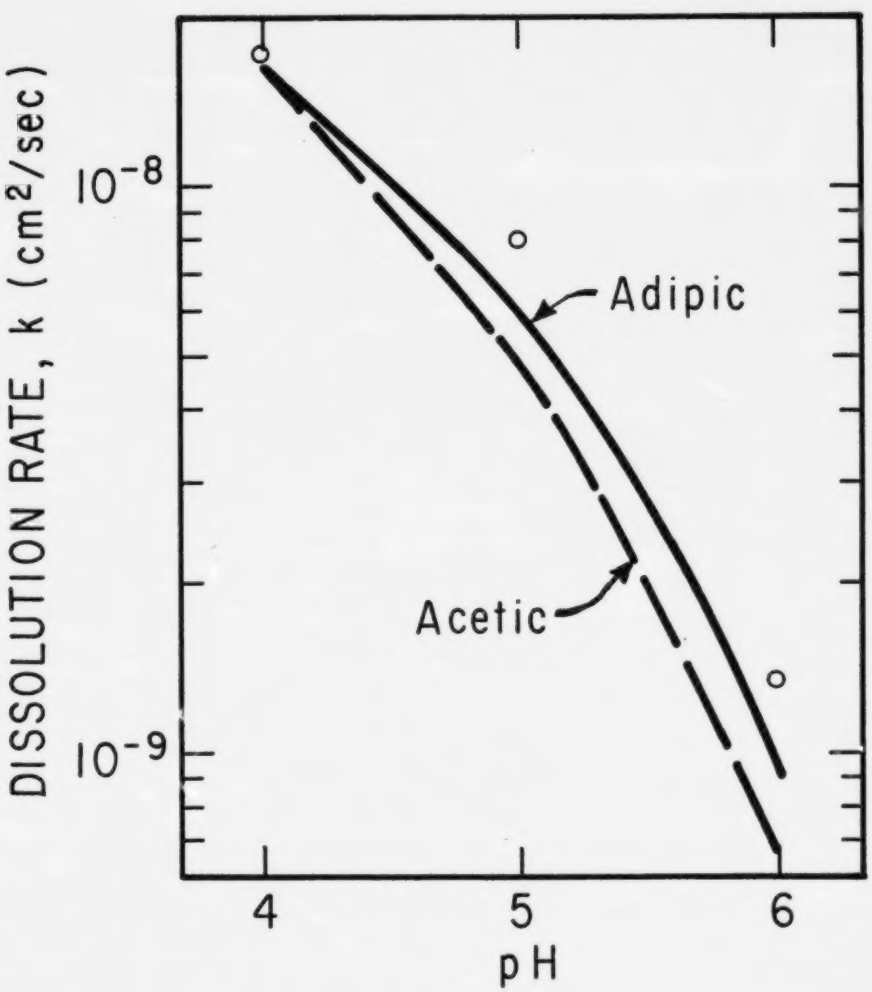

Figure 7. Dissolution Rate of $CaCO_3$ in 0.1 M $CaCl_2$ with N_2 Sparging at 25°C, and 3 mM Adipic or Acetic Acid.

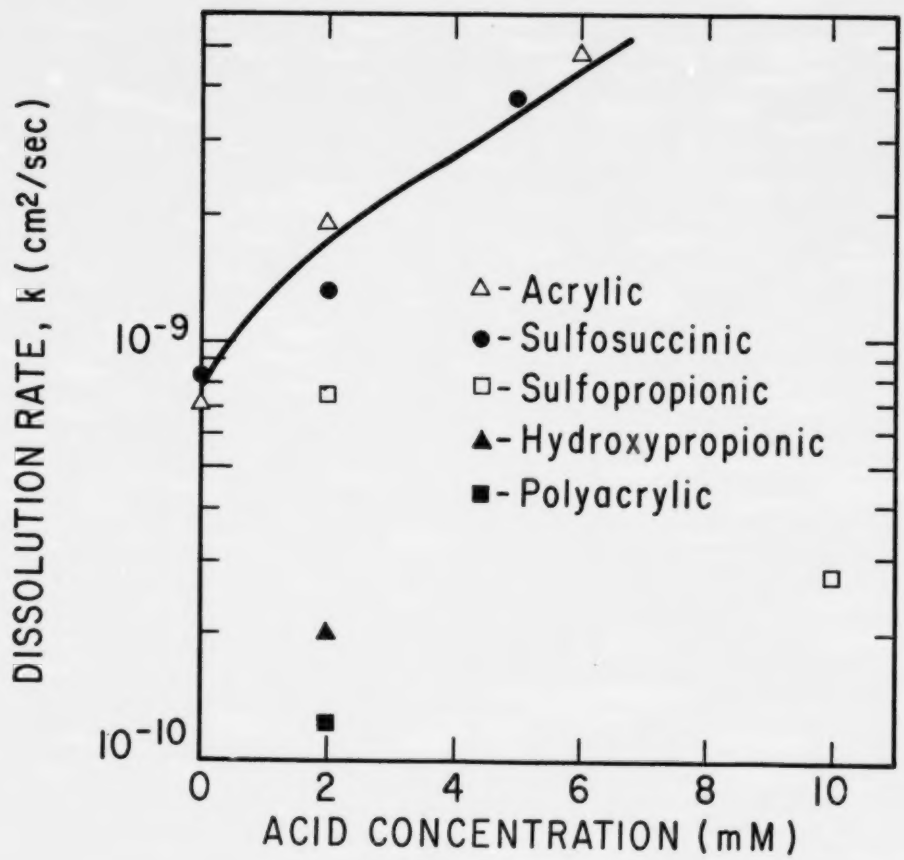

Figure 8. Effect of Organic Acids on Dissolution Rate in 0.1 M $CaCl_2$ with N_2 Sparging, 25°C and pH 5

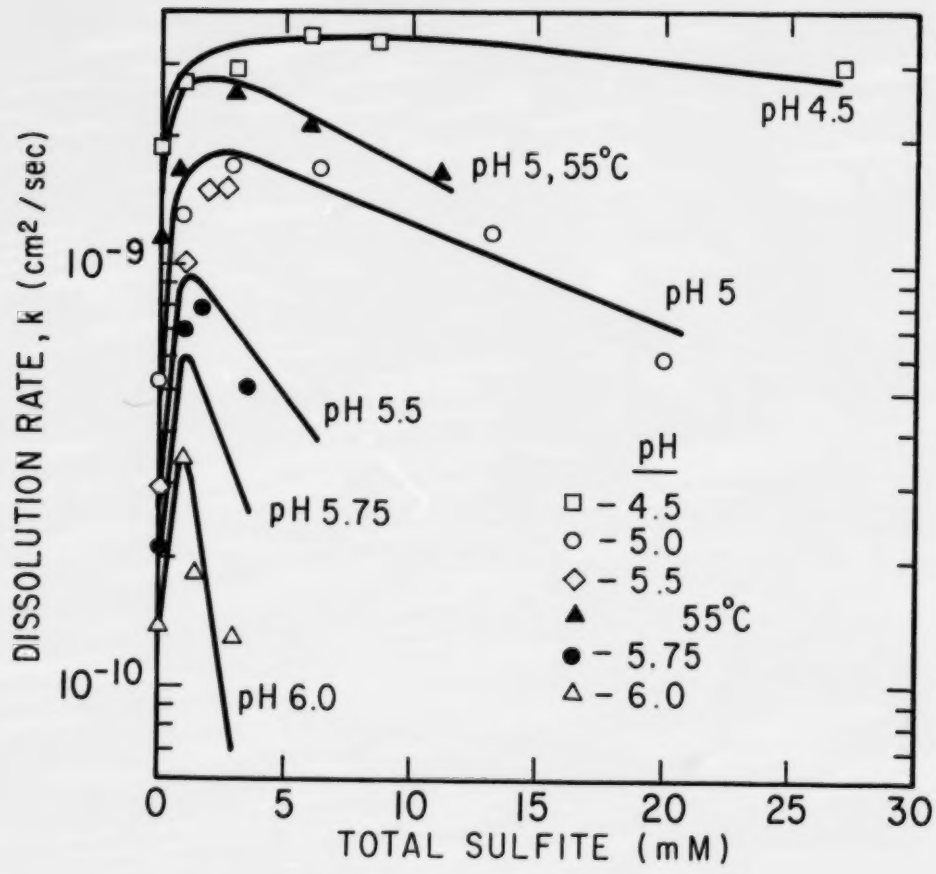

Figure 9. Effect of Sulfite on the Dissolution Rate of Reagent $CaCO_3$ at 25°C with N_2 Sparging, Curves calculated by the Mass Transfer Model Using the Equilibrium given by Figure 11.

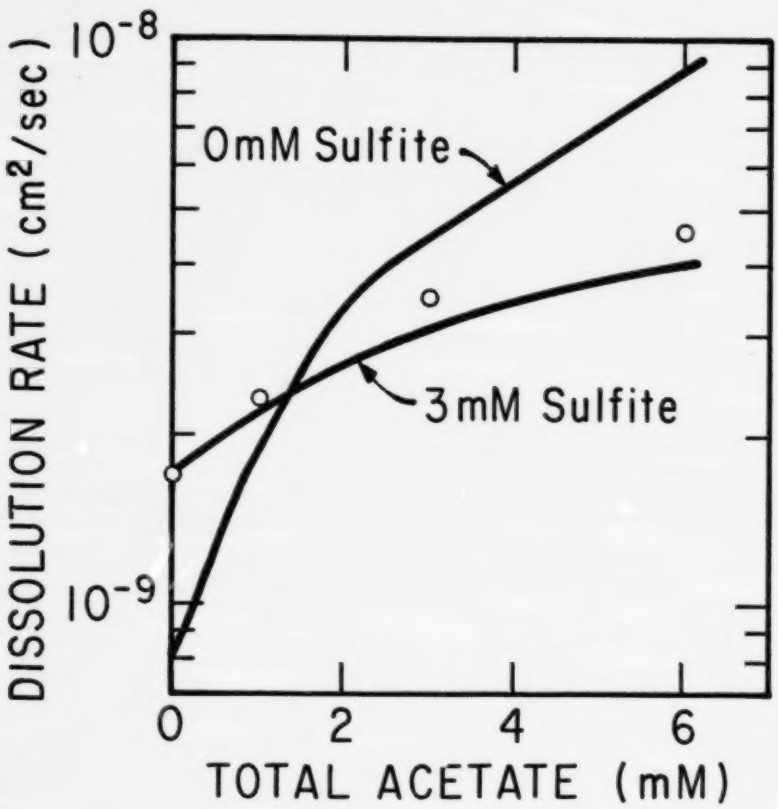

Figure 10. Effect of Acetate on Dissolution Rate with 3 mM Total Sulfite, pH 5 and 25°C

distinguishing characteristic of natural, ground limestones will be their particle size distribution. Limestone reactivity should be independent of internal surface area, grain size, and other such variables.

Effect of pH

Figures 4 and 5 show that dissolution rate is a strong function of pH. With CO_2 sparging at 25°C the dissolution rate decreases by a factor at 6.7 from pH 4.0 to pH 5.0. At these conditions the dissolution rate is controlled primarily by H^+ diffusion from the bulk solution with a stoichiometry given approximately by:

$$CaCO_3 + H^+ \rightleftarrows Ca^{++} + HCO_3^-$$

The adjusted model gives 0.36 cm/sec as the mass transfer coefficient of H^+ with a 10 μm particle. This compares with 0.05 cm/sec measured by Plummer et al (1979) with much larger particles.

Effect of CO_2

Figures 4 and 5 show that high CO_2 partial pressure generally enhances the dissolution rate by about 15 percent except close to equilibrium. Berner and Morse (1974) observed a similar effect with precipitated $CaCO_3$. At pH 4.5 to 5.0, CO_2 enhances the dissolution rate by diffusion from the bulk solution with the following net finite-rate reaction and stoichiometry:

$$CaCO_3 + CO_2 + H_2O \rightleftarrows Ca^{++} + 2HCO_3^-$$

At pH less than 4 to 4.5, the finite-rate CO_2 reaction produces CO_2 in the boundary layer and requires somewhat higher H^+ stoichiometry as follows:

$$CaCO_3 + 2H^+ \rightleftarrows Ca^{++} + CO_2 + H_2O$$

At pH 5.0, Plummer et al (1979) found that 1 atm CO_2 increased the dissolution rate of coarse Iceland spar by a factor of five. The participation of CO_2 is limited by a homogeneous reaction in the mass transfer boundary layer. The volume of the boundary layer increases faster than the surface area as the particle size increases. Therefore, a much larger effect is expected with corase particles.

With CO_2 sparging the calculated equilibrium pH in 0.1 M $CaCl_2$ is 5.6 at 25°C and 5.4 at 55°C. Therefore, CO_2 sparging inhibits dissolution above about pH 5.2.

Effect of Temperature

At pH 5.0 or less, Figures 4 and 5 show that the dissolution rate increases by a factor of 1.6 to 1.8 from 25 to 55°C. This gives an activation energy of about 4 kcal/gmol, corresponding to the effect of temperature on diffusivities.

Above pH 6.0, $CaCO_3$ dissolution is controlled mostly by diffusion of OH^- and HCO_3^- from the limestone surface. The driving force for this diffusion is determined to a large extent by the equilibrium:

$$CaCO_3 + H_2O \rightleftarrows Ca^{++} + HCO_3^- + OH^-$$

This equilibrium changes significantly with temperature. Therefore, at pH 6 to 6.5 with N_2 sparging, the rate increases by a factor of 3 from 25°C to 55°C, giving an activation energy of about 7 kcal/gmol. Other investigators have attributed this higher temperature dependence to surface kinetics, but these results showed that it arises from an effect of temperature on diffusivities and solution equilibria.

Effect of Organic Acids

Figures 6, 7, and 8 demonstrate the effect of organic acids on the dissolution rate at 25°C. Additives that provide buffer capacity between the bulk solution pH (4.0 to 5.5) and the pH at the limestone surface (5.5 to 8.0) enhance dissolution rate by providing an additional means of diffusing acidity to the limestone surface. Figure 6 shows that at pH 5.0, 3 mM total acetic acid enhances the dissolution rate a factor of 7. This enhancement is somewhat greater at higher pH, where H^+ diffusion is much more limited.

At pH 5, the effect of CO_2 is insignificant in the presence of acetic acid. With CO_2 sparging at pH 5.5, very near the equilibrium pH of 5.6, the calculated rates with acetic acid (Figure 6) are 2-3 times greater than the measured rates. This discrepancy may result from experimental pH error, or from error in accurately estimating the equilibrium pH.

Figure 7 shows that adipic acid is 20 to 50 percent more effective than acetic acid. Figure 8 shows that acrylic and sulfosuccinic acids are about

equivalent. However, hydroxypropionic, sulfopropionic, and polyacrylic acids inhibit limestone dissolution, probably by surface adsorption of polyacrylic acid. Sulfopropionic acid was synthesized by reaction of acrylic acid with $SO_3^=$ in the presence of air (Smith, 1981). Hydroxypropionic acid was synthesized by hydration of 2 M acrylic acid at 100°C in 1 M H_2SO_4 for 20 hours (Smith, 1981). Both of these procedures could give some polyacrylic acid impurities by free radical polymerization.

Effects of Sulfite

The effects of total dissolved sulfite are given in Figures 9 and 10. At low concentrations sulfite enhances dissolution by acting as a buffer. However, at concentrations greater than 1 mM, sulfite appears to inhibit $CaCO_3$ dissolution. This effect is more apparent at higher pH values. The range of sulfite concentration at which inhibition becomes apparent corresponds closely to the solubility of $CaSO_3$ solids in high pH solution, characteristic of the pH at the limestone surface. At lower pH values $CaCO_3$ dissolution rates do not actually decrease significantly until the bulk solution approaches the solubility limit of $CaSO_3$. All of the measured rates were well-behaved, therefore irreversible $CaSO_3$ blinding of the surface is not occurring.

Figure 10 shows that at pH 5 3 mM sulfite enhances dissolution with less than 2 mM acetate, but inhibits above 2 mM acetate.

The enhancing and inhibiting effect of sulfite can be modeled as a shift in equilibrium at the calcite surface. Thus, the equilibrium $[CaCO_3^\circ]$ is reduced by increased $[CaSO_3^\circ]$, much like a solid solution at the $CaCO_3$ surface. Using the general mass transfer model, the solution composition at the $CaCO_3$ surface was calculated from the experimental rate data.

Figure 11 shows that the calculated surface concentrations of $CaCO_3^\circ$ and $CaSO_3^\circ$ are correlated by the equation:

$$\log [CaCO_3^\circ] = -10.76 - 1.29 \log[CaSO_3^\circ] \qquad (38)$$

Thus, $CaSO_3^\circ$ concentration quantitatively reduces the equilibrium solubility of $CaCO_3^\circ$, probably by forming a solid solution or adsorption layer at the calcite surface. For $[CaSO_3^\circ]$ less than 0.05 mM, $[CaCO_3^\circ]$ at the surface is equal to its normal equilibrium value, 6.80×10^{-7} M. The calculated rate is

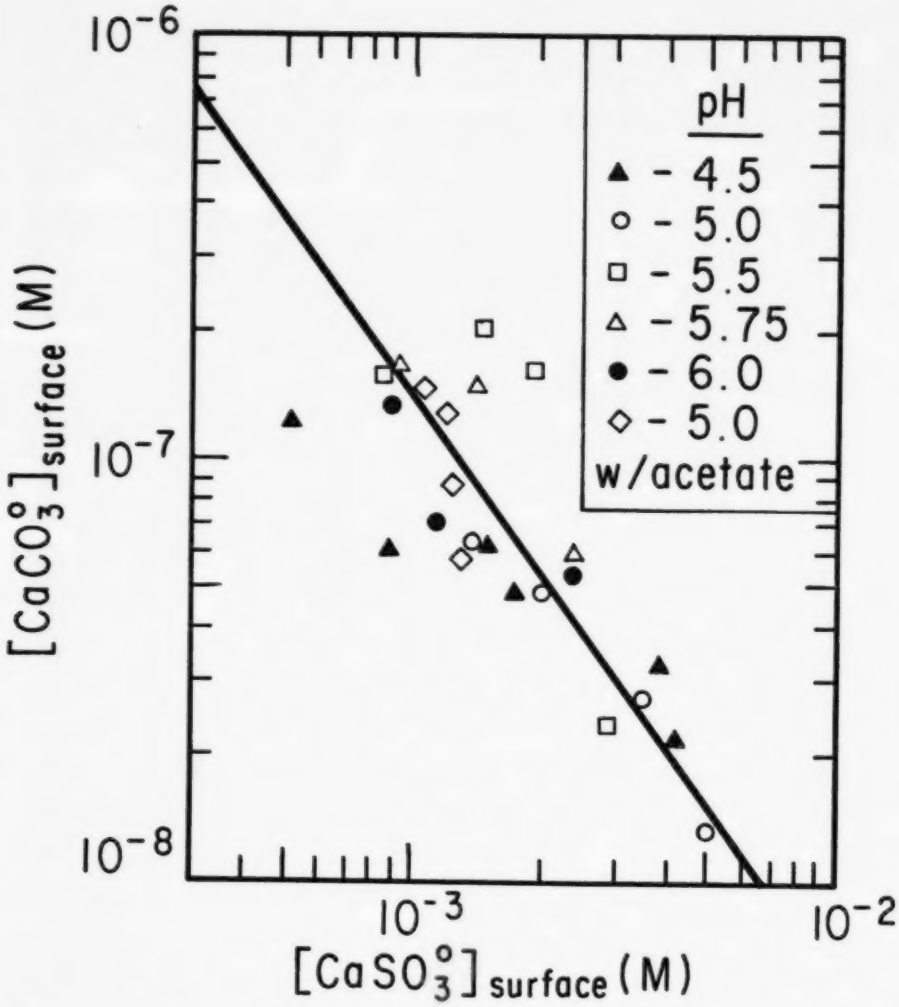

Figure 11. Calculated Solution Composition at $CaCO_3$ Surface, N_2 Sparging and 25°C

obtained by successive trial and error with β until the above solid solution equilibrium is satisfied.

As shown in Figure 9, the modified mass transfer model predicts the measured rate well at pH 4.5, 5.0, and 6.0, but deviates significantly at pH 5.5 and 5.75. These deviations may result from the sensitivity of the calculated rates to the estimated equilibrium constants and diffusivities used in the model. The maximum dissolution rates at each pH correspond roughly to the $CaSO_3$ solubility, shifting to higher sulfite concentrations at lower pH. A higher dissolution rate was observed at 55°C, but the rates are still modeled well by mass transfer with the same $CaSO_3^\circ$ equilibrium. It is significant that the solid solution equilibrium predicts well even with the higher rates in acetate buffer (Figure 10). Therefore, sulfite affects surface equilibrium, not surface kinetics.

Inhibition by sulfite is analogous to inhibition by phosphate (Berner and Morse, 1974; Sjoberg, 1981) and metal ions (Sjoberg, 1981; Terjeson et al., 1961; Koss and Moller, 1974). Inhibition by metal ions has also been modeled by a reduction in $CaCO_3$ solubility. Calcium phosphate and metal carbonates are relatively insoluble salts that could form adsorption layers or solid solutions at a calcite surface.

Sulfite inhibition is very significant for commercial applications in scrubber systems using $CaCO_3$ to produce $CaSO_3$ solids. $CaSO_3$ nucleation/crystallization may interact strongly with $CaCO_3$ utilization. Inhibitors of $CaSO_3$ crystallization, such as Mg^{++} or dissolved iron, may result in high $CaSO_3$ supersaturation which would in turn inhibit $CaCO_3$ dissolution. At very high $CaSO_3$ supersaturation irreversible blinding of the $CaCO_3$ surface could occur.

EFFECT OF TYPE AND GRIND

The effect of type and grind was determined by 31 experiments with 9 types of limestone and 19 grinds. The grinds included naturally distributed ground stone and screened fractions. Experiments were performed at 25°C in 0.1 M $CaCl_2$ at pH 4.0 or 5.0 with sparging by N_2 or CO_2.

For each experiment, the measured time to dissolve 50 percent of the available $CaCO_3$ (t_{50}) was compared to t_{50} calculated from equations (31) and (32) using the Coulter Counter size distribution. From several trails, a value of the adjustable parameter, B, in Eq. (28) was chosen for each pH and sparging condition that minimized the error in t_{50} prediction for all types and grinds of limestone tested.

Fitted values of B are given in Table 2 for the four solution conditions examined. Values of the rate parameter K in Eq. (31) were obtained using the unadjusted solution composition model for N_2 sparging with an empirical adjustment factor of 1.5 to account for nonspherical shape. The K values are equal to 80 percent of the k values in Figures 4-10.

The B value for N_2 sparging (low P_{CO_2}) gives the relative enhancement of mass transfer due to agitation. Because B is independent of chemical effects, it has the same value at pH 4 and 5.

At pH 4 or 5, diffusion of H^+ dominates the mass transfer process. With the H^+ diffusivity of 9.31×10^{-5} cm^2/sec and an estimated agitation power of 6.5 w/kg solution, the mass transfer coefficient for a 100-μm particle calculated from available correlations was 0.084 (Harriott), 0.075 (Levins and Glastonbury), and 0.029 cm/sec (Calderbank and Moo-Young). This suggests the correlation of Calderbank and Moo-Young, which extends over a 10^7 range of data but has a relative error of ± 50%, must be scaled by a factor of two. This is reflected in the Calderbank and Moo-Young prediction for B (Eq. (29)) of 190 cm^{-1}, about half of the fitted value of B of 400 cm^{-1}. Scaling Eq. (29) appropriately gives B as

$$B = \frac{0.167}{D} \left[\frac{\varepsilon \nu}{\rho^2} \right]^{1/4} \left[\frac{\nu}{D} \right]^{-2/3} \qquad (39)$$

Eq. (39) allows a calculation for B under widely varying conditions of agitation and solution composition and properties.

The predicted effects of high P_{CO_2} are substantiated by the B values for CO_2 sparging in Table 2. At pH 4, CO_2 sparging reduces B to 260 cm^{-1}. At pH 5, CO_2 sparging more than doubles B to 880 cm^{-1}.

The weak dependency of B on agitation power per unit mass indicates t_{50} is not greatly affected by increases in agitation above the minimum level necessary to fully fluidize the sample. This was verified by increasing agitation 1.44 times for a coarse sieve fraction (Brassfield 120-200) with no significant change in t_{50}. Early runs at lower speed may therefore be considered to have valid t_{50} values.

Table 3 gives predicted and measured values of t_{50} and t_{80} for all of the experiments. Predictions of the model for t_{50} extend over three orders of

TABLE 2: VALUES OF B FOR RATE EQ. (28) OBTAINED FROM THE EXPERIMENTAL DATA

Dissolution Condition	K (cm^2/min)	B (cm^{-1})	t_{50} meas/t_{50} calc Mean	Standard Deviation
pH 4, N_2 sparge	2.97×10^{-7}	400.	0.96	0.10
CO_2 sparge		260.	1.13	0.31
pH 5, N_2 sparge	3.26×10^{-8}	400.	1.04	0.16
CO_2 sparge		880.	0.95	0.24

TABLE 3: SUMMARY OF MEASURED AND PREDICTED VALUES OF TIME REQUIRED TO DISSOLVE 50% (t_{50}) AND 80% (t_{80}) OF THE INITIAL AVAILABLE $CaCO_3$.

Limestone Type	Grind	d_{50} (μm)	d_{90}/d_{50}	pH	Sparge	t_{50} meas(min)	t_{50} meas/calc	t_{80} meas(min)	t_{80} meas/calc
Ash Grove %A = 96.7[a]	-325	12.7	2.30	5	CO_2	7.88	0.99	32.6	1.17
Brassfield %A = 84.0	120-200	100	1.35	4	CO_2	39.0[b]	0.98	85.1	1.08
Fredonia %A = 95.0	Coarse	38.1	3.73	4	CO_2	6.95	1.16	57.1	1.33
	Extra Coarse	40.3	4.02	4	CO_2	6.10	0.91	38.7	0.79
	Feedbelt			5	N_2	3.91[b]	0.92[d]	60.2	1.32
	Fine	8.0	8.51	5	N_2	6.1	1.37	72.8	0.98
	100-140	130	1.20	4	CO_2	54.2	0.93	107	0.94
				4	N_2	40.0	0.95		
				5	CO_2	208[b]	1.05		
				5	N_2	494[b]	1.03	893	1.18
	120-200	125	1.24	4	CO_2	63.0	1.65[d]	131	1.68
	170-270	66	1.36	4	CO_2	14.6	0.71		
				4	N_2	13.9	0.87		
				5	CO_2	81.5	1.01		
				5	N_2	145	1.00		
	200-325	66.4	1.95	4	CO_2	22.0	0.90[d]	44.1	0.87
Georgia Marble %A = 96.5	Coarse	42.0	2.86	4	CO_2	11.9[b]	1.34	48.9[b]	1.34
				5	CO_2	47.0	1.17		
	Fine	24.0	2.06	5	N_2	27.0[c]	0.95	108	1.21
Longview %A = 95.0	Coarse	17.9	8.60	4	CO_2	2.80[b]	1.31	24.9	0.980
	Fine	15.0	3.63	5	CO_2	7.88[b]	0.87		
Maysville %A = 98.4	-325	8.3	4.31	4	CO_2	0.675[b]	1.01	3.54	0.794
Pfizer %A = 98.7	120-200	19.8	2.82	4	CO_2	3.70[d]	1.48	20.3	1.92
	200-325	21.8	2.34	4	CO_2	4.60[d]	1.63	23.6	2.02
Reagent Grade %A = 100		11.4	1.35	4	CO_2	1.26	1.07		
				4	N_2	1.17	1.07		
				5	CO_2	8.39	1.09		
				5	N_2	10.7	1.08		
Stoneman %A = 86.0	Coarse	40.3	2.90	4	CO_2	6.9[c]	0.90		
	Fine	22.0	2.30	5	CO_2	14.9	1.01	81.4	1.34
				5	N_2	20.3[c]	0.94		

a - %A = percent available for dissolution (wt % $CaCO_3$ + $MgCO_3$)
b - represents an average value from several runs
c - obtained in early apparatus with magnetic stirrer
d - 700 rpm

magnitude. The standard deviation of the t_{50} prediction varies from 10 percent with pH 4 and N_2 sparging to 30 percent with pH 4 and CO_2 sparging (Table 2). Lack of good fit may be attributed to error in experimental data or the Coulter Counter distribution used by the model. The low value of t_{50} predicted for Fredonia 120-200 at pH 4 and CO_2 sparging may be due to agitation levels too low to fully fluidize the sample. Fredonia Extra Coarse, Pfizer 120-200, and Pfizer 200-325 values may be in error because of problems with pH control at the time the data were collected.

For times other than t_{50}, the fit of the model to data is illustrated for three limestones by Figures 12, 13, and 14. The calculated and measured fraction remaining has been plotted versus normalized time, t/t_{50}. Deviations of the model from the data are greatest at the extremes from the point of superposition of $t/t_{50} = 1$. Relative fit of the model to data for long dissolution times is given by t_{80} measured to calculated ratios for many of the limestone types in Table 3.

The weak dependency of B on agitation power per unit mass indicates t_{50} is not greatly affected by increases in agitation above the minimum level necessary to fully fluidize the sample. Table 4 indicates the variation of t_{50} with agitation level for a coarse sieve fraction, Brassfield 120 to 200 mesh, and a coarse disperse limestone, Georgia Marble Coarse. The 28 percent decrease of t_{50} with increasing agitation from 660 to 1416 rpm for Brassfield 120-200 indicates a lack of fluidization at the lower speed. Increasing agitation from 655 to 2040 rpm, however, gives no significant change in t_{50} for Georgia Marble Coarse. In this case, no pronounced lack of fluidization is observed at the lower rpm due to the relatively small percentage of particles in the very coarse (120 to 200 mesh) range.

B is proportional to diffusivity to the -1/3 power (Eq. (38)). For a solution with 10 mM Na Acetate, the diffusivity is effectively that of HAc. In the base case of 0 mM NaAc, the effective diffusivity is approximately that of H^+ ion. Taking the ratio to the -1/3 power of HAc diffusivity to H^+ diffusivity gives B as

$$B = \left(\frac{1.19}{9.31}\right)^{-1/3} 400 \text{ cm}^{-1} = 794 \text{ cm}^{-1}$$

for NaAc solution.

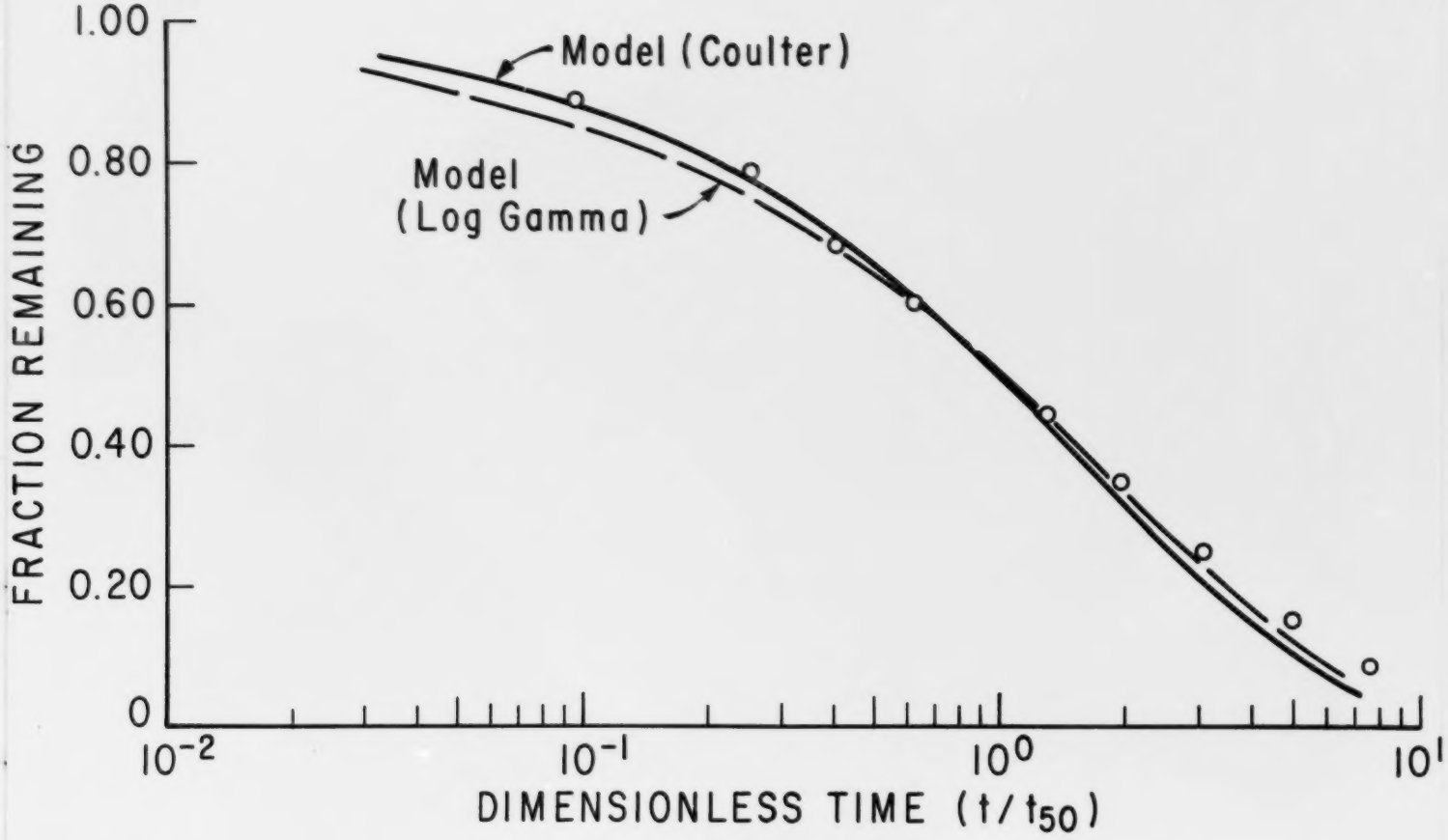

Figure 12. Dissolution Curves for Georgia Marble Fine at pH 5 with N_2 Sparging

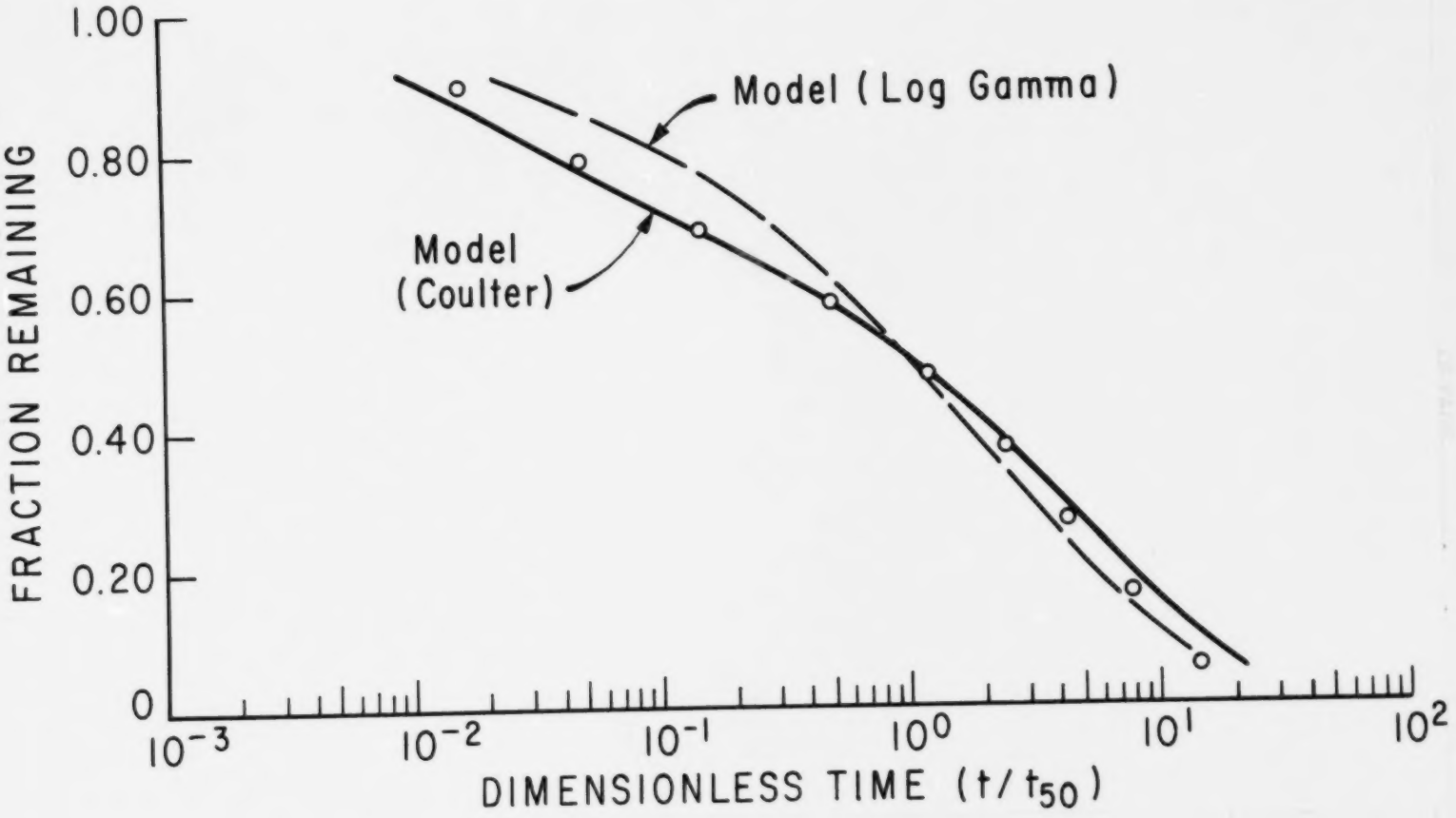

Figure 13. Dissolution Curves for Fredonia Extra Coarse at pH 4 with CO_2 Sparging

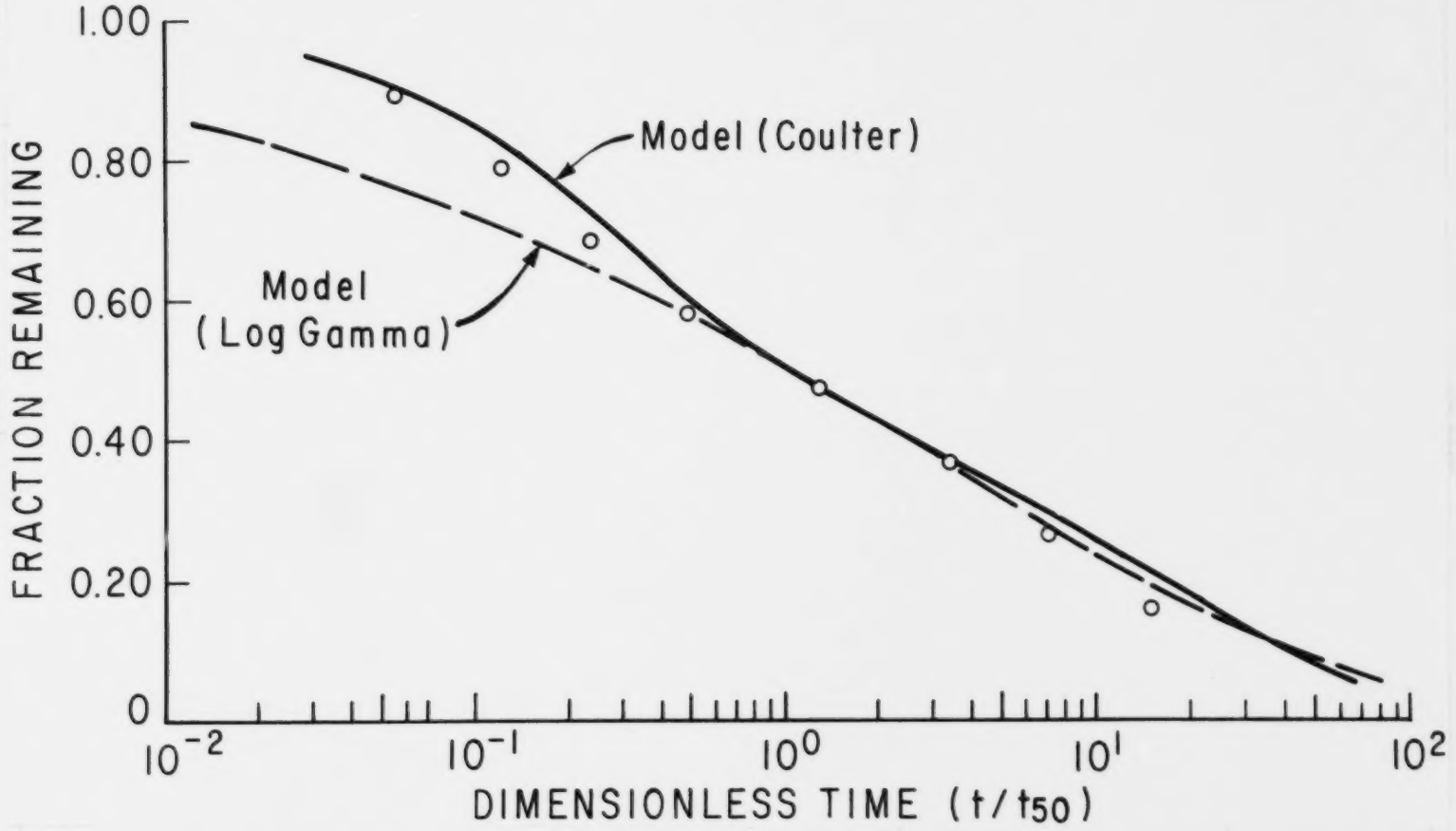

Figure 14. Dissolution Curves for Fredonia Fine at pH 5 with N_2 Sparging

TABLE 4: RELATIVE DISSOLUTION RATES AS A FUNCTION OF AGITATION LEVEL

Limestone Sample	Agitation Level (rpm)	t_{50}(min)
Brassfield 120-200	660	49.0
(pH 4.0, CO_2 sparge)	684	47.8
	1416	38.2
	2040	39.8
Georgia Marble Coarse	655	11.2
(pH 4.0, CO_2 sparge)	665	12.1
	720	12.1
	1360	12.2
	2400	11.4

This value of B was inserted in the mass transfer model and the resulting t_{50} compared with experimental values for Reagent $CaCO_3$ and Fredonia 100 to 140 sieve fraction with dissolution at pH 5 and 25°C in 0.1 M $CaCl_2$ with 10 mM sodium acetate (Table 5). The measured rate of dissolution is 27 to 47 percent slower than predicted.

STIRRED TANK CALCULATED RESULTS AND SO_2 REMOVAL

The U. S. EPA has sponsored a study of the relative reactivity of four limestone types as determined by relative SO_2 absorption in a pilot scrubber (Chang et al., 1982). The pilot scrubber, located at Research Triangle Park (RTP), was a three-stage turbulent contact absorber with a 7.5 m^3/min flue gas capacity. For each type and grind of limestone, SO_2 absorption was measured over 100 continuous hours of steady-state operation. Samples of limestones identical to those employed in the RTP scrubber studies were provided by the EPA for this investigation . Relative reactivity of these limestones versus stoichiometric ratio ($1/1-F_c$)) was calculated using the CSTR mass transfer model expressions for dissolution rate with integration over the Coulter Counter distributions (Eq. (35)).

Figures 15 and 16 give calculated stoichiometric ratios as a function of relative reactivity for all of the limestone types and grinds tested in the RTP pilot plant. SO_2 removal should be constant for a given relative reactivity. To get a relative reactivity of 10^{-3} μm^{-2}, Fredonia Feedbelt requires a stoichiometric ratio of 1.1 and Georgia Marble Coarse requires a stoichiometric ratio of 1.6. At low stoichiometry, the relative reactivity of the fine stones is in the sequence: Fredonia>Longview>Stoneman>Georgia Marble. At a stoichiometric ratio of 2.0 the relative reactivity of the coarse stones is in the sequence: Longview>Fredonia Coarse>Fredonia Extra Coarse>Stoneman>Georgia Marble. Except for Longview Coarse these calculated results are in qualitative agreement with the performance of the pilot scrubber.

Figure 17 gives a quantitative correlation of SO_2 removal with calculated relative reactivity. It shows general agreement of results from all stones except Fredonia Coarse which gives better SO_2 removal than expected and Georgia Marble Coarse which gives less SO_2 removal than expected. Predicted relative reactivity of Georgia Marble Coarse was also found to be 1.2 to 1.3 times greater than measured reactivity in laboratory experiments (Table 3).

TABLE 5: DISSOLUTION IN 10 mM NaAc SOLUTION, pH 5.0, N_2 SPARGE

$K=6.91 \times 10^{-7}$ cm^2/min, $B=400$ cm^{-1}

Limestone Type	t_{50} calc (min)	t_{50} meas/calc
Reagent $CaCO_3$	0.38	1.27
Fredonia 100-140	10.2	1.47

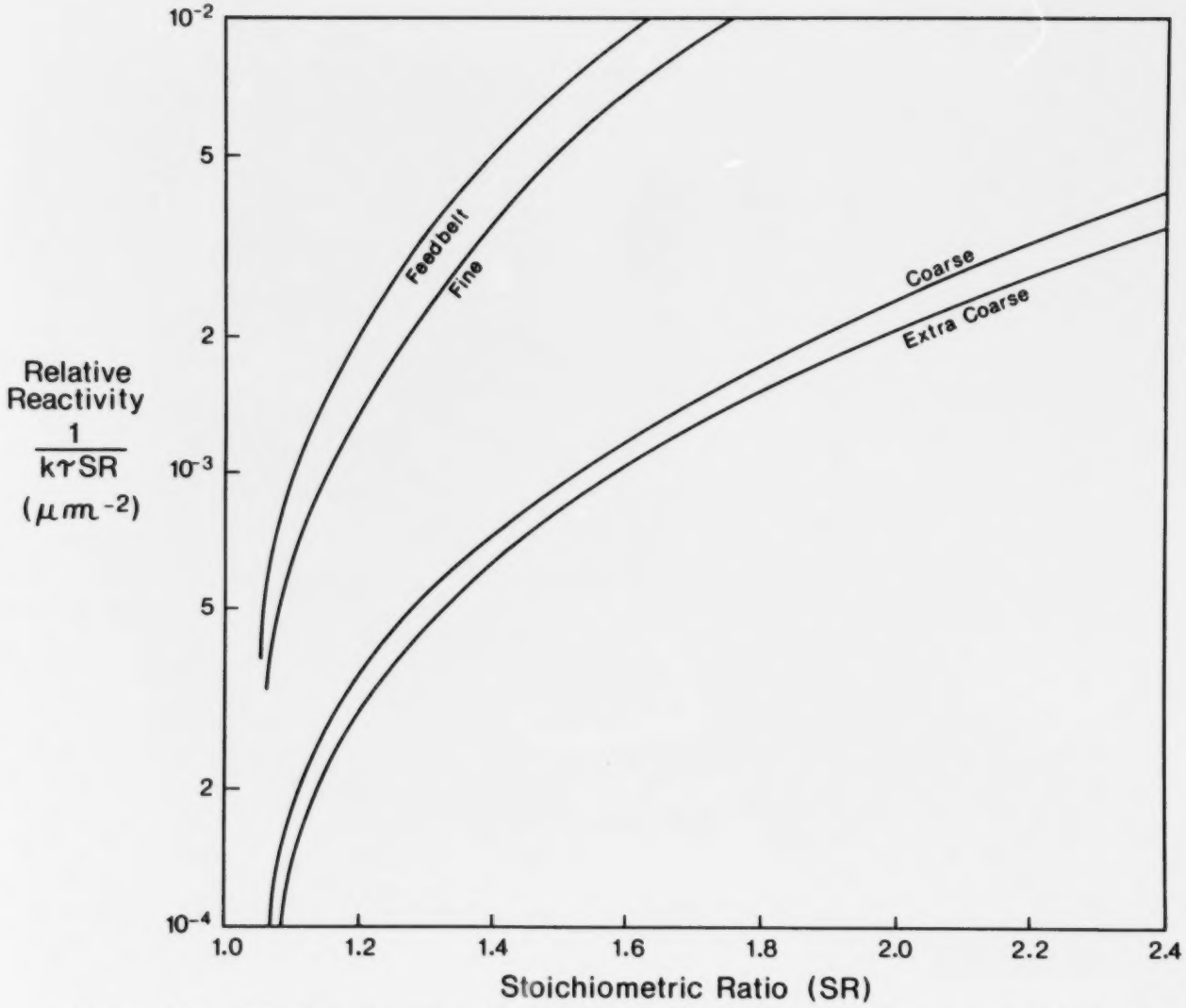

Figure 15. CSTR Mass Transfer Model Dissolution Rates for Fredonia Limestone Grinds

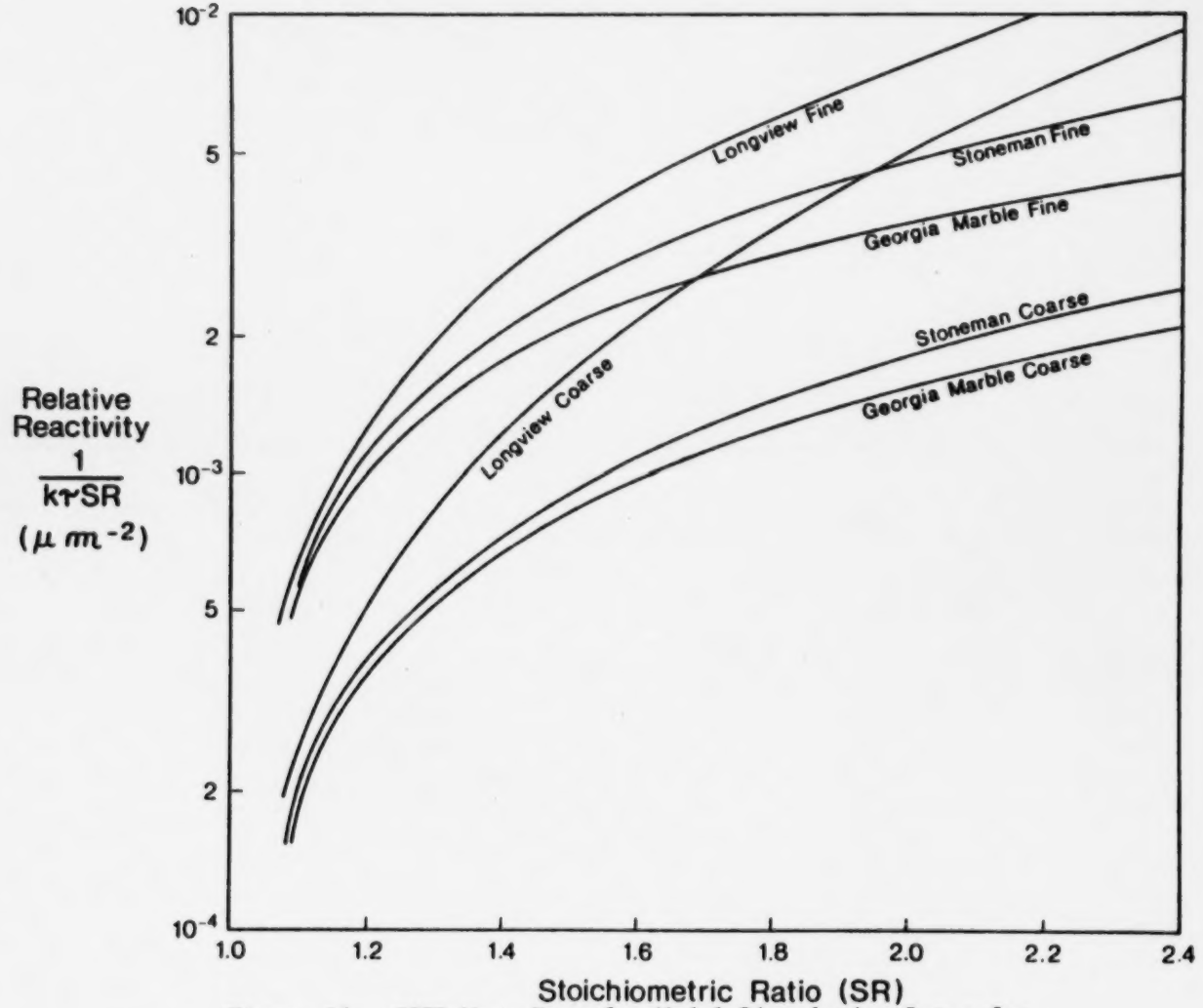

Figure 16. CSTR Mass Transfer Model Dissolution Rates for Various Limestone Types and Grinds

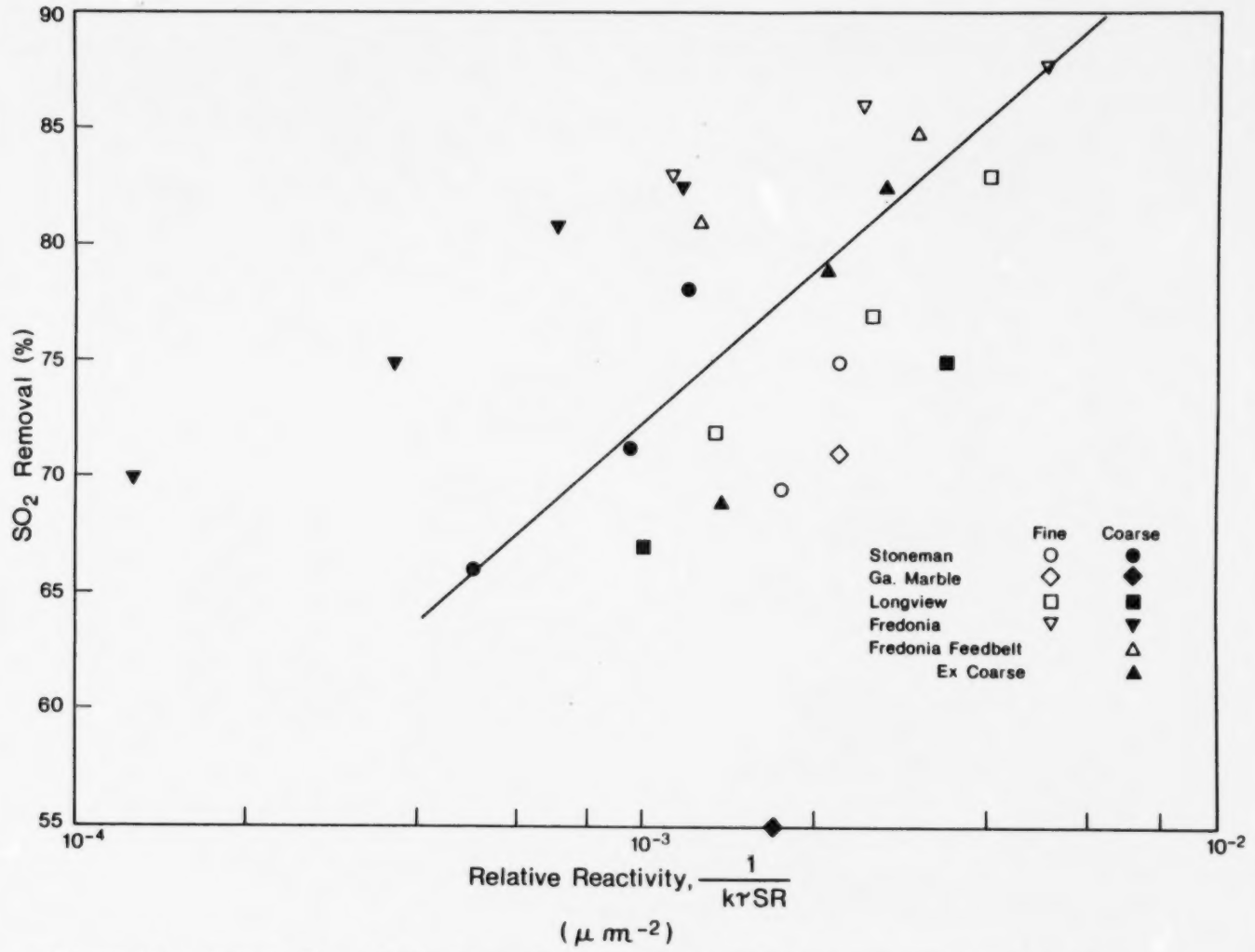

Figure 17. Correlation of SO_2 Removal with Limestone Relative Reactivity as Determined by CSTR Mass Transfer Model

This suggests that the measured particle size distribution is in error. The results with Fredonia coarse may be in error because of inaccurate measurement of SO_2 removal or inconsistent scrubber operation. Another possible source of error may be inconsistencies in particle size distribution from barrel to barrel of a given limestone sample.

RESULTS CALCULATED WITH A LOG GAMMA DISTRIBUTION

Dissolution rate for any limestone is apparently uniquely determined by extent of grinding. Actual determination of limestone particle size distribution by Coulter Counter measurements or similar means is difficult and costly to perform. The relative simplicity of pH-stat techniques in producing dissolution rate data suggests an easy method of accurately determining particle size distribution. Such a method would entail fitting rate data by the dissolution model using a mathematical distribution function with adjustable constants.

The size distribution of a crushed stone is frequently characterized as a log normal distribution (Aitchison and Brown, 1957). Based upon theoretical derivations, Schultz and Crouse (1973) propose a log gamma distribution as a better fit to crushed stone data. The log normal distribution includes a finite percentage of stones of unreasonably large diameter. In contrast, the log gamma distribution allows for a maximum particle size (d_{100}) and therefore better fits the coarse end of ground stone size distribution data.

The log gamma distribution is given by

$$f(3 \ln (d_{100}/d)) = \frac{\exp(-3 \ln(d_{100}/d)/\beta)(3 \ln(d_{100}/d))^{\alpha-1}}{\beta^{\alpha} \Gamma(\alpha)}$$

The parameter β is related to the characteristic mode of breakage for a given stone, and α increases with increasing breakage frequency. The mean and variance of the log gamma distribution are given respectively by

$$\mu = \alpha\beta$$

$$\sigma^2 = \alpha\beta^2$$

For large α, corresponding to long crushing times, the log gamma distribution asymptotically approaches the log normal.

In order to obtain a two parameter model it was assumed that the breakage parameter β could be given an average value that would characterize all limestones. The Coulter Counter distributions for the various grinds of the four stones used in the EPA pilot scrubber studies were found to give a β ranging from 1.15 to 2.80 (Table 6). A β of 2.0 was selected as best representing the limestone types and grinds that were examined.

Figure 18 gives general distributions with β equal to 2.0 as normalized diameter (d/d_{50}) versus cumulative volume percent.

For d_{90} and d_{50} obtained from size distribution data, Figures 19 and 20 may be used to obtain α and d_{100}. This method of fitting the log gamma distribution gives an exact fit to the data at d_{50} and d_{90}. The fine end of ground stone distributions represents a product due to particle-particle abrasion and is not well represented by the log gamma distribution. In addition, fitting the coarse end of the size distribution is most important as coarse particle dissolution is rate limiting in SO_2 absorption.

Table 6 compares the fitted values of α and d_{100} for β=2 to values calculated from the Coulter Counter distribution of three limestone samples. The t_{50} and t_{80} predictions of the model using the log gamma distribution are also compared to t_{50} and t_{80} values determined experimentally and from the model using the Coulter Counter distribution. Figures 12, 13, and 14 compare shapes of the two calculated curves with experimental dissolution data. The log gamma result is generally comparable to the Coulter Counter result for times greater than t_{50}. The deviation of the log gamma model for early times reflects the lack of fit to fine abrasion products.

For given values of d_{50} and α, cumulative dissolution of limestone in a CSTR may be predicted using Figures 21 and 22. Fraction remaining has been plotted against dimensionless time ($K\tau/d_{50}^2$) for d_{50} = 10 μm and d_{50} = 40 μm. Cumulative dissolution for median diameters other than 10 or 40 μm may be found by interpolation or extrapolation.

ADDITIONAL RESULTS

During this work additional rate data were obtained which are not amenable to quantitative modeling. These data were collected using at least one additional source of Reagent $CaCO_3$. This material was not sized on the Coulter Counter, and its size distribution was assumed to be the same as that used in the quantitative modeling. Therefore absolute rates reported in this

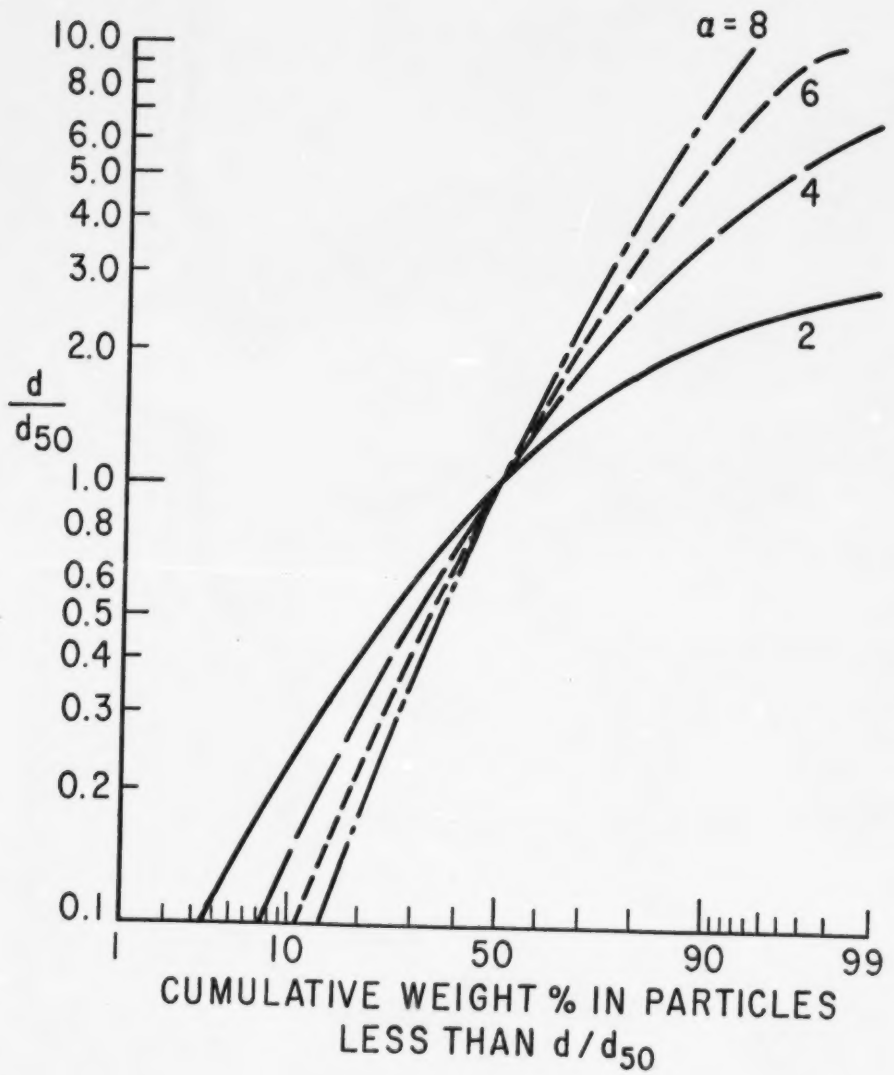

Figure 18. Generalized Log Gamma Distributions for $\beta = 2$

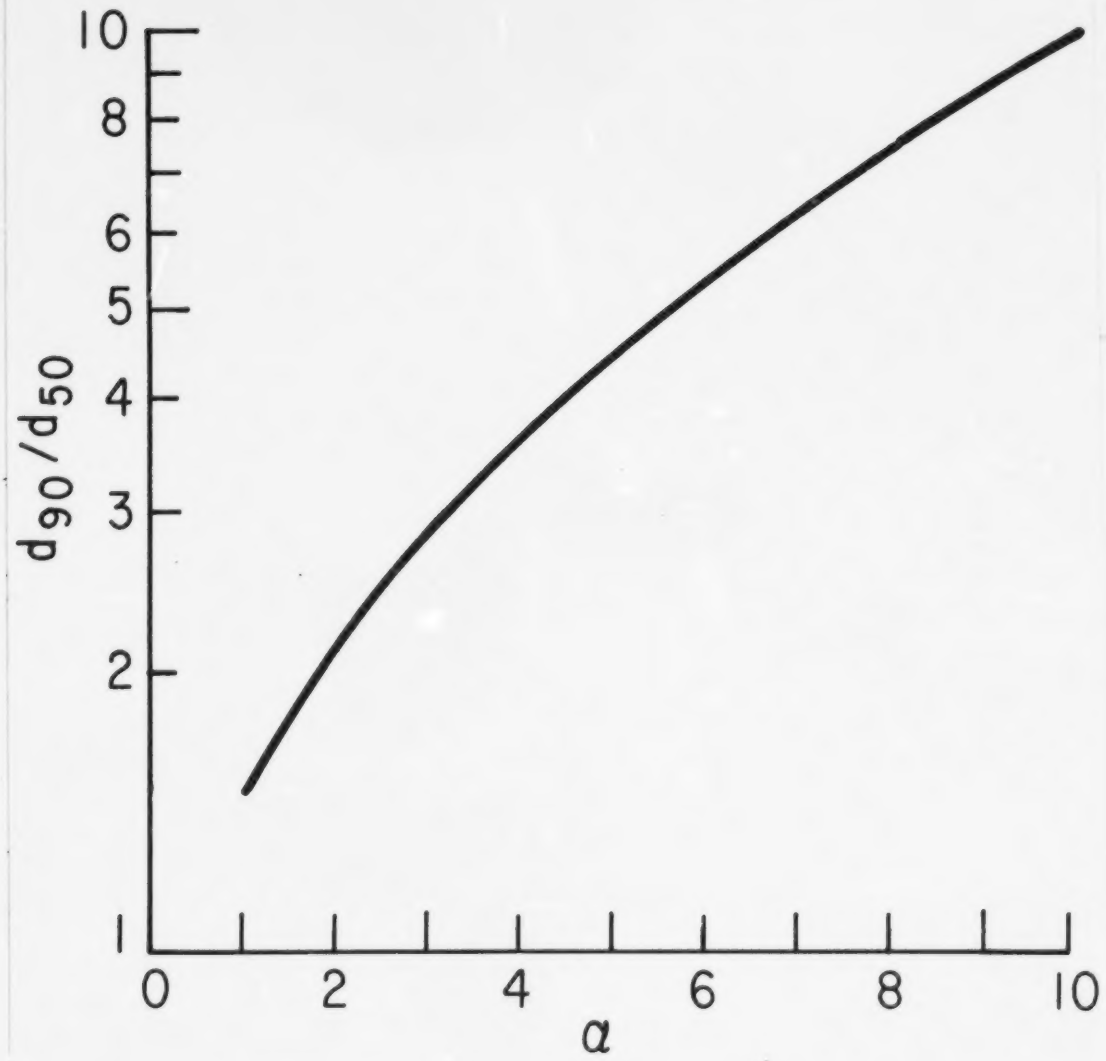

Figure 19. Correlation of α to Dispersivity Ratio d_{90}/d_{50} for Log Gamma Distribution, β = 2

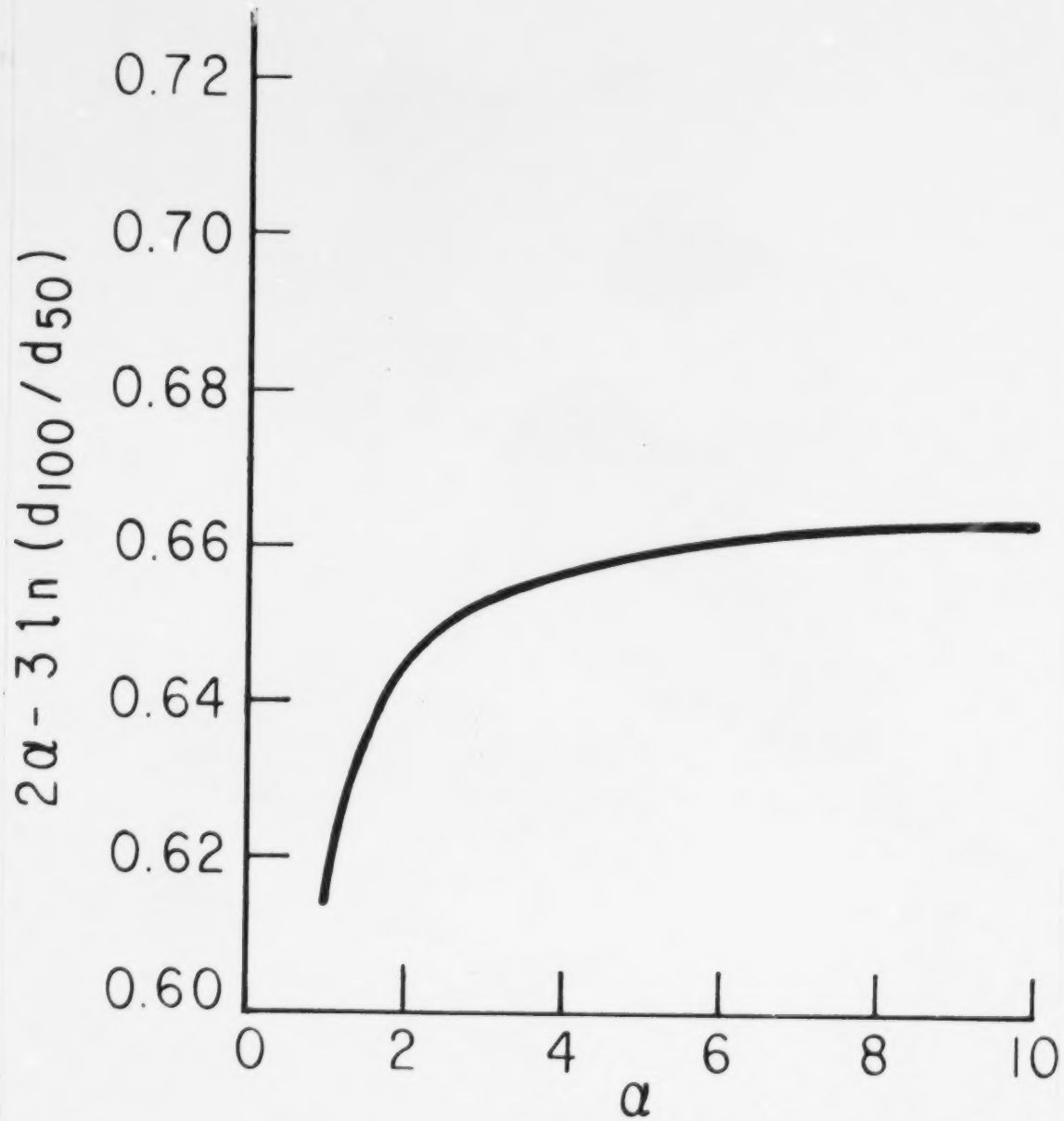

Figure 20. Correlation of d_{100} to α for Log Gamma Distribution, $\beta = 2$

TABLE 6: COMPARISON OF LOG GAMMA FIT WITH COULTER COUNTER DATA

Limestone (Grind)	Rigorous d_{100} (μm)	Rigorous α	Rigorous β	β = 2 d_{100} (μm)	β = 2 α	Measured time (min) t_{50}	Measured time (min) t_{80}	Measured time/Calculated time Coulter t_{50}	Measured time/Calculated time Coulter t_{80}	Measured time/Calculated time Log Gamma β=2 t_{50}	Measured time/Calculated time Log Gamma β=2 t_{80}
Fredonia (Extra Coarse)	460	3.45	2.44	650	4.5	6.1	38.7	0.91	0.79	1.30	1.59
Fredonia (Fine)	182	5.69	1.51	2357	8.86	6.1	72.8	1.37	0.98	1.46	1.25
Georgia Marble (Fine)	92	3.82	1.15	68.8	1.9	27.0	108	0.95	1.21	1.00	1.17

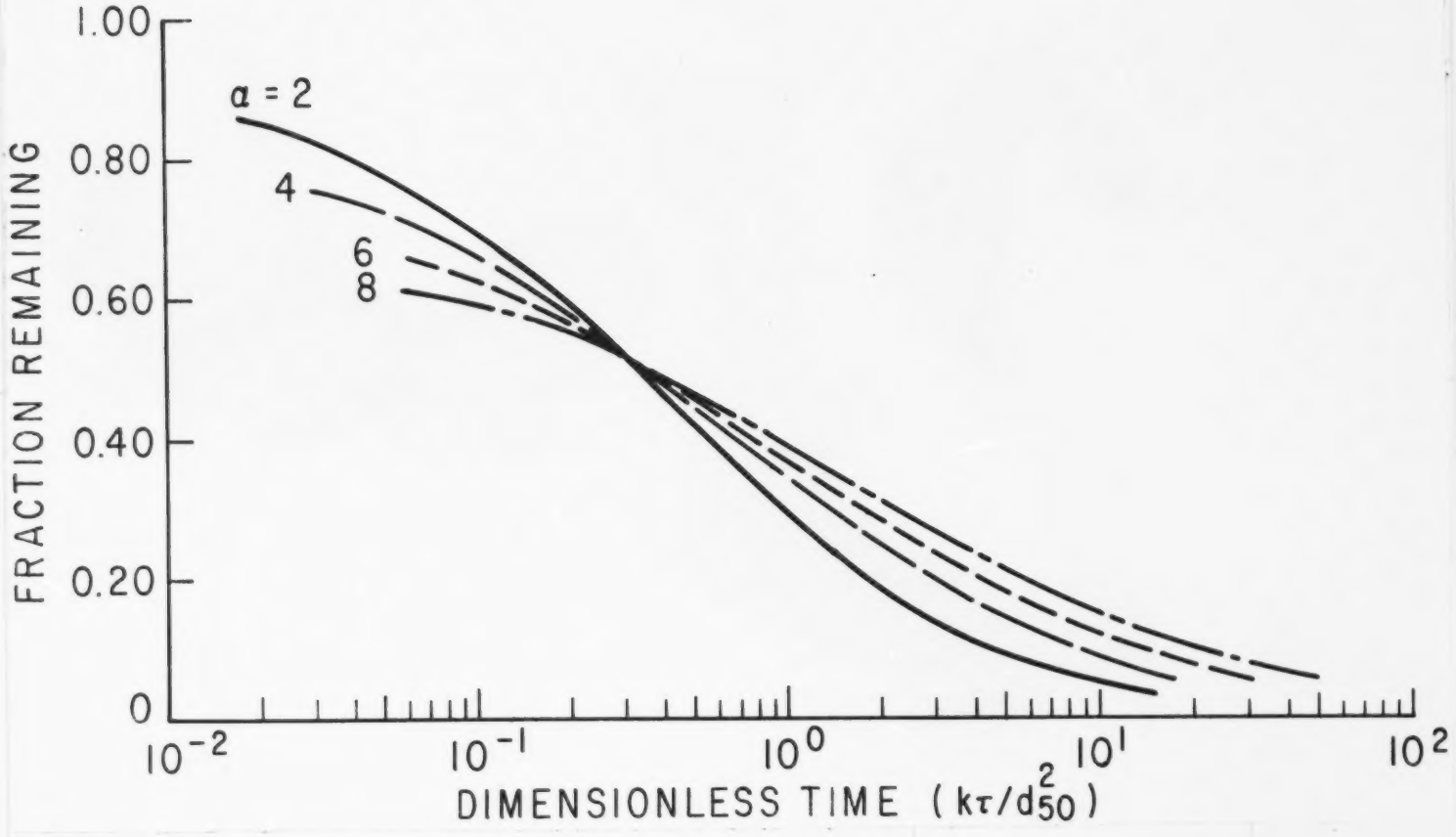

Figure 21. CSTR Dissolution Curves Based on Log Gamma Distributions, $\beta = 2$, $d_{50} = 10\mu m$

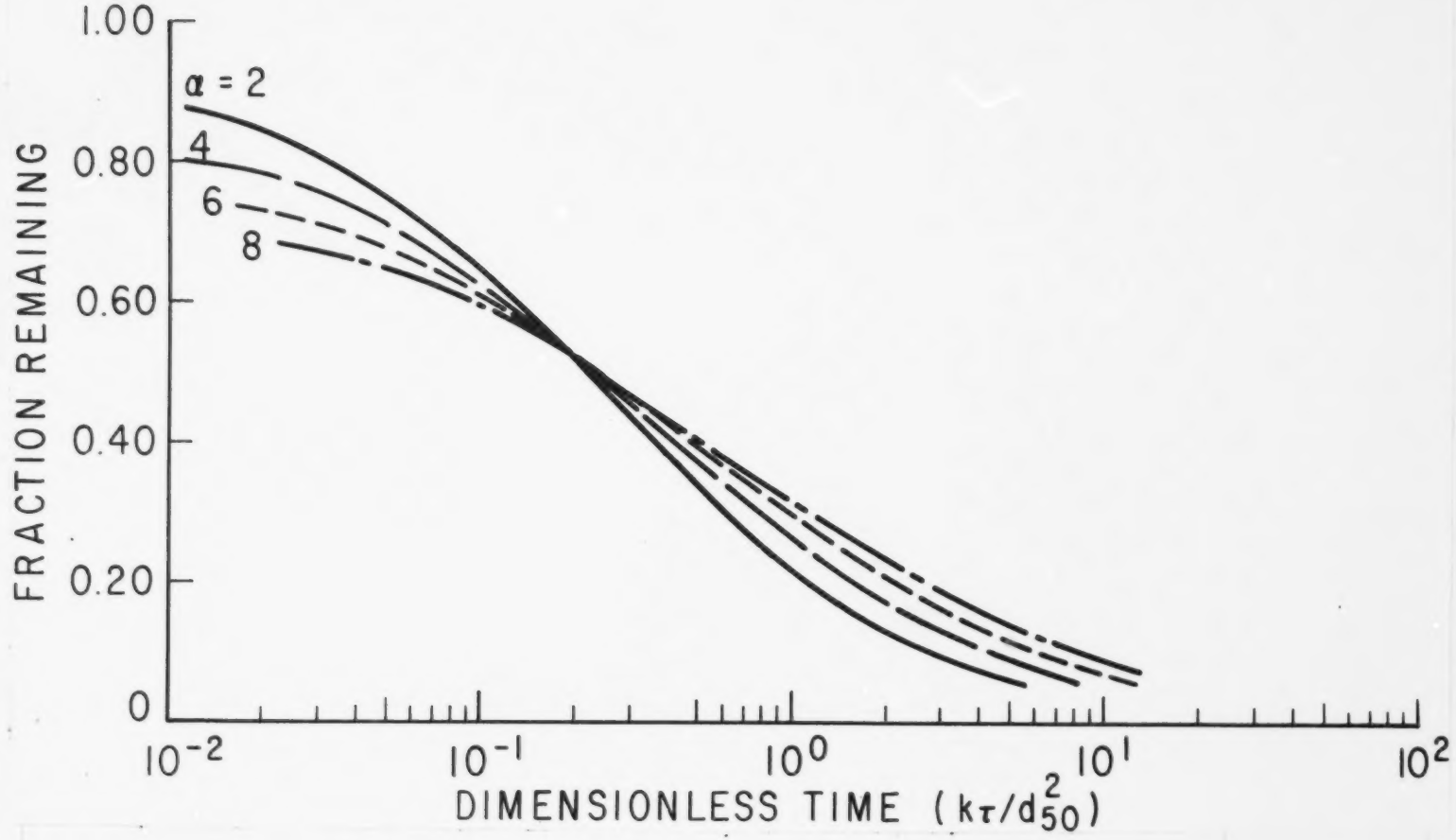

Figure 22. CSTR Dissolution Curves Based on Log Gamma Distributions, $\beta = 2$, $d_{50} = 40$ μm

section are not directly comparable with those reported earlier. However each set of data reported here is internally consistent and shows the relative effects of specific variables. These data were all collected at 25°C unless otherwise noted.

Effects of Mg^{++}, Mn^{++}, and Fe^{++}

Work by Koss and Moller (1974) suggests that heavy metals may inhibit limestone dissolution by surface adsorption with a shift in the effective solubility. Figure 23 shows the effect of Mn^{++} and Mg^{++} in 0.1 M sulfate solution. No effect was observed at pH 5, because the solid/solution equilibrium has no effect on dissolution rate. The maximum effect was observed at pH 6.5 with N_2 sparging with zero initial Ca^{++} or 2.5 mM Ca^{++} at 50 percent dissolution. Under these conditions dissolution is enhanced primarily by the hydrolysis equilibrium:

$$CaCO_3 + H_2O \rightleftarrows Ca^{++} + HCO_3^- + OH^-$$

Therefore, the dissolution rate is sensitive to surface equilibrium. The rate was reduced by a factor of 1.6 by 0.1 M Mg^{++} and a factor of 7.7 by 0.01 M Mn^{++}.

Figures 24 and 25 give the effect of dissolved Fe^{++} with CO_2 and N_2 sparging, respectively. Experiments were performed with a nominal concentration of 1 mM $FeSO_4$ in 0.1 M Na_2SO_4. The maximum effect was observed at pH 4.0 with CO_2 sparging, when the dissolution rate was reduced by a factor of 1.8. There was precipitated iron present in all of the experiments, therefore the maximum effect at pH 4.0 probably results from increased Fe^{+2} solubility at low pH.

Effects of Sulfite in Sulfate Solutions

Figures 26 and 27 give effects of sulfite in 1 M Na_2SO_4 at pH 6.5 and 0.3 M $MgSO_4$ at pH 5.0, respectively. These experiments were performed with Reagent $CaCO_3$ by adding $NaHSO_3/Na_2SO_3$ and $CaCl_2$ to the sulfate solutions.

Figure 26 shows a strong effect of both Ca^{++} and $SO_3^=$ on the dissolution rate in 1 M Na_2SO_4. As in 0.1 M $CaCl_2$ at pH 5 (Figure 9), increasing total dissolved sulfite initially increases the dissolution rate by buffering, and then reduces the dissolution rate by the effect of sulfite adsorption on the solid/solution equilibrium. In the absence of dissolved sulfite, reduced Ca^{++}

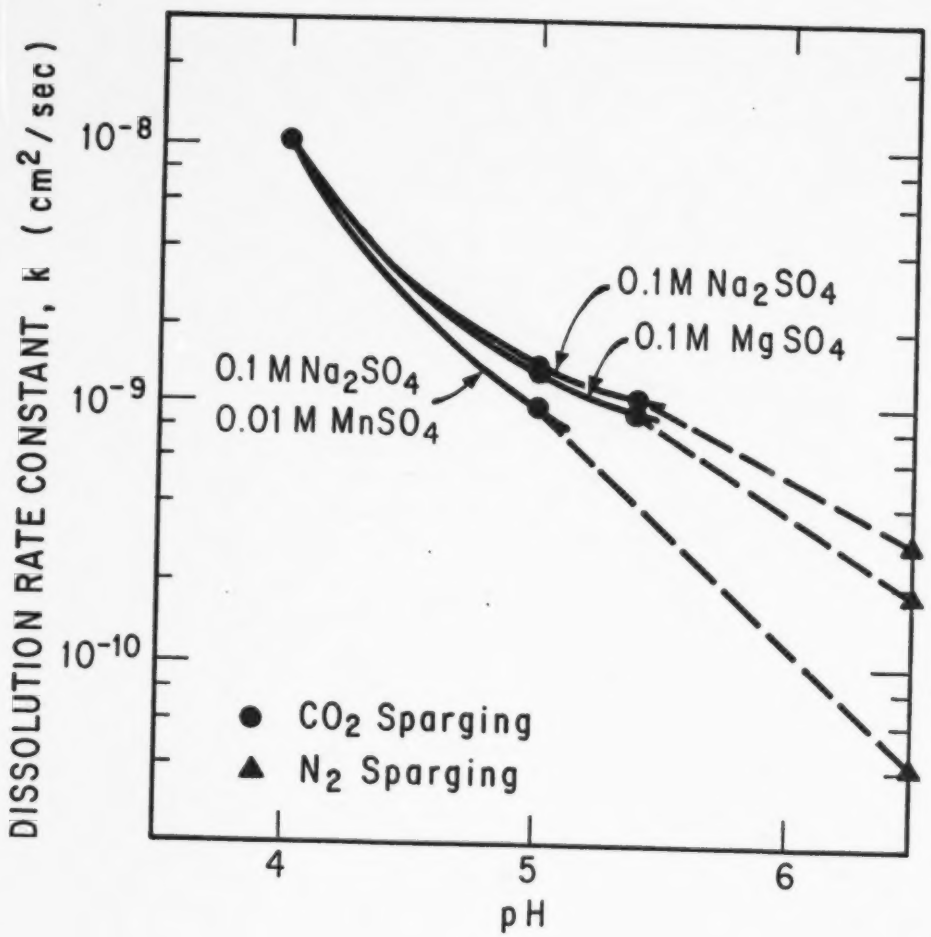

Figure 23. Effect of Mn and Mg on Reagent $CaCO_3$ Dissolution, 25°C, 2.5 mM Ca^{++}

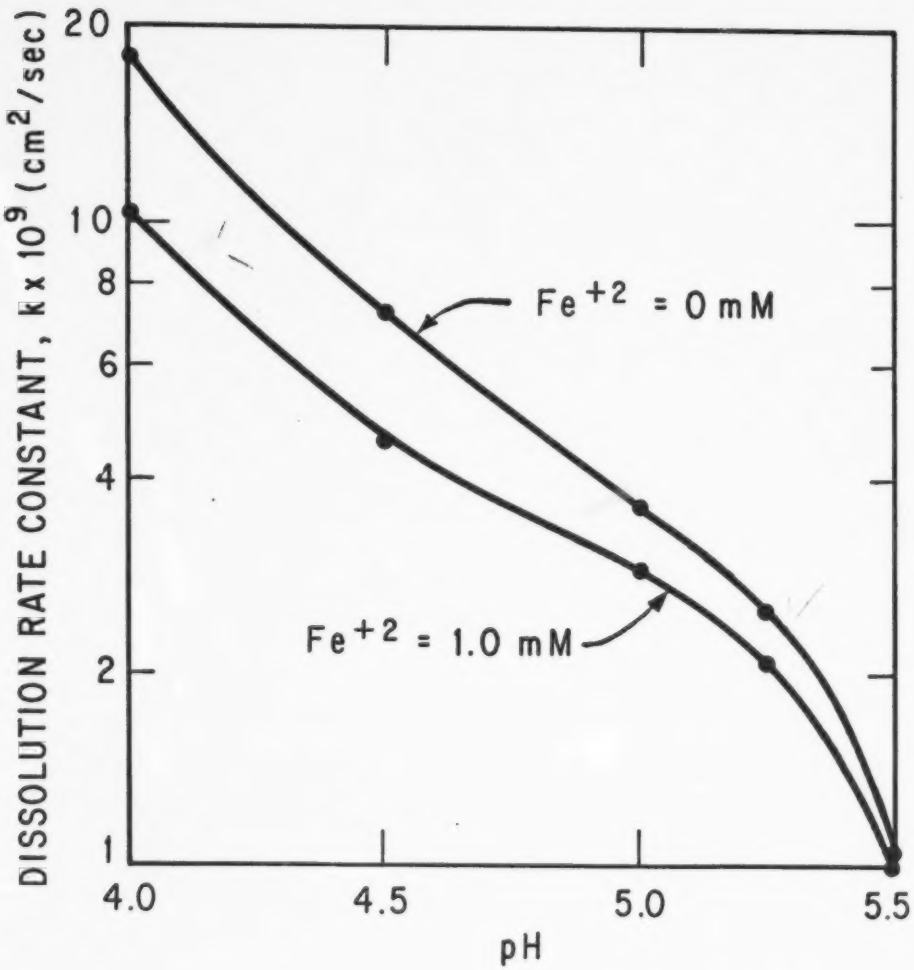

Figure 24. Effect of Fe^{+2} on Reagent $CaCO_3$ Dissolution, CO_2 Sparging, 0.1 M Na_2SO_4, 25 mM Ca^{++}, 25°C

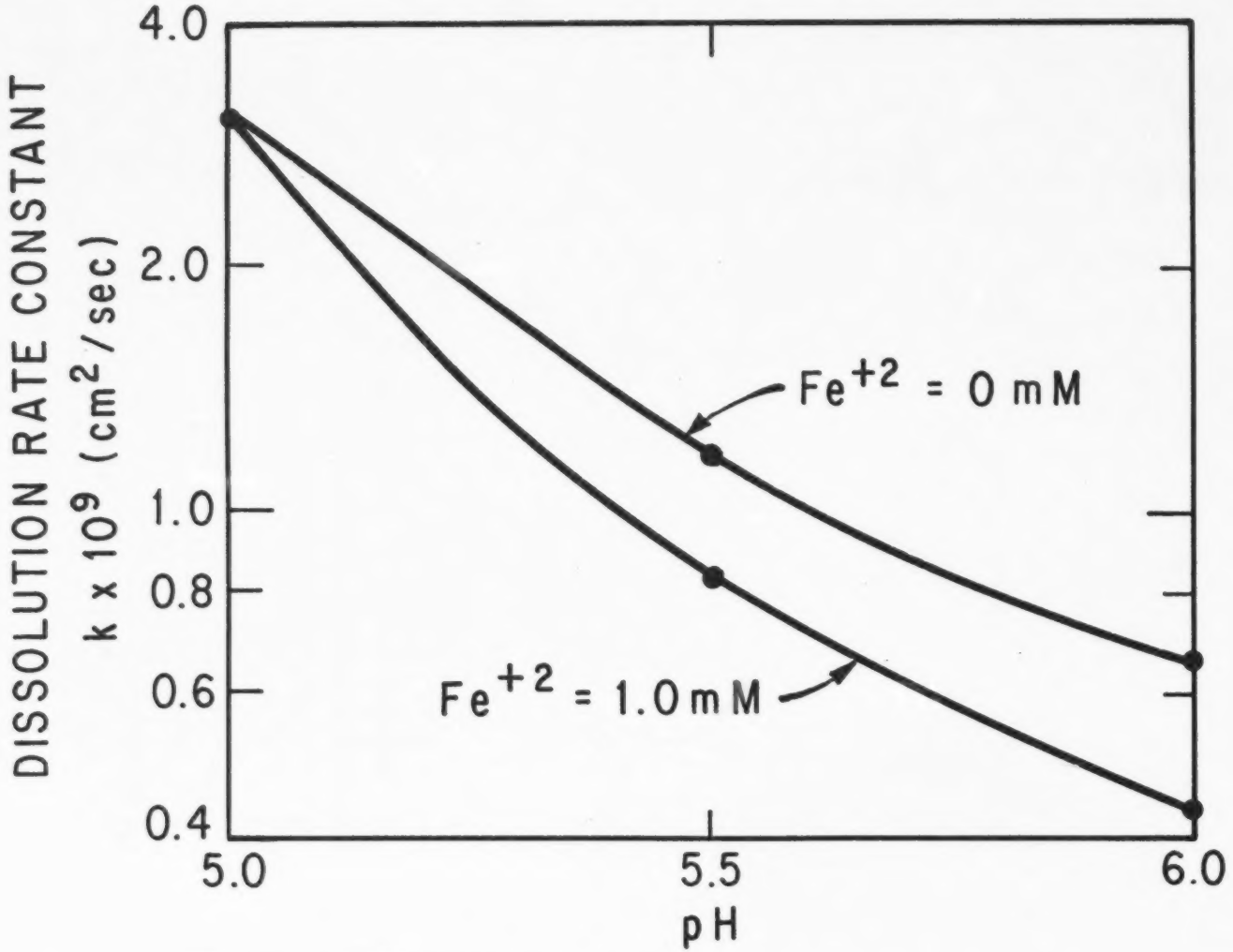

Figure 25. Effect of Fe^{+2} on Reagent $CaCO_3$ Dissolution, N_2 Sparging, 0.1 M Na_2SO_4, 2.5 mM Ca^{++}, 25°C

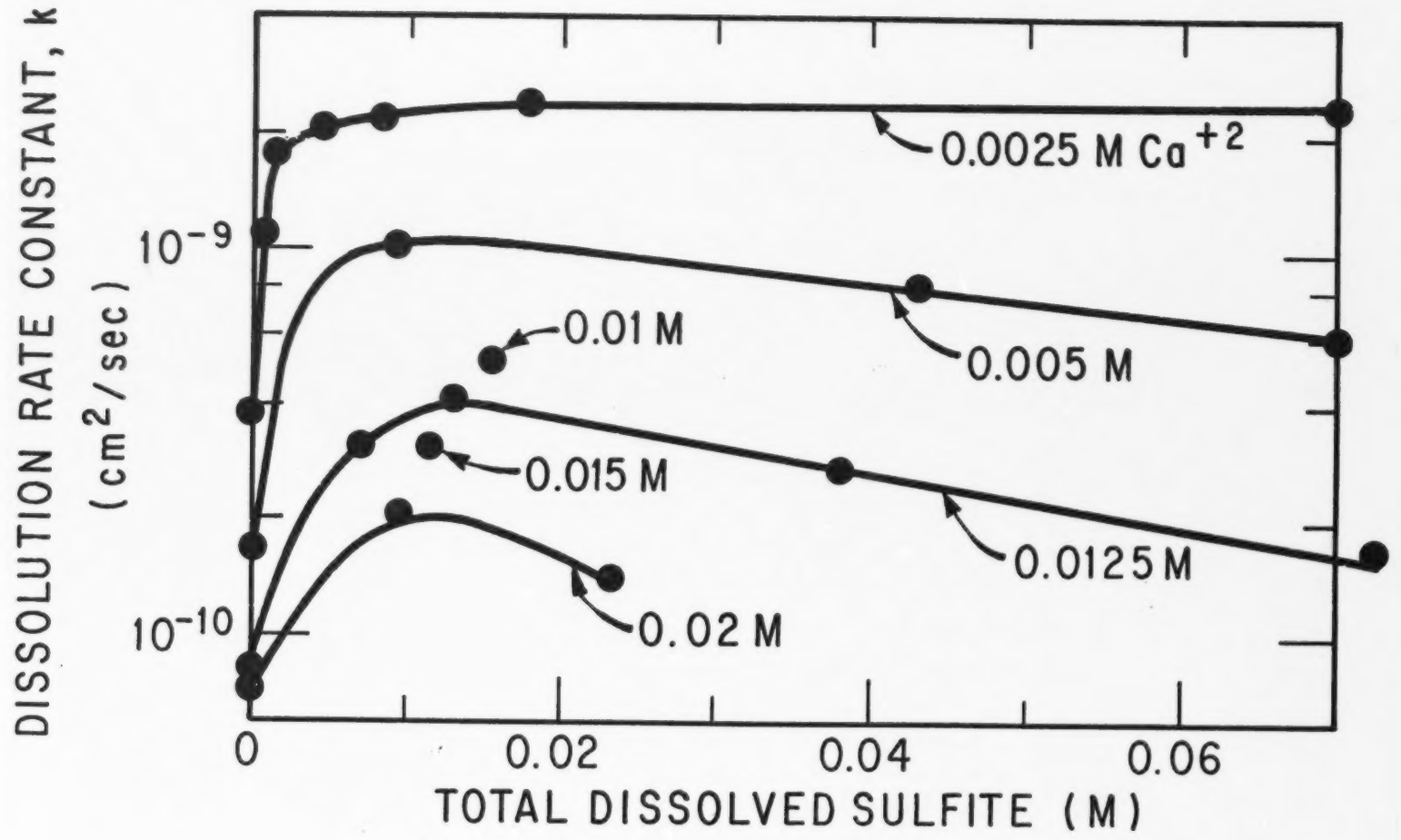

Figure 26. Effect of Dissolved Sulfite on Reagent $CaCO_3$ Dissolution in 0.3 M $MgSO_4$, N_2 Sparging, pH 6.5, 25°C

enhances the dissolution rate by increasing the contribution of the hydrolysis reaction:

$$CaCO_3 + H_2O \rightleftarrows Ca^{++} + HCO_3^- + OH^-$$

In the presence of sulfite, reduced calcium also enhances the dissolution rate by shifting the surface equilibrium:

$$CaCO_3 \cdot CaSO_3 + H_2O \rightleftarrows 2\ Ca^{++} + SO_3^{=} + HCO_3^- + OH^-$$

Figure 27 shows similar effects in 0.3 M $MgSO_4$ with N_2 sparging. Dissolved sulfite enhances the dissolution rate by as much as a factor of 15.

Effects of Ionic Strength

The dissolution rate of Reagent $CaCO_3$ was measured at pH 5 with N_2 sparging in solutions containing 0.1 M $CaCl_2$ plus variable quantities of $CaCl_2$, $MgCl_2$, and NaCl. The results are given in Figure 28. The dissolution rate appears to be correlated with ionic strength rather than calcium concentration. It decreases by a factor of 3.1 from 0.1 M $CaCl_2$ (ionic strength 0.3) to 1.0 M $CaCl_2$ (ionic strength 3.0).

At pH 5 with N_2 sparging, the dissolution is controlled primarily by the diffusion of H^+. Increased ionic strength could only decrease the dissolution rate by decreasing the diffusivity of H^+ or by increasing the activity coefficient of H^+. Figure 27 also shows the diffusivity of H^+ as measured in NaCl solution (Roberts and Northey, 1972). In 3 M NaCl it is a factor of 2.2 less than in infinitely dilute solution. Therefore, the effect of ionic strength on H^+ diffusivity is the dominant factor.

Effects of CO_2, Sulfite, and Temperature with Coarse Limestone

Experiments were performed at pH 5.0 with a coarse screened fraction (100-140 mesh) of Fredonia limestone to quantify interactions of sulfite and temperature with the contribution of the CO_2 reaction. The results are presented in Figure 29 and Table 7 as values of $1/t_{50}$, which should be proportional to the dissolution rate.

At 25°C in 0.1 M Na_2SO_4 with 2.5 mM Ca^{++}, $1/t_{50}$ is larger with CO_2 sparging by 0.004 to 0.013 min^{-1} as total dissolved sulfite varies from zero to 25 mM (Figure 29). The change in the absolute CO_2 enhancement of the

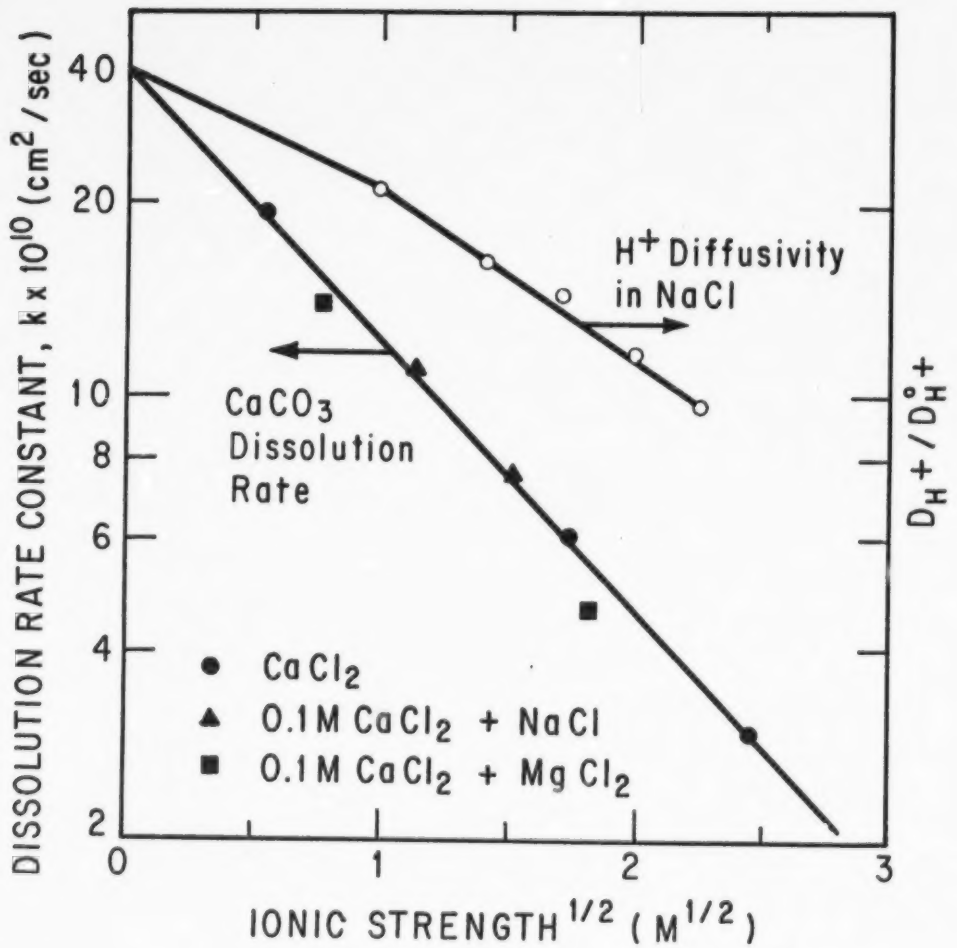

Figure 28. Effect of Ionic Strength on Reagent $CaCO_3$ Dissolution, pH 5, 0.1 M $CaCl_2$, N_2 Sparging, 25°C, and on H^+ Diffusion in NaCl

TABLE 7: DISSOLUTION OF 100-140 MESH FREDONIA, pH 5.0

Solution	T(°C)	Sparge	$1/t_{50}(min^{-1})$
0.1 M Na_2SO_4 2.5 mM Ca^{++}	25	N_2	0.0053
		CO_2	0.0091
0.1 M $CaCl_2$	25	N_2	0.0020
		CO_2	0.0050
	55	N_2	0.0030
		CO_2	0.0083

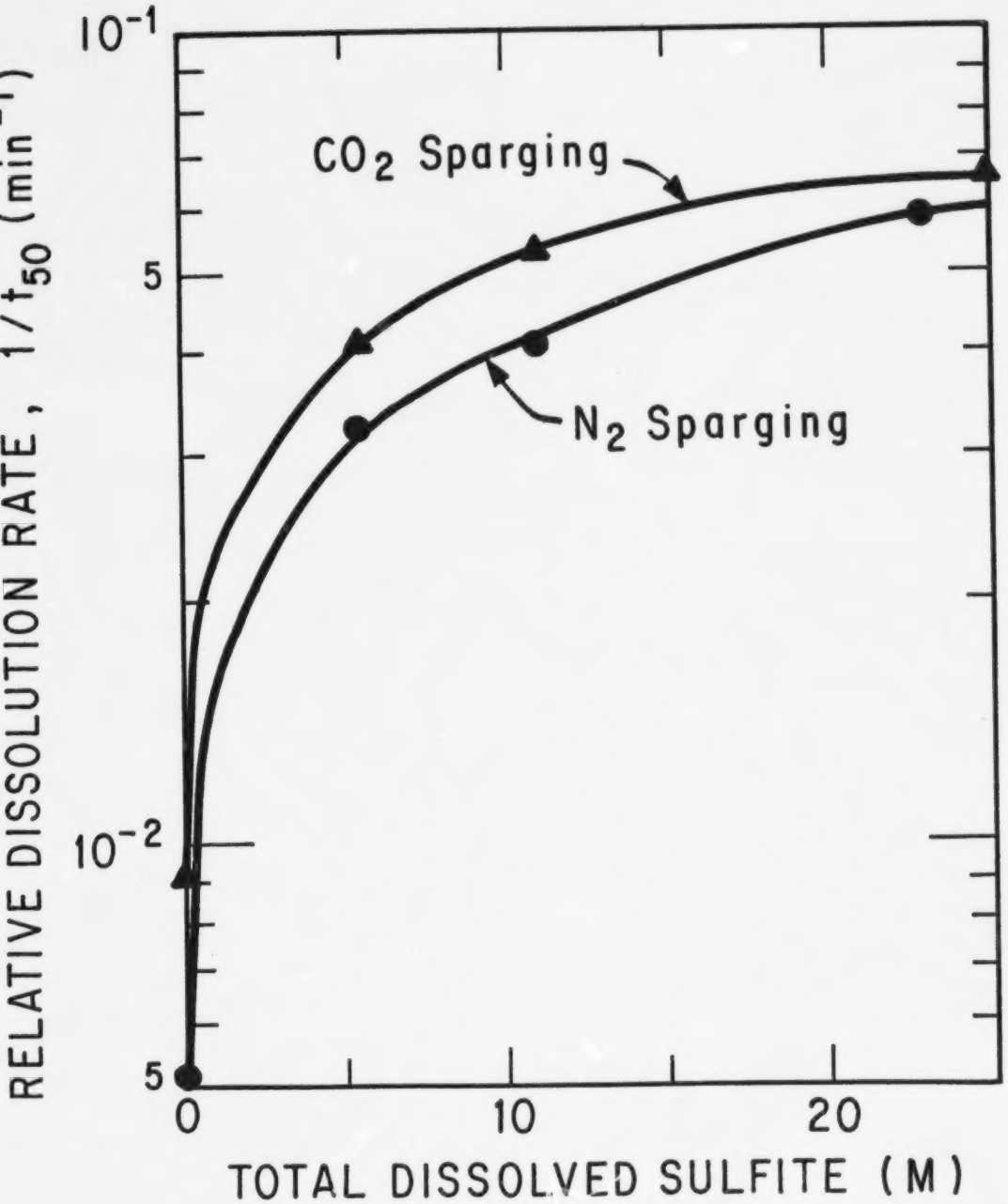

Figure 29. Effect of Dissolved Sulfite on Dissolution of Fredonia 100-140 Mesh, 0.1 M Na_2SO_4, 2.5 mM Ca^{++}, pH 5, 25°C

dissolution rate with dissolved sulfate is probably not statistically significant since at 11 mM sulfite the absolute contribution of 0.013 min^{-1} represents a relative increase of only 30 percent. On a relative basis, CO_2 sparging increases the $CaCO_3$ dissolution rate a factor of 1.8 at zero sulfite, but only by a factor of 1.12 at 25 mM sulfite.

Table 7 compares values of $1/t_{50}$ for $CaCO_3$ dissolution without dissolved sulfite. The dissolution rate is 1.8 to 2.5 times faster with 2.5 mM Ca^{++} than with 0.1 M Ca^{++}. It is about 1.5 to 1.7 times faster at 55°C than at 25°C. CO_2 sparging enhances the dissolution rate by a factor of 1.7 to 2.8. It has less relative effect at low Ca^{++} because the absolute rates are generally faster. There appears to be little interaction of the CO_2 effect with temperature.

Effects of Other Buffers

The dissolution of Reagent $CaCO_3$ was measured at pH 5, 0.1 M $CaCl_2$, 25°C, and CO_2 sparging with variable quantities of glycolic acid and waste boiler cleaning acid. The waste acid was analyzed by ion exclusion chromatography to contain 0.6 M formic acid and 0.3 M glycolic acid plus a large quantity of dissolved iron. The dissolution results are presented in Table 8. Glycolic acid at 10 mM enhanced the dissolution rate by a factor of two. The waste cleaning acid also enhanced the dissolution rate.

The effect of ethylenediamine (EDA) on Reagent $CaCO_3$ dissolution was determined at pH 6.0 in 0.1 M $CaCl_2$ with N_2 sparging. Experiments were performed at both 25 and 55°C. The effective pK_a value of ethylenediamine was earlier found to be 7.30 at 27°C and 6.55 at 55°C in 0.1 M $CaCl_2$ (Cavanaugh, 1978). Therefore it should be an effective buffer for enhancing limestone dissolution. The results are given in Table 9. Ten mM EDA enhanced the dissolution rate by a factor of 8.0 at 25°C, but by only a factor of 2.0 at 55°C.

Effect of Gypsum Saturation

Reagent grade $CaCO_3$ was dissolved at pH 5 with CO_2 sparging in 0.1 M $CaCl_2$ with variable quantities of Na_2SO_4. The results are presented in Table 10. The dissolution rate is essentially independent of sulfate concentration up to 25 mM, which is supersaturated to gypsum. Therefore gypsum does not inhibit $CaCO_3$ dissolution as $CaSO_3$ does.

TABLE 8: EFFECTS OF BOILER CLEANING ACID (0.6 M glycolic, 0.3 M formic, plus Fe) ON DISSOLUTION OF REAGENT $CaCO_3$, pH 5, 0.1 M $CaCl_2$, 25°C, CO_2 SPARGING

Acid	Dissolution Rate Constant $kx10^9 (cm^2/sec)$
0	1.11
10 mM Glycolic	2.07
10 mM Glycolic 10 mM $FeSO_4$	1.06
35 mM cleaning acid	1.95
10 mM cleaning acid	1.85

TABLE 9: EFFECTS OF ETHYLENEDIAMINE ON REAGENT $CaCO_3$ DISSOLUTION, pH 6.0, 0.1 M $CaCl_2$, N_2 SPARGING

Ethylenediamine (mM)	T(°C)	Dissolution Rate Constant $kx10^{10}(cm^2/sec)$
0.0	25	1.44
10.0	25	12.1
0.0	55	4.0
10.0	55	9.8

TABLE 10: EFFECT OF GYPSUM SATURATION ON REAGENT $CaCO_3$ DISSOLUTION, 25°C, pH 5, 0.1 M $CaCl_2$, CO_2 SPARGING

Na_2SO_4 (mM)	Dissolution Rate Constant $kx10^{10}$ (cm^2/sec)
0	10.5
5	9.8
10	11.6
15	11.4
20	6.2
25	10.3

Effect of Solids Concentration

At pH 5 with CO_2 sparging, addition of 1.0 M gypsum solids increased the $CaCO_3$ dissolution rate less than 15 percent.

Experiments were performed with variable quantities of Reagent $CaCO_3$ at pH 5 and 25°C with CO_2 sparging in 0.1 M $CaCl_2$. The solution was titrated with 10 N H_2SO_4. Ten g gypsum seed was added to the initial solution. Table 11 gives the results.

The apparent dissolution rate increases linearly with initial $CaCO_3$ concentration. At 0.25 M $CaCO_3$ the rate is about two times faster than at 0.005 M $CaCO_3$. At pH 5, CO_2 enhances the dissolution rate. With increased $CaCO_3$ solids concentration, CO_2 stripping from the solution may not keep up with the increased rate of CO_2 generation by $CaCO_3$ dissolution. Therefore CO_2 may accumulate in the solution and give the enhanced rate of dissolution. The conversion of HCO_3^- to CO_2 may also not keep up with the rate of $CaCO_3$ dissolution.

Therefore, the pH-stat apparatus is not suitable for rate measurements at high solids concentration.

Dissolution of Dolomite

The dissolution rate of a natural dolomite ($MgCO_3 \cdot CaCO_3$) was measured as a function of pH in 0.1 M $MgCl_2$ and 0.1 M $CaCl_2$ at 25°C and 55°C. The screened dolomite sample (Thornton, -325 mesh) was obtained from Radian. Its size distribution is given in Appendix A.

The data have been interpreted assuming that the dolomite dissolution rate is controlled by surface reaction kinetics and is proportional to the surface area. If the rate per unit surface area is given by k_s, the total fraction of undissolved dolomite is given by:

$$F = \sum_{j=1}^{n} \phi_j \left(1 - \frac{2k_s t}{\rho_m d_j}\right)^3$$

The value of the rate constant, k_s (gmol/cm^2-sec), has been calculated for each experiment from the measured t_{50} and the particle size distribution.

Figure 30 gives the measured values of the dissolution rate and $1/t_{50}$. Above pH 3 the dissolution rate appears to be directly proportional to H^+ activity. At pH 4 to 6 and 25°C the dissolution rates in 0.1 M $MgCl_2$ are twice as fast as in 0.1 M $CaCl_2$. At 55°C, the dissolution rates were 2.5 (pH 6)

TABLE 11: EFFECT OF REAGENT $CaCO_3$ SOLIDS CONCENTRATION, pH 5.0, CO_2 SPARGING, 0.1 M $CaCl_2$, TITRATION BY 10 N H_2SO_4

Initial $CaCO_3$ (M)	Agitator Speed (rps)	Dissolution Rate Constant $kx10^{10}$ (cm^2/sec)
0.005	12	8.7
0.05	12	9.0
0.05	12	10.1
0.05	24	11.2
0.125	12	10.3
0.25	12	17.0
0.25	24	19.6

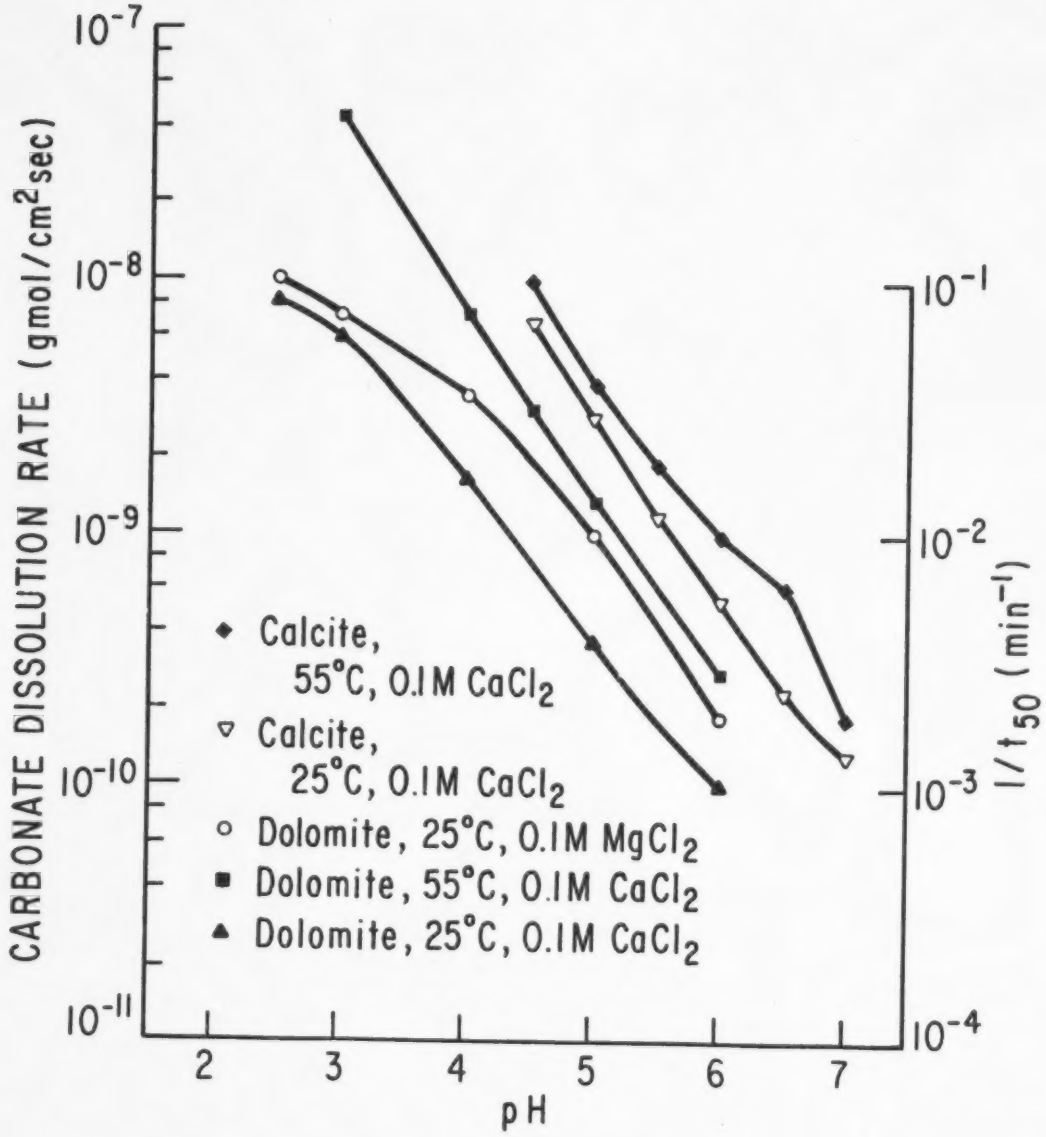

Figure 30. Comparison of Dissolution Rates of Calcite and Dolomite With the Same Particle Size Distribution, N_2 Sparging

to 7.0 (pH 3) times faster that at 25°C, giving an activation energy of 6 to 12 kcal/gmol.

Figure 30 also gives values of $1/t_{50}$ calculated from the dolomite particle size distribution using Eq. (23) and k values from the simplified, stagnant model for calcite dissolution. Because the median size of the Thornton dolomite is about 25 μm, the actual rates of mass transfer would be somewhat greater than shown in Figure 30. Calcite dissolves about 5 times faster than dolomite at 25°C and about 3.5 times faster at 55°C.

Table 12 gives additional results with sodium acetate (NaAc) and with NaCl and $MgCl_2/CaCl_2$ solutions. Sodium acetate had no significant effect in 0.1 M $MgCl_2$. In 0.1 M $CaCl_2$ at pH 4, 20 mM NaAc increased the dissolution rate a factor of 1.5. This effect is far less than that observed in calcite dissolution, which is controlled by H^+ diffusion.

The dissolution rates with 0.3 M NaCl and 0.05 M $MgCl_2$/0.05 M $CaCl_2$ were about the same and equal to the geometric mean of the rates at 0.1 M $CaCl_2$ and 0.1 M $MgCl_2$.

These data all strongly suggest that dolomite dissolution is controlled by surface reaction kinetics. The dissolution rates are 3.5 to 5 times slower than predicted by mass transfer. The activation energy is 6 to 12 kcal/gmol, which is significantly greater than expected from simple diffusion processes (3-4 kcal/gmol). The observed effects of Ca^{++} and Mg^{++} could not be predicted from a simple mass transfer model.

Because dolomite dissolution is controlled by surface reaction kinetics, it will probably not be enhanced by dissolved sulfite and may even be substantially inhibited by sulfite adsorption. Therefore, dolomite will probably dissolve 3 to 20 times slower than calcite in an actual scrubber system.

TABLE 12: DISSOLUTION OF THORNTON DOLOMITE, -325 MESH, 25°C, N_2 SPARGING

pH	Solution Composition	t_{50} (min)	Carbonate Dissolution Rate x 10^{10} (gmol/cm^2-sec)
4.0	0.1 M $CaCl_2$	64.5	16.2
	+ 2 mM NaAc	51.0	20.4
	+ 5 mM NaAc	46.9	22.2
	+20 mM NaAc	44.0	23.8
5.0	0.1 M $CaCl_2$	286	3.64
	+ 2 mM NaAc	198	5.26
4.0	0.1 M $MgCl_2$	31.1	33.6
	+ 2 mM NaAc	30.6	34.0
	+ 5 mM NaAc	29.0	36.0
	+20 mM NaAc	34.0	30.6
4.0	0.05 M $MgCl_2$ + 0.05 M $CaCl_2$	45.8	22.8
4.0	0.3 M NaCl	48.6	21.8

SECTION 6

CONCLUSIONS

The pH-stat method is effective for determining the absolute or relative reactivity of a ground limestone sample. Rate data can be obtained at practically any constant solution composition from 0 to 100% dissolution of the sample. Relative reactivity is independent of solution composition and temperature and can be determined at 25°C in a simple solution. No solution or solid analyses are necessary since the dissolution rate is obtained directly from the titration volume. The method can be performed manually with a pH meter and a burette or automatically with an appropriate pH titrimeter.

The dissolution rate of relatively pure limestone (>85% $CaCO_3$) is controlled by mass transfer, not by surface reaction kinetics. The mass transfer model accurately predicts effects of solution composition, particle size distribution, and temperature. The two adjustable constants in the model are within a factor of 1.5 of values predicted by theory or previous correlations of mass transfer in stirred tanks. The mass transfer rates are a strong function of agitation only when solids are settled out of the solution.

Diffusion of H^+, OH^-, and buffer species usually dominates the mass transfer rate. Accurate modeling requires careful accounting for the diffusivity and equilibria of each solution species in the mass transfer boundary layer. Buffers such as $SO_3^=/HSO_3^-$, adipic acid, and ethylenediamine can substantially increase the dissolution rate at concentrations as low as 1 mM.

At pH values less than 5.5, temperature affects only diffusivities, resulting in an effective activation energy of 4 kcal/gmol. At higher pH values, OH^- diffusion can be important and temperature can also affect solution equilibria, resulting in a greater effective activation energy.

Dissolved CO_2 can reduce the dissolution rate by the extent that it affects solid/solution equilibrium. This equilibrium is accounted for in the mass transfer model but is usually important only if the bulk solution pH is

within 0.5 units of the equilibrium pH. CO_2 can also enhance the dissolution rate as the CO_2/HCO_3^- buffer. However, this buffer reaction occurs at a finite rate and is important only with larger limestone particles in the absence of $SO_3^=/HSO_3^-$ and other buffers.

Limestone type affects the $CaCO_3$ dissolution rate primarily by its effect on the particle size distribution. The rate of mass transfer may also have some limited variation with particle shape, but it should not vary with factors such as internal surface area, grain size, or minor chemical impurities. A large fraction of dolomite or other inerts will affect the dissolution rate. Dolomite dissolves 3 to 10 times slower than calcite of equivalent particle size.

The Coulter Counter can be used with $CaCl_2$ electrolyte to obtain particle size distributions at 0.7 to 160 μm. When supplemented by wet sieving at larger sizes, the comprehensive size distribution can be effectively used by the mass transfer model to predict dissolution rates. A generalized log gamma size distribution model can be used to infer a size distribution from pH-stat rate data or to predict a dissolution rate from a less comprehensive size distribution measurement.

Dissolved sulfite and metal ions such as Fe^{++}, Mn^{++}, and Mg^{++} inhibit limestone dissolution. $CaSO_3$ or metal carbonates appear to adsorb on the $CaCO_3$ surface and reduce the effective solubility of $CaCO_3$. The mass transfer model is still effective with sulfite inhibition if the $CaCO_3$ solubility is expressed as a function of dissolved $CaSO_3$ at the $CaCO_3$ surface. Because of its beneficial buffer effects, dissolved $SO_3^=/HSO_3^-$ causes actual rate reduction only at concentration levels greater than expected in saturated $CaSO_3$ solution. Similarly, inhibition is only important when the bulk solution is near equilibrium with $CaCO_3$ solids or with the adsorption layer.

High ionic strength inhibits $CaCO_3$ dissolution by reducing the diffusivity of H^+. It may also reduce the diffusivities of other important solution species. These effects should also be important for other phenomena involving liquid phase diffusion, including SO_2 gas/liquid mass transfer and $CaSO_3$ dissolution.

Limestone dissolution is relatively fast, especially in the presence of dissolved sulfite. Therefore, absorber feed solution tends to be near equilibrium with $CaCO_3$ solid or with the $CaCO_3/CaSO_3$ adsorption layer. Furthermore,

a substantial fraction of $CaCO_3$ can dissolve at the lower pH in the absorber, even though the residence time is much shorter than in the hold tank. Since the hold tank is near equilibrium, it should be sized not for limestone dissolution, but for $CaSO_3/CaSO_4$ crystallization.

SECTION 7

RECOMMENDATIONS

Additional measurements of $CaCO_3$ dissolution rate should be made with high suspended solids concentration (1 to 15 percent). This project measured dissolution rate with 0.05 percent solids. At higher solids concentration, the mass transfer coefficient should be reduced by particle-particle interaction and agglomeration. These effects may be a function of limestone type. These experiments will need to be performed in a pH-stat with continuous liquid removal, because gas sparging cannot remove CO_2 at a sufficient rate.

Better measurements of diffusivities are needed for H^+, OH^-, HCO_3^-, $SO_3^=$, Ca^{++}, and other solution species in concentrated electrolytes such as 0.1 to 2.0 M $CaCl_2$, $MgSO_4$, or Na_2SO_4. Additional measurements of $CaCO_3$ dissolution in these electrolytes could be used to infer diffusivities. Other more direct measurements of diffusivities would also be useful.

Careful measurements of $CaCO_3$ dissolution rate are needed in solutions near the equilibrium pH. This project measured few data closer than 0.2 pH units to equilibrium. Inhibition by $SO_3^=$, metal ions, and Mg^{++} will be most evident in this zone and the measurements could be used to establish the pseudo-equilibrium relationships. Most absorber hold tanks will also operate near equilibrium.

Careful measurements of $CaCO_3$ reactivity at high utilization are needed to establish second-order effects of limestone type. At 80 to 100 percent limestone utilization, dolomite and inert impurities will dominate the remaining solids and may affect dissolution of the remaining $CaCO_3$ by blinding or by giving artificially large particles. Careful dissolution rate and particle size measurements will be required to separate these effects.

LITERATURE CITED

Aitchison, J. and J.A.C. Brown, The Lognormal Distribution, Cambridge University Press, Cambridge (1957).

Albery, W. J., A. R. Greenwood, and R. F. Ribble, Trans. Far. Soc., 63, 360 (1967).

Barton, P., and T. Vatanatham, Env. Sci. and Tech., 10, 262 (1976).

Berner, R. A., and J. W. Morse, Amer. J. Sci., 274, 108 (1974).

Calderbank, P. H. and M. B. Moo-Young, Chem. Eng. Sci., 16 39-54 (1961).

Cavanaugh, C. M., M.S. Thesis, University of Texas at Austin, Austin, Texas (1978).

Chan, P.K.R., M.S. Thesis, University of Texas, Austin, Texas, 1981.

Chan, P. K., and G. T. Rochelle, ACS Symp. Ser., 188, 75-97 (1982).

Chang, C-S., J. H. Dempsey, R. H. Borgwardt, G. T. Rochelle, and A. J. Toprac, Env. Prog., 1(1), 59-65 (1982).

Drehmel, D. C., "Limestone Types for Flue Gas Scrubbing," Proceedings of Second International Lime/Limestone Wet-Scrubbing Symposium, Vol. I, pp. 167-194, U. S. Environmental Protection Agency, APRD-1161, 1972.

Erga, O., and S. G. Terjesen, Acta. Chem. Scand., 10, 872 (1956).

Garrels, R. M., and M. E. Thompson, Am. J. Sci., 260, 57 (1962).

Harned, H. S., and F. T. Bonner, J. Am. Chem. Soc., 67, 1026 (1945).

Harned, H. S., and S. R. Scholes, Jr., J. Am. Chem. Soc., 63, 1706 (1941).

Harriott, P., AIChE J., 27, 93-101 (1962).

Jeffrey, G. H., and A. I. Vogel, J. Chem. Soc., 21 (1935).

Koss, V., and P. Moller, Z. Anorg. Allg. Chem., 410, 165 (1974).

Landolt-Bornstein Physikalisch-Chemische Tabbellen, Bd. II-7 225, Springer-Verlag, Berlin, Germany (1960).

Levins, D. M. and J. R. Glastonbury, Trans. Instu. Chem. Engrs., 50, 32-41, 132-146, (1972).

Lewis, J. B., J. Appl. Chem., 5, 225 (1955).

Lowell, P. S., D. M. Ottmers, K. Schwitzgebel, T. I. Strange, and D. W. Deberry, "A Theoretical Description of the Limestone Injection - Wet Scrubbing Process," PB 193-029, U. S. Environmental Protection Agency (1970).

Meserole, F. B., private communication (1982).

Meserole, F. B., R. L. Glover, and D. A. Stewart, "Laboratory Studies to Determine the Major Factors Which Affect Limestone Dissolution and the Availability of Magnesium in Limestone," presented at the ACS National Meeting, Atlanta, GA, March 29-30, 1981.

Morse, J. W., Amer. J. Sci. 274, 97 (1974).

Nielsen, K. L., "Method in Numerical Analysis," 2nd Edition, New York, MacMillan (1964).

Ottmers, D., J. Phillips, C. Burklin, W. Corbett, N. Phillips, and C. Shelton, "A Theoretical and Experimental Study of the Lime/Limestone Wet Scrubbing Process," EPA Report No. EPA-650/2-75-006 (1974).

Pinsent, R. W., L. Pearson, and F. J. W. Roughton, Trans. Far. Soc., 52, 1512 (1956).

Plummer, L. N., T. M. L. Wigley, and D. L. Parkhurst, Amer. J. Sci., 278, 179 (1978).

Plummer, L. N., D. L. Parkhurst, and T. M. L. Wigley, ACS Symp. Ser., 93, 537 (1979).

Roberts, N. K. and H. L. Northey, J. Chem. Soc. (A), 1971, 2572-74.

Rochelle, G. T., "Process Synthesis and Innovation in Flue Gas Desulfurization," EPRI FP-463-SR (1977).

Rochelle, G. T., and C. J. King, Chem. Eng. Prog., 74, 65 (1978).

Schultz, D. M. and C. F. Crouse, So. African Statist. J., 7, 143-152 (1973).

Sherwood, T. K., R. L. Pigford, and C. R. Wilke, "Mass Transfer," McGraw-Hill (1975).

Sjoberg, E. L., Geochim. Cosmochim. Act., 40, 441 (1976).

Sjoberg, E. L., Stock. Contr. Geol., 32(1), 1 (1981).

Smith, R. C., M.S. Thesis, The University of Texas at Austin, Texas (1981).

Tartar, H. V., and H. H. Garretson, J. Am. Chem. Soc. 63, 808 (1941).

Terjesen, S. G., O. Erga, G. Thersen, and A. Ve, Chem. Eng. Sci. 14, 227 (1961).

Toprac, A. J., M.C. Thesis, The University of Texas, Austin, Texas (1981).

Toprac, A. J., and G. T. Rochelle, Env. Prog., 1(1), 52-58 (1982).

Weems, W. T., M.S. Thesis, The University of Texas, Austin, Texas (1981).

APPENDIX A
PARTICLE SIZE DISTRIBUTIONS

The Coulter Counter determines the number and size of particles suspended in a conductive liquid by forcing the suspension to flow through a small aperture and monitoring an electrical current which also passes through the aperture. As a particle passes through the aperture, it changes the resistance between the electrodes. This produces a current pulse of short duration having a magnitude proportional to the particle volume. The measurements obtained from the Coulter Counter are differential percent volume versus volumetric size, and cumulative percent volume versus volumetric size. A single aperture can generate a size distribution with 14 fractions from 2 to 40 percent of the aperture diameter. By wet sieving the sample, successively smaller apertures may be employed to generate size distributions over large ranges. The overlapping size fractions between apertures may be ratioed and averaged to provide a scaling factor that is applied to the smaller distribution. When overlapping of distributions is completed, the final distribution may be normalized to 100 percent for the entire range.

Use of the 19 and 800 μm apertures theoretically allows for Coulter Counter distributions extending from 0.4 to 800 μm. In practice, however, the 30 μm tube was found to be the smallest that was free from electrical noise and aperture blockage problems. The 400 μm tube is the largest amenable to the sample stand employed. The 100 μm tube was found to be useful for the intermediate range.

The Coulter Counter Model TA II consists of three units: the Sample Stand, the Main Unit, and the X-Y recorder. In the unit employed in this investigation, the main unit additionally contained the Population Accessory built into the base. The Population Accessory contains a tape printer from which volume percent for each channel was obtained. The X-Y recorder plots of differential and cumulative volume percent were used for qualitative judgments of data validity and distribution overlaps.

The electrolyte employed was 0.18 M $CaCl_2$. Dissolution of $CaCO_3$ sample was found to occur during measurements when employing an electrolyte

of 1 percent NaCl saturated with $CaCO_3$. 0.18 M $CaCl_2$ or 1 mM sodium triphosphate in 1 percent sodium chloride was found to prevent any significant dissolution over time. The electrolyte must be highly filtered for valid particle distribution measurements. A Coulter Filtration System was employed for this purpose. Prefiltration of the electrolyte is necessary to prevent premature fouling of the filtration system filters. This was accomplished by filtering the electrolyte five to eight times through standard filter paper in a vacuum system.

Calibration of the aperture tubes was performed using the built-in meter. Dry limestone sample was introduced into a well-rinsed round bottom beaker full of filtered electrolyte to produce a concentration index reading of about five percent. The sample was dispersed by high speed operation of the agitator for about a minute. The agitator speed was reduced during measurement to prevent electrical noise.

Tabulated size distributions for all limestone types and grinds used in this investigation are presented in Tables A-1 through A-4.

TABLE A-1 : Differential and Cumulative Limestone Particle Size Distributions, Volume percent

SIZE (μm)	Ashgrove		Fredonia Fine		Georgia Marble Fine		Maysville		Stonemen Fine	
	Dif[a]	Cum[b]	Dif	Cum	Dif	Cum	Dif	Cum	Dif	Cum
0.630			0						0.3	100.0
0.794			0.2	100.0					0.4	99.7
1.00			0.9	99.8	0.1	100.0			1.0	99.3
1.26	0		2.2	98.9	0.2	99.9	0		1.8	98.2
1.59	0		4.4	96.7	0.3	99.7	0		2.4	96.4
2.00	0.5	100.0	5.5	92.3	0.5	99.4	2.2	100.0	2.6	94.0
2.52	1.2	99.5	9.1	86.7	0.8	98.9	4.8	97.8	2.8	91.4
3.17	2.8	98.3	10.5	77.7	1.2	98.1	8.8	93.0	3.2	88.6
4.00	5.0	95.5	8.0	67.2	2.0	96.9	12.3	84.2	3.0	85.4
5.04	7.6	90.5	5.1	59.2	2.4	94.9	11.6	71.9	3.0	82.3
6.35	9.3	82.8	4.1	54.0	3.4	92.5	9.2	60.3	3.5	79.3
8.00	11.3	73.5	3.9	49.9	4.4	89.1	6.7	51.1	3.9	75.8
10.08	11.4	62.1	3.6	46.0	6.0	84.7	6.0	44.4	4.8	71.9
12.7	11.4	50.7	3.7	42.4	8.6	78.7	5.7	38.4	6.2	67.1
16.0	11.8	39.2	3.9	38.7	11.1	70.1	5.7	32.7	7.7	60.8
20.2	11.1	27.3	3.9	34.8	12.6	59.0	6.2	27.0	8.9	53.1
25.4	10.6	16.2	4.5	30.9	14.3	46.4	7.3	20.8	11.4	44.2
32.0	4.2	5.5	4.6	26.4	13.2	32.1	7.7	13.5	11.6	32.8
40.3	1.3	1.3	5.5	21.8	10.2	18.9	4.8	5.8	11.5	21.2
50.8	0	0	5.2	16.3	4.8	8.7	1.0	1.0	6.8	9.7
64.0	0	0	4.6	11.1	2.6	3.9	0	0	2.5	2.9
80.6			3.8	6.5	1.3	1.3	0	0	0.5	0.5
101.6			2.3	2.7	0	0			0	0
128.0			0.3	0.4	0	0			0	0
161.0			0	0						
297.0			0	0						
420.0										
595.0										

[a] Dif = Volume fraction between designated size and next largest size.

[b] Cum = Volume fraction larger than designated size.

TABLE A-2: Differential and Cumulative Limestone Particle Size Distributions, Volume Percent

Size	Fredonia 120-200 mesh		Fredonia 200-325 mesh		Fredonia Coarse		Fredonia Extra-Coarse		Georgia Marble Coarse		Longview Coarse		Reagent Fisher 2		Stone-man Coarse	
(μm)	Dif[a]	Cum[b]	Dif	Cum	Dif	Cum	Dif	Cum	Dif	Cum	Dif	Cum	Dif	Cum	Dif	Cum
0.630					0		0.2	99.9	0		0.6	100.0			0.1	99.6
0.794					0.4	100.3	0.3	99.7	0.2	100.0	0.6	99.4			0.5	99.5
1.00					1.1	99.9	0.6	99.4	0.3	99.8	1.1	98.8			0.8	99.0
1.26					2.0	98.8	1.0	98.8	0.4	99.5	1.9	97.7			1.5	98.2
1.59					3.1	96.8	1.8	97.8	0.7	99.1	2.5	95.8			1.8	96.7
2.00					4.2	93.7	2.6	96.0	0.9	98.4	3.0	93.3			1.9	94.9
2.52					5.3	89.5	4.1	93.4	1.2	97.5	3.6	90.3	0		1.9	93.0
3.17					5.1	84.2	5.0	89.3	1.6	96.3	4.7	86.7	0		2.1	91.1
4.00					3.7	79.1	4.6	84.3	1.8	94.7	5.3	82.0	0.2	100.4	1.9	89.0
5.04					2.8	75.4	3.5	79.7	1.6	92.9	5.7	76.7	1.4	100.2	1.8	87.1
6.35					2.4	72.6	3.0	76.2	1.8	91.3	5.3	71.0	6.7	98.8	1.9	85.3
8.00					2.2	70.2	2.6	73.2	2.5	89.5	5.0	65.7	22.1	92.1	2.3	83.4
10.08					2.2	68.0	2.7	70.6	3.2	87.0	3.8	60.7	39.2	70.0	3.0	81.1
12.7					2.5	65.8	3.1	67.9	4.3	83.8	4.4	56.9	25.6	30.8	4.0	78.1
16.0			0	0	2.9	63.3	3.3	64.8	5.1	79.5	4.0	52.5	4.6	5.2	4.9	74.1
20.2			0	0	3.3	60.4	3.6	61.5	5.9	74.4	3.7	48.4	0.4	0.6	5.5	69.2
25.4	0	0	0.2	99.8	4.1	57.1	4.0	57.9	7.7	68.5	3.9	44.7	0.2	0.2	6.5	63.7
32.0	0	0	0.5	99.6	4.7	53.0	4.2	53.9	8.5	60.8	3.8	40.8	0	0	7.1	57.2
40.3	0.7	99.5	11.5	99.1	5.8	48.3	5.6	49.7	9.6	52.3	4.2	37.0	0	0	8.4	50.1
50.8	0.9	99.8	46.1	87.6	7.2	42.5	6.3	44.1	9.8	42.7	4.9	32.8			7.5	41.7
64.0	1.1	97.9	30.8	41.5	7.4	35.3	6.3	37.8	9.0	32.9	4.4	27.9			9.0	34.2
80.6	8.3	96.8	6.4	10.7	8.8	27.9	7.4	31.5	8.4	23.9	6.3	23.5			9.9	25.3
101.6	35.6	88.5	2.4	4.3	8.5	19.1	8.3	24.1	6.7	15.5	8.7	17.2			8.5	15.3
128.0	51.1	52.9	1.9	1.9	4.9	10.6	6.3	15.8	4.8	8.8	6.7	8.5			4.1	6.8
161.0	1.8	1.8	0	0	3.2	5.7	5.9	9.5	3.0	4.0	1.6	1.8			2.1	2.7
210.0	0	0	0	0	1.7	2.5	2.7	3.6	0.8	1.0	0.2	0.2			0.5	0.6
297.0	0	0	0	0	0.6	0.8	0.7	0.9	0.2	0.2	0	0			0.1	0.1
420.0					0.2	0.2	0.2	0.2	0	0					0	0
595.0						0	0	0								

[a]Dif = Volume fraction between designated size and next largest size.

[b]Cum = Volume fraction larger than designated size.

TABLE A-3: Differential and Cumulative Limestone Particle Size Distributions, Volume Percent

Size	Brassfield 120-200 mesh		Pfizer 120-200 mesh		Pfizer 200-325 mesh		Thornton -325 mesh	
(μm)	DIF[a]	CUM[b]	DIF	CUM	DIF	CUM	DIF	CUM
0.630								
0.794								
1.00								
1.26			0		0			
1.59			0		0			
2.00			0.9	99.8	0.9	100.0		
2.52			2.6	98.9	1.3	99.1	1.7	99.9
3.17			3.7	96.3	2.2	97.8	2.5	98.2
4.00			4.1	92.5	3.1	95.6	3.2	95.7
5.04			4.6	88.5	3.4	92.5	3.9	92.5
6.35			5.2	83.9	3.7	89.1	4.6	88.6
8.00			6.1	78.7	3.9	85.4	5.1	84.0
10.08			6.6	72.6	5.3	81.5	6.1	78.9
12.7			8.0	66.0	6.6	76.2	6.9	72.8
16.0			8.9	58.0	7.6	69.6	8.3	65.9
20.2			9.5	49.1	9.0	62.0	9.5	57.6
25.4	0		10.7	39.6	10.9	53.0	10.6	48.1
32.0	0		8.6	28.9	13.5	42.1	12.3	37.5
40.3	0.4	100.1	7.6	20.3	17.7	28.6	12.2	25.2
50.8	0.8	99.7	7.1	12.7	9.8	10.9	7.9	13.0
64.0	9.0	98.9	4.0	5.6	0.9	1.1	5.1	5.1
80.6	47.4	89.9	1.6	1.6	0.2	0.2		
101.6	40.7	42.5	0	0	0	0		
128.0	1.4	1.8	0	0	0	0		
161.0	0.4	0.4						
203.0								

[a]DIF = Volume fraction between designated size and next largest size.

[b]CUM = Volume fraction larger than designated size.

TABLE A-4: Differential and Cumulative Particle Size Distributions, Volume Percent

Size (μm)	Fredonia Feedbelt		Longview Fine		Fredonia 100-140		Fredonia 170-270	
	DIF[a]	CUM[b]	DIF	CUM	DIF	CUM	DIF	CUM
0.630	0.4	100.0	0.1	100.0				
0.794	0.7	99.6	0.1	99.9				
1.00	1.3	98.9	1.2	99.8				
1.26	2.4	97.6	2.0	98.6				
1.59	3.9	95.2	2.7	96.6				
2.00	5.9	91.3	3.0	93.9				
2.52	7.9	85.4	3.8	90.9				
3.17	8.5	77.5	4.7	87.1				
4.00	7.5	69.0	4.9	82.4				
5.04	6.6	61.5	5.5	77.5				
6.35	5.9	54.9	5.5	72.0				
8.00	5.7	49.0	5.8	66.5				
10.08	5.2	43.3	6.3	60.7				
12.7	4.8	38.1	6.4	54.4				
16.0	4.7	33.3	6.7	48.0				
20.2	4.7	28.6	6.8	41.3			0.2	100.0
25.4	4.6	23.9	6.9	34.5			0.4	99.7
32.0	4.5	19.3	7.6	27.6			0.7	99.3
40.3	4.5	14.8	8.3	20.0	0.2	100.0	7.0	98.6
50.8	3.8	10.3	6.3	11.7	0.4	99.8	27.8	91.6
64.0	3.5	6.5	4.0	5.4	0.4	99.4	36.5	63.8
80.6	1.7	3.0	1.1	1.4	0.6	99.0	26.1	27.3
101.6	1.2	1.3	0.3	0.3	43.7	98.4	1.2	1.2
128.0	0.1	0.1	0	0	52.0	54.7	0	
161.0	0		0	0	2.7	2.7	0	
210.0	0							
297.0								
420.0								
595.0								

[a] DIF = Volume fraction between designated size and next largest size.

[b] CUM = Volume fraction larger than designated size.

APPENDIX B

COMPOSITIONS OF LIMESTONE SAMPLES

Limestone Type	Percentage				
	Available Carbonate[a]	$CaCO_3$	Dolomite	$MgCO_3$	Insolubles
Ash Grove	96.7	96.7	0.9	0	2.43
Brassfield	84.0	84.0	15.2	0	0.8
Fredonia	95.0	95.0	3.2	0	1.8
Georgia Marble	95.9	95.9	2.2	0	1.9
Longview	95.0	94.9	3.4	0	1.7
Maysville	88.9	88.8	9.6	0.1	1.5
Pfizer	98.7	95.2	1.0	3.50	0.3
Stoneman	88.0	88.0	9.9	0	2.1
Thornton	-	-	(100)	-	-

[a] Available carbonate as $CaCO_3$, Equal to molar sum of $CaCO_3$ and $MgCO_3$.

APPENDIX C

NOMENCLATURE

a = activity, M

$\% A$ = weight percent of limestone available for dissolution

B = mass transfer enhancement factor, cm^{-1}

ΔC = concentration gradient of solution species from limestone particle surface to bulk solution, moles/liter

d, d_p = diameter of limestone particle, cm

d_{50} = particle diameter corresponding to 50 cumulative weight percent of limestone size distribution, cm

d_{90} = particle diameter corresponding to 90 cumulative weight percent of limestone size distribution, cm

d_{100} = largest particle diameter of limestone size distribution, cm

D = diffusivity, cm^2/sec

D_s = diameter of propeller, cm

D_T = diameter of tank, cm

f, f_j = fraction undissolved of a limestone particle with an initial volume, V_j

F_a = Faraday Number, 23,062 cal/volt-equiv

F, F_b = total fraction undissolved limestone of a ground sample dissolving in batch

F_c = total fraction undissolved limestone of a ground sample dissolving in a CSTR

ΔH = apparent heat of reaction, kcal/gmol

K = dissolution rate parameter, cm^2/min

K_j = Equilibrium Constant, M

k = dissolution rate parameter, cm^2/sec

k_L = mass transfer coefficient, cm/sec

M = molarity, gmol/liter

n_j = charge on the jth ion

N_{Re} = Reynolds number for particle with velocity v with respect to the fluid $d_p v/\nu$

N_{Sh} = Sherwood number = $k_L d_p/D$

N_{Sc} = Schmidt number = ν_c/D

P_{CO_2} = partial pressure of CO_2 in solution, atm

pH = negative logarithm of hydrogen ion activity

R = universal gas constant, 0.08205 liter-atm/gmol- K

V, V_p = volume of a limestone particle, cm^3

V_j = initial volume of limestone particle corresponding to size fraction ϕ_j, cm^3

r = distance from center of sphere, cm

T = temperature, K

t = time, min

t_{44} = time required to dissolve 44 percent of sample, min

t_{50} = time required to dissolve 50 percent of limestone sample, min

t_{80} = time required to dissolve 80 percent of limestone sample, min

x = dimensionless distance, 1-d/2r

Greek Letters

α = breakage frequency parameter, log gamma distribution

α_i, β_i = constants of integration M cm^2/sec

β = breakage mode parameter, log gamma distribution

γ = activity coefficient

$\Gamma(\alpha)$ = Gamma function with argument α

ε = agitation power per gram solution, cm^2/sec^3

μ = mean of random variable 3 ln (d_{100}/d)

η = viscosity, poise

ν = kinematic viscosity of solution, cm^2/sec

λ_o = equivalent ionic conductivity at infinite dilution, cm^2/gmol-ohm

ρ = density of solution, gm/cm^3

ρ_m = molar density of limestone, $moles/cm^3$

σ = standard deviation of random variable 3 ln (d_{100}/d)

τ = mean residence time of CSTR, min

ϕ_j = fraction of limestone particles with initial diameter V_j

[ ] = concentration, M